



KENTUCKY TRANSPORTATION CENTER

**SEISMIC EVALUATION OF THE TENNESSEE RIVER
BRIDGES ON I-24 IN WESTERN KENTUCKY**



UNIVERSITY OF KENTUCKY

College of Engineering



OUR MISSION

We provide services to the transportation community through research, technology transfer and education.
We create and participate in partnerships to promote safe and effective transportation systems.

OUR VALUES

Teamwork

Listening and communicating along with courtesy and respect for others.

Honesty and Ethical Behavior

Delivering the highest quality products and services.

Continuous Improvement

In all that we do.

Research Report
KTC-06-24/SPR206-00-5F

SEISMIC EVALUATION OF THE TENNESSEE RIVER BRIDGES ON INTERSTATE 24 IN WESTERN KENTUCKY

By

Tong Zhao

Visiting Professor, Kentucky Transportation Center

Wei-Xin Ren

Formerly Visiting Professor, Kentucky Transportation Center

Issam E. Harik

Professor of Civil Engineering and Head, Structures Section,
Kentucky Transportation Center

and

Jin-Dong Hu

Visiting Professor, Kentucky Transportation Center

Kentucky Transportation Center
College of Engineering, University of Kentucky

in cooperation with

Transportation Cabinet
Commonwealth of Kentucky

and

Federal Highway Administration
U.S. Department of Transportation

The contents of this report reflect the views of the authors who are responsible for the facts and accuracy of the data presented herein. The contents do not necessarily reflect the official views or policies of the University of Kentucky, the Kentucky Transportation Cabinet, nor the Federal Highway Administration. This report does not constitute a standard, specification or regulation. The inclusion of manufacturer names or trade names are for identification purposes and are not to be considered as endorsement.

September 2006

Technical Report Documentation Page

1. Report No. KTC-06-24/SPR206-00-5F		2. Government Accession No.		3. Recipient's Catalog No.	
4. Title and Subtitle SEISMIC EVALUATION OF THE TENNESSEE RIVER BRIDGES ON INTERSTATE 24 IN WESTERN KENTUCKY				5. Report Date September 2006	
				6. Performing Organization Code	
				8. Performing Organization Report No. KTC-06-24/SPR206-00-5F	
7. Author(s): T. Zhao, W.X. Ren, I.E. Harik, and J.D. Hu					
9. Performing Organization Name and Address Kentucky Transportation Center College of Engineering University of Kentucky Lexington, Kentucky 40506-0281				10. Work Unit No. (TRAIS)	
				11. Contract or Grant No. KYSPR 206	
				13. Type of Report and Period Covered Final	
12. Sponsoring Agency Name and Address Kentucky Transportation Cabinet State Office Building Frankfort, Kentucky 40622				14. Sponsoring Agency Code	
15. Supplementary Notes Prepared in cooperation with the Kentucky Transportation Cabinet and the U.S. Department of Transportation, Federal Highway Administration.					
16. Abstract This report presents the seismic evaluation of the approaches and parallel bridges on I-24 crossing the Tennessee River between Marshall and Livingston counties in Western Kentucky. The main bridges are steel tied-arch bridges. The bridges are situated within the influence of the New Madrid Seismic Zone. The seismic evaluation program consisted of field testing, 3-dimensional finite element modeling and seismic response analysis. The dynamic properties of the main bridges are determined through field testing, and are used to calibrate the finite element models. The finite element model is then subjected to time histories of the 250-year and 500-year earthquake events. Stresses and displacements for these events are found to be within the acceptable limits. Analytical results indicate that the main bridge will withstand the 250-year and 500-year earthquakes without any significant damage and no loss-of-span. The supports with fixed bearings on the pier of the main bridge need to be retrofitted for the 500-year earthquake event. The approach spans are analyzed using the response spectrum method with simplified single-degree-of-freedom models. Some supports on the approach spans are found to be vulnerable to shear failure of anchor bolts under the 250-year earthquake. All supports on the piers of the approach spans need to be retrofitted for the 500-year earthquake event. Additional anchor bolts or other retrofit measures at the bearings are recommended.					
17. Key Words Seismic Evaluation; Finite Element Model; Time-History Analysis; Response Spectral Analysis; Field Testing; Interstate 24; Kentucky.			18. Distribution Statement Unlimited with approval of Kentucky Transportation Cabinet		
19. Security Classif. (of this report) Unclassified		20. Security Classif. (of this page) Unclassified		21. No. of Pages 123	22. Price

EXECUTIVE SUMMARY

Background

The need for evaluating the seismic adequacy of the existing infrastructure has come into focus following the damage and collapse of numerous bridge structures during recent earthquakes. For example, the 1989 Loma Prieta earthquake and 1994 Northridge earthquake brought attention to the seismic risks to bridges and elevated highway structures. In particular, the seismic evaluation and rehabilitation of older bridges in regions of high seismicity, where bridges were designed prior to the advent of modern seismic design codes.

Research Objectives

The main objective of this investigation is to assess the structural integrity of the I-24 Bridge over the Tennessee River connecting Marshall and Livingston counties in Western Kentucky (Figures 1 – 3). Due to its importance, the bridge will be evaluated for the 250-year and the maximum credible 500-year earthquakes. The definition of the 250-year event is: the peak horizontal particle acceleration, at the top of bedrock, which has a 90% probability of not being exceeded in 250 years (i.e. 10% probability of exceedance). Likewise, the 500-year earthquake event has a 90% probability of not being exceeded in 500 years. The investigation considers both the main bridge and the approach spans. To achieve this objective, the scope of the work is divided into the following tasks: 1) Field testing of the main bridge; 2) Finite element modeling and calibration; 3) Time-history seismic response analysis; and 4) Seismic response of the approach spans using the response spectrum method.

Field Testing

The ambient vibration properties of the main bridge are determined through field ambient vibration testing under traffic- and wind-induced excitation. The purpose of field testing is to determine the natural frequencies and the associated mode shapes. These vibration properties are subsequently used as the basis for calibrating the three-dimensional finite element model for seismic response analysis.

Finite Element Modeling

The three-dimensional finite element model of the main bridge is constructed using SAP2000 computer program and is used for the calculation of free vibration and seismic response analysis. Free vibration analysis is a key process in the dynamic analysis of the bridge structure. The natural frequency and mode shapes succinctly describe the dynamic characteristics of a complex structure. The analytical model is calibrated by comparing the free vibration analysis results with the ambient vibration properties obtained from the field testing.

Seismic Evaluation of the Main Bridge

Once calibrated, the finite element model is used for seismic response analysis. The three-dimensional model of the main bridge is subjected to the time histories of the 250-year and 500-year earthquakes to determine the maximum displacements at joints, stresses in members, and forces on the bearings.

Seismic Evaluation of the Approach Bridge

The approach spans are idealized as a simple structural system depending on the type of the bearings on the top of the piers. This simple structural system is regarded as the single degree of freedom system (SDOF) for the analytical model of the approach spans. Then seismic response of the approach spans is analyzed using the response spectrum method to determine the maximum displacements and forces.

Conclusions and Recommendations

The seismic analyses indicate that the main bridge can resist the 250-year and 500-year earthquake events without yielding of the main structural members or loss-of-span at supports. The supports with fixed bearings on the pier of the main bridge need to be retrofitted under 500-year earthquake event.

For the approach spans, some supports on the approach spans are found to be vulnerable to shear failure of anchor bolts under the 250-year earthquake (Figure 4). All supports on the piers of the approach spans need to be retrofitted under the 500-year earthquake event (Figure 5). Therefore, retrofitting of the bearings on the approach span piers is recommended.

NOTE: This report is the fifth (5 th) in a series of seven reports for Project SRP 206: “Seismic Evaluation of I-24 Bridges”. The seven reports are:	
Report Number:	Report Title:
(1) KTC-06-20/SPR206-00-1F	Seismic Evaluation of I-24 Bridges and Embankments in Western Kentucky – Summary Report
(2) KTC-06-21/SPR206-00-2F	Site Investigation of Bridges along I-24 in Western Kentucky
(3) KTC-06-22/SPR206-00-3F	Preliminary Seismic Evaluation and Ranking of Bridges along I-24 in Western Kentucky
(4) KTC-06-23/SPR206-00-4F	Detailed Seismic Evaluation of Bridges along I-24 in Western Kentucky
(5) KTC-06-24/SPR206-00-5F*	Seismic Evaluation of the Tennessee River Bridges on I-24 in Western Kentucky
(6) KTC-06-25/SPR206-00-6F	Seismic Evaluation of the Cumberland River Bridges on I-24 in Western Kentucky
(7) KTC-06-26/SPR206-00-7F	Seismic Evaluation and Ranking of Bridge Embankments along I-24 in Western Kentucky

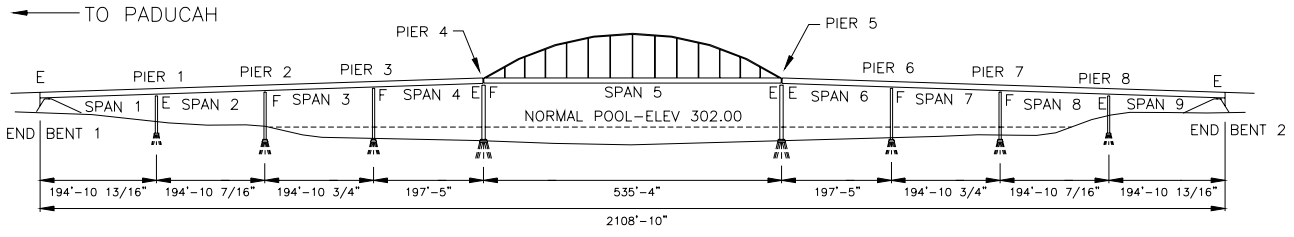
* Denotes current report



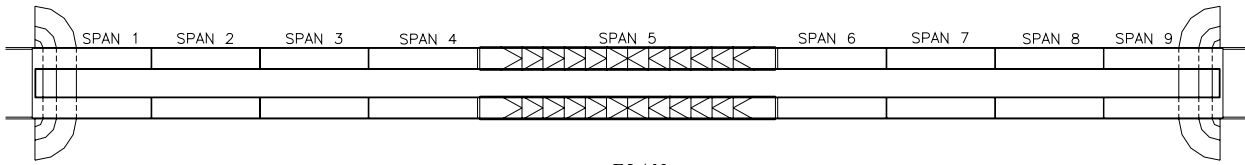
Figure 1. View of Tennessee River Bridges on I-24



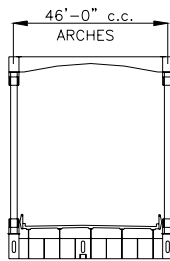
Figure 2. Side View Showing the Main Span of the Tennessee River Bridge on I-24



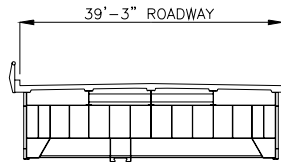
ELEVATION



PLAN



SECTION THRU TIED ARCH SPAN



SECTION THRU GIRDER SPAN

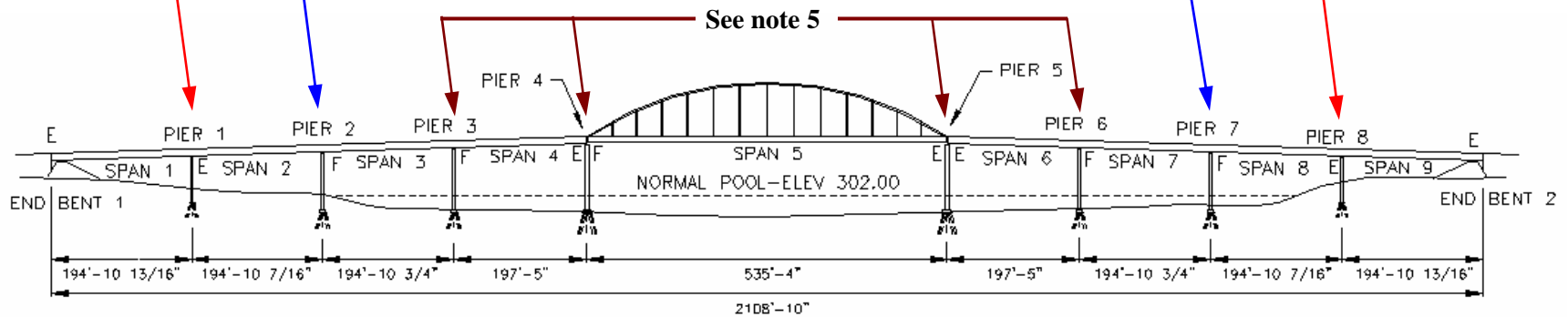
Figure 3. Layout of the Tennessee River Bridges on I-24

For each of the two bearings on Pier 1 or Pier 8 in the parallel bridges:

- Existing Shear Capacity: 1,509 kN (339 kips) - Refer to Notes 1 and 2
- Shear Demand: 3,661 kN (823 kips) - Refer to Note 4

For each of the two bearings on Pier 2 or Pier 7 in the parallel bridges:

- Existing Shear Capacity: 2,263 kN (509 kips) - Refer to Notes 1 and 3
- Shear Demand: 2,536 kN (570 kips) - Refer to Note 4



- Note 1:** The existing Shear Capacity of the bolts is derived under the assumption that the strength of the bearings remained the same since the bridge was constructed.
- Note 2:** The two bearings on Pier 1 or Pier 8 in the parallel bridges are expansion bearings in the longitudinal direction and fixed in the transverse direction. The shear capacity and demand are determined for the transverse direction.
- Note 3:** The bearings on Piers 2, 3, 6 and 7 in the parallel bridges are fixed bearings in both the longitudinal and transverse directions. The shear capacity and demand are determined from the resultant of the capacities in both directions.
- Note 4:** The shear capacity can be increased by: 1) providing additional bolts, and/or 2) replacing the existing bolts with higher strength bolts, or 3) replacing the bearings with seismic isolation bearings.
- Note 5:** The bearings at Piers 3, 4, 5 and 6 do not require any retrofit.

Figure 4. Retrofit Recommendations for the Tennessee River Bridge on I-24 in Western Kentucky for the 250-Year Seismic Event

(Note: A 250-year event is an event with 90% probability of not being exceeded in 250 years)

For each of the two bearings on Pier 1 or Pier 8 in the parallel bridges:

- Existing Shear Capacity: 1,509 kN (339 kips) - Refer to Notes 1 and 2
- Shear Demand: 7,321 kN (1,646 kips) - Refer to Note 4

For each of the two bearings on Pier 2 or Pier 7 in the parallel bridges:

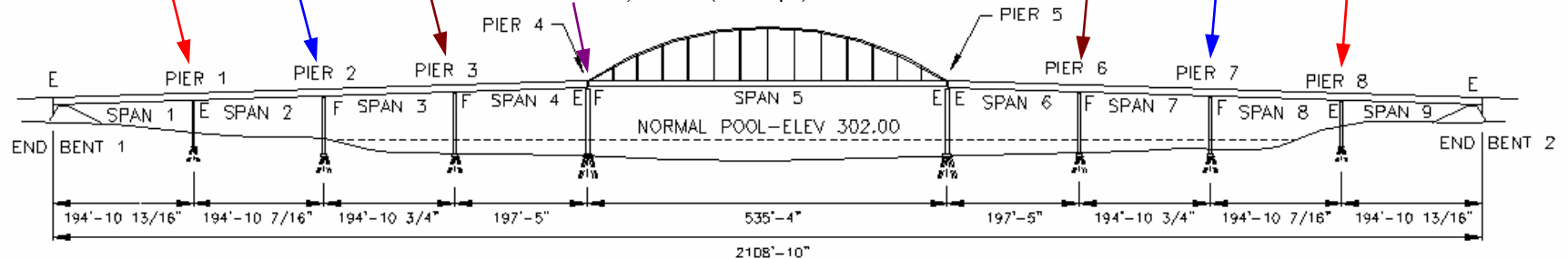
- Existing Shear Capacity: 2,263 kN (509 kips) - Refer to Notes 1 and 3
- Shear Demand: 3,981 kN (895 kips) - Refer to Note 4

For each of the two bearings on Pier 3 or Pier 6 in the parallel bridges:

- Existing Shear Capacity: 2,263 kN (509 kips) - Refer to Notes 1 and 3
- Shear Demand: 2,765 kN (622 kips) - Refer to Note 4

For each of the two bearings on Pier 4 of the main span in the parallel bridges:

- Existing Shear Capacity: 2,053 kN (462 kips) - Refer to Notes 1 and 3
- Shear Demand: 3,221 kN (724 kips) - Refer to Note 4



Note 1: The existing Shear Capacity of the bolts is derived under the assumption that the strength of the bearings remained the same since the bridge was constructed.

Note 2: The two bearings on Pier 1 or Pier 8 in the parallel bridges are expansion bearings in the longitudinal direction and fixed in the transverse direction. The shear capacity and demand are determined for the transverse direction.

Note 3: The bearings on Piers 2, 3, 6 and 7 in the parallel bridges are fixed bearings in the both the longitudinal and transverse directions. The shear capacity and demand are determined from the resultant of the capacities in both directions.

Note 4: The shear capacity can be increased by: 1) providing additional bolts, and/or 2) replacing the existing bolts with higher strength bolts, or 3) replacing the bearings with seismic isolation bearings.

Note 5: The bearings at Pier 5 do not require any retrofit.

Figure 5. Retrofit Recommendations for the Tennessee River Bridge on I-24 in Western Kentucky for the 500-Year Seismic Event
(Note: A 500-year event is an event with 90% probability of not being exceeded in 500 years)

ACKNOWLEDGEMENTS

The financial support for this project was provided by the Kentucky Transportation Cabinet and The Federal Highway Administration. The help of John Flekenstein and Clark Graves in coordinating and conducting the bridge testing is especially noteworthy. The authors would like to acknowledge the cooperation, suggestions, and advise of the members of the study advisory committee. Special thanks to Dr. Shien T. Wang, Professor of Civil Engineering at the University of Kentucky, for his help and suggestions. The authors are also grateful to Peng Yuan, Gehan Elsayed and Kheng Chye Lim, and Robert Goodpaster for their help.

TABLE OF CONTENTS

EXECUTIVE SUMMARY	i
ACKNOWLEDGEMENTS	vii
TABLE OF CONTENTS	viii
LIST OF TABLES	x
LIST OF FIGURES	xi
1. INTRODUCTION	1
1.1 General	1
1.2 Field Testing	1
1.3 Earthquake Background	2
1.4 Scope of the work	3
2. DESCRIPTION OF THE BRIDGES	5
2.1 General	5
2.2 Bridge Superstructure	5
2.3 Bridge Bearings	5
2.4 Bridge Substructure	6
3. FIELD TESTING AND SYSTEM IDENTIFICATION	7
3.1 General	7
3.2 Instrumentation	7
3.3 Testing Procedure and Data Record	8
3.4 Data Processing	8
3.5 System Identification from Ambient Measurements	9
3.6 Peak Picking (PP) System Identification	10
3.7 Stochastic Subspace Identification (SSI)	12
3.8 Summary	14
4. FINITE ELEMENT MODELING AND FREE VIBRATION ANALYSIS	16
4.1 General	16
4.2 Finite Element Model	16
4.3 Free Vibration Analysis	17
4.4 Finite Element Model Calibration and Verification	20
5. SEISMIC EVALUATION OF THE MAIN BRIDGE	22
5.1 General	22
5.2 Seismic Response Analysis	23
5.3 Seismic Evaluation	23

6. SEISMIC EVALUATION OF THE APPROACH SPANS	25
6.1 General	25
6.2 Structural Modeling	25
6.3 Seismic Response Analysis	26
6.4 Capacity/Demand Ratios	26
7. CONCLUSIONS AND RECOMMENDATIONS	28
7.1 General	28
7.2 Main Bridge	28
7.3 Approach Spans	29
REFERENCES	30

LIST OF TABLES

Table No.	Description	Page No.
3.1	Different stations per setup	34
4.1	Comparisons of dead load deformation	35
4.2	Identified and calculated frequencies	35
4.3	Natural frequencies and mass participation of the main span of the bridge for Modal-1	36
4.4	Natural frequencies and mass participation of the main span of the bridge for Modal-2	37
5.1	Maximum seismic stresses of the bridge elements resulting from the combined loading of DL+EQ	38
5.2	Maximum seismic forces and stresses at bottom of Pier 5 and Pier 4 resulting from 250-year event	39
5.3	Maximum seismic forces and stresses at bottom of Pier 5 and Pier 4 resulting from 500-year event	40
5.4	Maximum seismic shear forces at two fixed bearings over Pier 4 and the Seismic Shear Force Capacity/Demand ratios (rC/D) for each anchor bolt	41
5.5	Displacement Capacity/Demand ratios of the bearings over Pier 5	42
6.1	Calculation of weight for SDOF system	43
6.2	Seismic force of the approach bridge	43
6.3	Longitudinal displacement of the approach bridge	43
6.4	Seismic shear force Capacity/Demand ratios (rC/D) for each anchor bolt	44
6.5	Displacement C/D ratios for expansion bearings of the approach bridge	45

LIST OF FIGURES

Fig. No.	Description	Page No.
2.1a	Roadway view of Tennessee River Bridges on I-24	46
2.1b	Side view of Tennessee River Bridges on I-24	46
2.1c	Side view showing the main span of Tennessee River Bridges on I-24	47
2.1d	View showing the roadway of Tennessee River Bridges on I-24	47
2.1e	Side view showing the approach span of Tennessee River Bridges on I-24	48
2.1f	Bottom view showing the bearings of Tennessee River Bridges on I-24	48
2.2	Layout of Tennessee River Bridges on I-24	49
2.3	Main span plan and elevation views of Tennessee River Bridges	50
2.4	View showing the superstructure under roadway of Tennessee River Bridges	51
2.5	Expansion bearing of Tennessee River Bridges	51
3.1	Triaxial accelerometers mounted on the aluminum block	52
3.2	Data acquisition system on site	53
3.3	Measurement station setup	54
3.4a	Raw longitudinal time history data at station L8	55
3.4b	Raw longitudinal power spectral density at station L8	55
3.5a	Raw transverse time history data at station L8	56
3.5b	Raw transverse power spectral density at station L8	56
3.6a	Raw vertical time history data at station L8	57
3.6b	Raw vertical power spectral density at station L8	57
3.7a	Resampled longitudinal time history data at station L8	58
3.7b	Resampled longitudinal power spectral density at station L8	58
3.8a	Resampled transverse time history data at station L8	59
3.8b	Resampled transverse power spectral density at station L8	59
3.9a	Resampled vertical time history data at station L8	60
3.9b	Resampled vertical power spectral density at station L8	60
3.10a	Full average normalized power spectral density	61
3.10b	Longitudinal average normalized power spectral density	61
3.10c	Transverse average normalized power spectral density	62
3.10d	Vertical average normalized power spectral density	62
3.11a	Stabilization diagram of longitudinal data	63
3.11b	Stabilization diagram of transverse data	63
3.11c	Stabilization diagram of vertical data	64
3.12a	The first vertical mode shape	65
3.12b	The second vertical mode shape	66
3.12c	The third vertical mode shape	67
3.13a	The first transverse mode shape	68
3.13b	The second transverse mode shape	69
4.1	3-D view of the FE models	70
4.2	Mode shape of the first natural frequency for Model-1	71
4.3	Mode shape of the second natural frequency for Model-1	72
4.4	Mode shape of the third natural frequency for Model-1	73

4.5	Mode shape of the fourth natural frequency for Model-1	74
4.6	Mode shape of the fifth natural frequency for Model-1	75
4.7	Mode shape of the sixth natural frequency for Model-1	76
4.8	Mode shape of the seventh natural frequency for Model-1	77
4.9	Mode shape of the eighth natural frequency for Model-1	78
4.10	Mode shape of the ninth natural frequency for Model-1	79
4.11	Mode shape of the tenth natural frequency for Model-1	80
4.12	Mode shape of the first natural frequency for Model-2	81
4.13	Mode shape of the second natural frequency for Model-2	82
4.14	Mode shape of the third natural frequency for Model-2	83
4.15	Mode Shape of the Seventh Natural Frequency for Model-2	84
4.16	Mode shape of the eighth natural frequency for Model-2	85
4.17	Mode shape of the thirteenth natural frequency for Model-2	86
4.18	Comparison of 1st vertical mode shapes	87
4.19	Comparison of 2st vertical mode shapes	87
4.20	Comparison of 1st transverse mode shapes	88
5.1	Time history-response spectra identification map of the Commonwealth of Kentucky for 250-year event earthquake	89
5.2	Time history-response spectra identification map of the Commonwealth of Kentucky for 500-year event earthquake	93
5.3	Time-history of relative longitudinal displacement between top and bottom of the bearings on Pier 5 for 250-year event (Case-1, $\xi=0.05$)	97
5.4	Time-history of relative longitudinal displacement between top and bottom of the bearings on Pier 5 for 250-year event (Case-2, $\xi=0.05$)	98
5.5	Time-history of relative longitudinal displacement between top and bottom of the bearings on Pier 5 for 500-year event (Case-1, $\xi=0.05$)	99
5.6	Time-history of relative longitudinal displacement between top and bottom of the bearings on Pier 5 for 500-year event (Case-2, $\xi=0.05$)	100
6.1	Expansion bearing for Pier 1 and Pier 8	101
6.2	Fixed bearing for Pier 2, Pier 3, Pier 6 and Pier 7	101
6.3	Calculation model for the longitudinal analysis	102
6.4	Response spectra for the horizontal component of the 250-year event for counties identified by 0.15g-1 (Damping ratio=0.00 and 0.05)	103
6.5	Response spectra for the transverse component of the 250-year event for counties identified by 0.15g-1 (Damping ratio=0.00 and 0.05)	104
6.6	Response spectra for the horizontal component of the 500-year event for counties identified by 0.30g-1 (Damping ratio=0.00 and 0.05)	105
6.7	Response spectra for the transverse component of the 500-year event for counties identified	

by 0.30g-1 (Damping ratio=0.00 and 0.05)

106

1. INTRODUCTION

1.1 General

Recent earthquakes, 1989 Loma Prieta earthquake [EERI 1990] and 1994 Northridge earthquake [EERI 1995], caused the severe damages and collapse of a considerable amount of bridge structures. The seismic evaluation and rehabilitation of older bridges in regions of high seismicity, which were designed prior to the current advanced seismic design codes and have not yet been subjected to a severe earthquake, is a matter of growing concern. Despite the fact that only California and Alaska have suffered earthquake related bridge damage and failure, these events have raised public concern on a national level.

Seismic design of the bridges throughout most of the United States is governed by AASHTO Standard Specifications for Highway Bridges, Division I-A (1996). Use of the AASHTO Standard Specifications is intended: 1) to allow the structure to yield during a major earthquake, 2) to allow damage (yielding) only in the areas that are accessible (visible) and repairable, and 3) to prevent collapse even during very large earthquakes (NHI 1996).

Unfortunately, numerous bridges in Kentucky are lack of seismic considerations in their initial design. Recently however, several long span bridges in Kentucky designed prior to the application of advanced seismic design codes have been evaluated for seismic loads. They are the Brent-Spence bridge on I-75 (Harik et al 1997a,b), the US51 bridge in Ballard County (Harik et al 1998), the US 41 Southbound and Northbound bridges in Henderson County (Harik et al 1999a,b).

After seismic evaluation, if the bridge is found to be deficient it must be retrofitted. Nevertheless, not all the bridges in the highway transportation system need to be retrofitted simultaneously. Only those bridges with the highest priority should be retrofitted first. The bridge retrofit priority is based on seismic rank, importance, nonseismic deficiencies, and other factors such as network redundancy.

This work concentrates on the seismic evaluation of the I-24 Bridge over the Tennessee River in Western Kentucky. The bridge connects US interstate highway I-24 across the Tennessee River between Marshall and Livingston Counties in Kentucky. Due to its importance, the bridge is to be evaluated for the 250-year event and the maximum predictable 500-year event earthquakes.

1.2 Field Testing

Field testing of bridges has become an integral part of the seismic evaluation process in order to eliminate the uncertainties and assumptions involved in analytical modeling. Full-scale dynamic tests on structures can be performed in a number of ways. Hudson (1977) describes the different types of testing as: 1) free vibration tests, including i) initial displacement as in the pullback, quick-release test, and ii) initial velocity from impacts; 2) forced vibration tests, including i) steady-state resonance testing, ii) variable frequency excitation including sweep, rundown, random and pulse sequences, and iii) transient excitations including earthquakes, wind, traffic, and explosions. Shelley (1995) provides a very informative discussion of the advantages and disadvantages of the various

test methods used on highway bridges.

An alternative technique used to dynamically test bridges is the ambient vibration testing through measurement of the bridge response under normal traffic and wind. The ambient vibration testing does not affect the traffic on the bridge because it uses the traffic and wind as natural excitation. This method is obviously cheaper than the forced vibration testing since no extra equipment is needed to excite the structure. However, relatively long records of response measurements are required and the measurement data are highly stochastic. Consequently, the system identification results are not always satisfied. In the context of ambient vibration testing only response data of ambient vibrations are measurable while actual loading conditions are unknown. A system identification procedure will therefore need to base itself on output-only data. System identification using ambient vibration measurements presents a challenge requiring use of special identification techniques, which can deal with very small magnitudes of ambient vibration contaminated by noise without the knowledge of input forces. The ambient vibration testing has been used by a number of researchers (Abdel-ghaffer and Scanlan 1985a,b; Alampalli and Fu 1994; Buckland et al. 1979; Doll 1994; Farrar et al. 1995; Harik et al. 1993; Paultre et al. 1995; Saiidi et al. 1994; Shahawy 1995; Ventura et al. 1994; Wendichansky et al. 1995).

For the Tennessee River Bridge, on-site dynamic testing was performed by way of ambient vibration testing under natural excitation such as traffic, wind and their association. Since the main bridge is symmetric, ambient vibration measurements are carried out only on one-half of the span. The measured data are the acceleration-time histories. The dynamic characteristics (frequencies and mode shapes) of the bridge were extracted from the peak picking of the average normalized power spectral densities (ANPSDs) in frequency domain and stochastic subspace identification in time domain. These vibration properties are subsequently used as a basis for calibrating the finite element model of the bridge.

1.3 Earthquake Background

Tennessee River Bridge is located on the boundary of Marshall and Livingston counties, Kentucky. This location is near the New Madrid Seismic Zone, site of four of the most severe earthquakes known to have occurred in American history (Johnston 1982, 1985, Johnston and Nava 1985, Street et al. 1996). The seismic zone is named for the town of New Madrid, Missouri, epicenter of the third of the great earthquakes. Each of the massive earthquakes is estimated to have had a Richter magnitude over 8.0 and each of the main shocks was followed by a protracted series of strong aftershocks. The main shocks were felt throughout all of the Central United States, most of the Eastern United States, as well as parts of Canada.

The first two events of the most severe earthquakes occurred on December 16, 1811, at 3 and 6 a.m. local time; the third event followed on January 23, 1812, at 8 a.m. local time. Inhabitants reported that the earth to be rolling in waves a few feet in height during the main shocks. On February 7, 1812, at 2 a.m. local time, the fourth and strongest of the main shocks occurred. Denoted the “hard shock”, this temblor created waterfalls on the Mississippi River and caused it to flow backward, locally, for several hours. This earthquake dramatically altered the region’s landscape. Several islands in the Mississippi disappeared altogether. Present-day Reelfoot Lake, in

Kentucky and Tennessee, was created during the February hard shock. It is estimated the quake to have had a Richter magnitude of up to 8.8 (Johnston 1985b).

Some seismographs were mounted in the New Madrid Seismic Zone since 1974. More than 2000 earthquakes had been instrumentally detected in this region during the first 9 years (Johnston 1985). Although 97% of these are too small to be felt, roughly a Richter magnitude of 2.5, an earthquake occurs in the region, on average, every 48 hours (Johnston 1982). This activity makes the New Madrid Seismic Zone the most hazardous zone in the east of the Rocky Mountains (Johnston 1985).

Considering of the potential damages from a large New Madrid earthquake, or other less severe quakes, the Kentucky Transportation Cabinet funded the research project Evaluation and Analysis of Innovative Concepts for Bridge Seismic Retrofit. Research was conducted by the Kentucky Transportation Center at the University of Kentucky. Fundamental to this research project was the characterization of the seismic potential affecting Kentucky from known seismic zones as well as unknown “local” events. Results from this seismological assessment of Kentucky were published in Source Zones, Recurrence Rates, and Time Histories for Earthquakes Affecting Kentucky (Street et al., 1996). Its objective is to develop earthquake time-histories for use in the design of transportation facilities throughout the commonwealth. Three main tasks were covered in this report: 1) definition and evaluation of earthquakes in seismic zones that have the potential to generate damaging ground motions in Kentucky, 2) specification of the source characteristics, accounting for the spreading and attenuation of the ground motions to top-of-bedrock at sites in Kentucky, and 3) determination of seismic zoning maps for the Commonwealth based on peak-particle accelerations, response spectra, and time-histories.

1.4 Scope of the Work

Due to the importance of the I-24 Bridge over the Tennessee River, this bridge is to be evaluated for the 250-year event and the maximum predictable 500-year event earthquakes. During a 250-year event, the bridge is required to remain in the elastic range without any disruption to traffic. During a 500-year event, partial damage will be permitted on the bridge; however, the bridge has to remain accessible to emergency and official vehicles. In order to achieve this objective, the scope of work was divided into four tasks as: 1) Field testing of the main bridge, 2) finite element modeling, 3) time history seismic response analysis of the main bridge, and 4) seismic response of the approach bridges using response spectrum method.

The ambient vibration properties of the main bridge are determined through field testing under traffic and wind induced excitation. The purpose of measuring the ambient vibration properties is to determine the mode shapes and the associated natural frequencies. Full-scale ambient or forced vibration tests have been used extensively in the past to determine the dynamic characteristics of highway bridges (Abdel-ghaffer and Scanlan, 1985a,b).

Then, the three dimensional finite element model of the main bridge is created for free vibration and seismic response analyses. The model is first calibrated by comparing the free vibration analysis results with ambient vibration properties from field testing. After the calibration,

the model can be used for seismic time-history analysis to determine the maximum displacements at joints, stresses in critical members and shear forces on bearings under 250-year event and 500-year event earthquakes.

Time-histories developed in Street's report were used in the seismic evaluation of the Tennessee River Bridge. Effects of these artificial earthquakes were calculated for bedrock elevation at the county seat of the two counties. These acceleration time-histories were derived through the use of random vibration analysis and taking into consideration the probability of earthquakes from nearby seismic zones, the attenuation of ground motions with distance in the Central United States, and the possibility of a random event occurring outside of the generally recognized seismic zones (Street et. al., 1996).

The approach spans are idealized as a simple structural system depending on the type of the bearings on the top of the piers. This simple structural system is regarded as the single degree of freedom system (SDOF) for the mathematical model of the bridge. Then seismic response of the approach spans is analyzed using response spectrum method to determine the maximum displacements and shear forces.

2. DESCRIPTION OF THE BRIDGES

2.1 General

The parallel Tennessee River Bridges, on I-24 in Western Kentucky, are the steel plate-girder bridges. Each entire bridge, shown in Figures 2.1 and 2.2, consists of nine spans symmetrically located on both sides of the tied-arch span with the total length of 643 m (2108 ft 10 in.). The main span of the bridge is one span of the steel-girder tied-arch with a span length of 163 m (534 ft 4 in.). Both bridges were originally designed by Kroboth Engineers, Inc. and Sverorup & Parcel and Assoc., Inc. in 1969. Figure 1 shows the side view of the arch span of the Tennessee River bridges. The plan and elevation of the steel-girder tied-arch span are as shown in Figure 2.3.

2.2 Bridge Superstructure

The superstructure of the bridge is described in terms of the vertical load system, the lateral load system, the floor system and the bracings. The main arch span is supported by 2 wall type piers, 2 girders and an arch. The tied-arch span consists of 28 horizontal brace members, 11 vertically braced members, 2 portal braced members, and 24 diagonally braced members. The 26 main suspended steel wire ropes are vertically attached on both sides of the arch and are suspending the floor system. Each of these 26 main ropes consists of 4 smaller wire ropes with an area of 13.35 cm² (2.07 square inches) each.

The floor system consists of a 203.2 mm (8 in.) thick concrete slab supported by five longitudinal stringers (typical W30×116 spaced at 2.838 m or 111.75 in.). The stringers are placed on the transverse built-up floor beams and braced by four transverse members (typical MC18×42.7). The typical sections of the floor beams are 1,778mm × 11.1mm (70 in. × 0.438 in.) in webs and 406.4mm (16 in.) cover plates. The floor beams span 14.021 m (46 ft) between the main wire rope suspenders.

2.3 Bridge Bearings

For the main tied-arch span, the superstructure is supported by fixed bearings at Pier 4 and by expansion bearings at Pier 5. The expansion bearings permit longitudinal translation and longitudinal rotation. The fixed bearings only allow longitudinal rotation. The fixed bearing is a standard pinned bearing design that bears on a cast steel bottom shoe. The upper shoe is bolted to the bottom flange of the steel girder and the bottom shoe is rigidly attached to the pier via anchor bolts. The expansion bearing consists of pin and roller combinations to allow rotation and translation. The top shoe of this bearing is connected to the bottom flange of the steel girder, which is then connected to the pin. The slots in the bottom flange of the steel girder allow longitudinal translation. The view of the expansion bearing is shown in Figure 2.5.

2.4 Bridge Substructure

The whole bridge is supported by eight wall type piers in the middle and by two end bents at both ends. The main tied-arch span (Span 5) is supported by two river piers 4 and 5. These two piers are 29.7 m (97.5 ft) tall and 18.3 m (60 ft) wide. They consist of two large taped shafts (approximately 3.66 m or 12 ft in diameter) connected by a 4-foot thick wall supported by the pile foundation.

3. FIELD TESTING AND SYSTEM IDENTIFICATION

3.1 General

On-site dynamic testing of a bridge provides an accurate and reliable description of its real dynamic characteristics. Two main types of dynamic bridge testing are Forced Vibration Test and Ambient Vibration Test.

In the first method, the structure is excited by artificial means such as shakers or drop weights. By suddenly dropping a load on the structure, a condition of free vibration is induced. The disadvantage of this method is that traffic has to be shut down for a rather long time, especially for large structures, e.g. long-span bridges with many test setups. It is clear that this can be a serious problem for intensively used bridges. In contrast, ambient vibration testing does not affect the traffic on the bridge because it uses the traffic and wind as natural excitation. This method is obviously cheaper than forced vibration testing since no extra equipment is needed to excite the structure. However, relatively long records of response measurements are required and the measurement data are highly stochastic. Consequently, the system identification results are not always that good.

For the Tennessee River Bridge on I-24 in Western Kentucky, the field dynamic testing has been performed on the main arch bridge in the way of ambient vibration test. The ambient vibration measurements are carried out on the whole arch span. Field testing was conducted on December 01, 1999. Testing was conducted on the northbound bridge only. All measurements were taken by placing the instruments on the pavement. Instruments were placed on the pavement due to the limited access to the actual floor beams and the time constraints involved. Each instrument was placed with its longitudinal axis aligned parallel to the longitudinal direction of the bridge. The ambient vibration measurements under traffic- and wind-induced excitations were recorded at 15 locations on the both sides (right lane and left lane) of the northbound bridge. The system identification is performed by rather simple peak picking method in the frequency domain and more advanced stochastic subspace identification technique in the time domain.

3.2 Instrumentation

The equipment used to measure the acceleration-time responses of instrumentation consisted of triaxial accelerometers (Figure 3.1) linked to its own data acquisition system (Figure 3.2). The system contained a Keithly MetraByte 1800HC digital recording strong motion accelerograph. Two units contained internal accelerometers, while the two remaining units were connected to Columbia Research Labs, SA-107 force balance accelerometers. The accelerometers are capable of measuring accelerations up to 2g at frequencies up to DC-50Hz. The data was stored in a personal computer at one of the base stations for further processing. The instrumentation placement for testing was to set up four accelerometers on a given segment of the bridge along with fixed reference base station accelerometers at a minimum of two other locations on the bridges. The recording devices were triggered by a computer at one of the base stations to synchronize the start and stop of the accelerometers.

Sets of three accelerometers were mounted to aluminum blocks in orthogonal directions to

form a tri-axial accelerometer station. A block was positioned at each station with the accelerometers oriented in the vertical, transverse and longitudinal directions. To prevent any shifting of the accelerometers during testing, 25-pound bags of lead shot were laid on top of the accelerometer blocks once in position. To ensure the blocks were placed in level, adjustable feet and carpenter's level were attached to each block. Accelerometers were connected to the data acquisition system by shielded cables.

Eight test setups were conceived to cover the planned testing area of the main arch span of the bridge. As a result, a total of 30 locations (15 points per side) were measured. A reference location, hereinafter referred to as the base station, is selected based on the mode shapes from the preliminary finite element model. Each setup group is composed of three base tri-axial accelerometer stations and four moveable tri-axial accelerometer stations. The detailed test setups and a view on the measurement locations are shown as Figure 3.3.

3.3 Testing Procedures and Data Record

Four test setups for each of the right-hand lane and left-hand lane were measured for the whole main arch span. Table 3.1 shows the distribution of the different stations (locations) per setup. The base station accelerometers remained in their original positions for each test setup. Testing began at the east end of the bridge and progressed to the west end of the span. in the right hand lane. The same series of tests were repeated for the left-hand lane. For each setup, the tests yielded a total of twelve sets of data from moveable stations and nine sets of base station data. The test locations, station names, and data file names are included in Table 3.1.

The sampling frequency on site was chosen to as high as 1000 Hz to capture the short-time transient signals of the ambient vibration in full detail. The ambient excitation of the bridge was then simultaneously recorded for 60 seconds at all accelerometers and the base stations, which results in a total of 60,000 data points per data set (channel). Once the data was collected, the moveable stations were moved to the next locations while the base stations remained stationary. This sequence was repeated eight times to get measurements on all stations on the northbound lane. During all tests, normal traffic was allowed to flow over the bridge at normal speeds.

3.4 Data Processing

The raw data from the tests displayed a series of data that showed the acceleration of the bridge in one of the three axial directions with respect to time. Thus, a time-history record of accelerations for the bridge was created. The measured data were first detrended. This treatment enables the removal of the DC-components that can badly influence the identification results. The Figures 3.4a, 3.5a and 3.6a show the raw acceleration time-history measurement data of Station L8 (mid-span) in triaxial directions respectively. Figures 3.4a, 3.5a and 3.6a are acceleration-time history measurements visualized in the time domain, while Figures 3.4b, 3.5b and 3.6b the corresponding Power Spectral Density (PDS) visualized in the frequency domain.

The sampling frequency on site was chosen to be as high as 1000Hz to capture the transient signals of ambient vibration resulting frequency range from 0 to 500Hz. For most bridges, however,

the frequency range of interest lies between 0 and 10 Hz, containing at least the first ten eigen frequencies. So the resampling of the raw measurement data is necessary. It is important to proceed with this now, because afterwards other preprocessing steps will go much faster due to the reduced amount of data. Re-sampling and filtering out the 500Hz to 12.5Hz range is the same as decimating (=low-pass filtering and re-sampling at a lower rate) 40 times. The decimating 40 times of raw data results in $60000/40=1500$ data points and an excellent frequency range from 0 to 12.5 Hz. A nice power spectral density diagram can be obtained. A smaller interval would reduce the number of points too much. Figures 3.7, 3.8 and 3.9 give the resampled longitudinal, transverse and vertical acceleration time data and corresponding Power Spectral Density at the Station L8. This results in a noise-free signal as shown in Fig. 4.7 and Fig.4.8. Now, the data are ready for the system identification to extract the eigen-frequencies and mode shapes.

3.5 System Identification from Ambient Measurements

System identification is originally a topic of control engineering. However, it has recently received world-wide attention for various applications. In the context of civil engineering, structures such as bridges or buildings are considered as the system and identification means the extraction of modal parameters (eigen-frequencies, damping ratios and mode shapes) from dynamic measurements. These modal parameters will serve as basis or input for finite element model updating, damage identification algorithms in detecting and locating the possible damage in structures, and safety evaluation after the structure has suffered heavy damages from events such as an earthquake. These modal parameters will also be essential in the monitoring of structures in service and the controlling of structures.

Over the past decades, the system identification of civil engineering structures has developed very fast. Techniques such as modal testing and modal analysis have become available and widely used (Ewins 1986; Maia et al. 1997). Basically, the system identification procedure is carried out according to both input and output measurement data through the frequency response functions (FRFs) in the frequency domain or impulse response functions (IRFs) in the time domain. For civil engineering structures there is normally no difficulty to obtain the output measurements (dynamic responses). The structural dynamic responses are the direct records of the sensors that are installed at several locations of the structure. However, the input or excitation of the real structure in the operational condition often hardly realizes. It is extremely difficult to measure the input dynamic forces acting on a large-scale structure. Although forced excitations (such as heavy shakers and drop weights) and correlated input-output measurements are sometimes available, testing or structural complexity and achievable data quality restrict these approaches to dedicated applications.

On the other hand, ambient excitations such as traffic, wave, wind, earthquake and their combination are environmental or natural excitations. The ambient vibration has the advantage of being inexpensive since no equipment is needed to excite the structure. Also the service state of the structure does not have to be interrupted by using this technique. The ambient vibration measurements have been successfully applied to many large structures, for instance, the Golden Gate Bridge (Abdel-Ghaffer and Scanlan 1985a,b) and the Brent-Spence Bridge (Harik et al. 1997a,b) to evaluate the seismic safety.

Ambient excitation does not lend itself to FRFs or IRFs calculations because the input force cannot be measured. In this case only response data of ambient vibrations are measurable while actual loading conditions are unknown. A system identification procedure will therefore need to base itself on output-only data. System identification using ambient vibration measurements presents a challenge requiring the use of special identification techniques, which can deal with very small magnitudes of ambient vibration contaminated by noise without the knowledge of input forces. There have been several ambient vibration system identification techniques available that were developed by different investigators or for different uses such as:

- Peak-picking from the power spectral densities (PSDs) (Bendat and Piersol 1993);
- Auto Regressive-Moving Average (ARMA) model based on discrete-time data (Andersen et al. 1996);
- Natural excitation technique (NExT) (James et al. 1995);
- Stochastic subspace methods (Van Overschee and De Moor 1996);

An extensive literature review on system identification techniques using ambient vibration measurements can be found in Van der Auweraer et al. (1999) and De Roeck et al. (2000). In fact, the mathematical background for many of these methods is often very similar, differing only from implementation aspects (data reduction, type of equation solvers, sequence of matrix operations, etc.).

In present study, both rather simple peak picking (PP) method in frequency domain and more advance stochastic subspace identification method in time domain are used to make sure the right frequencies and mode shapes have been selected. The data processing and system identification are carried out by the MACEC, a Matlab-based program of modal analysis for civil engineering construction (De Roeck and Peeter 1999).

3.6 Peak Picking (PP) System Identification

The peak picking system identification technique is a rather simple frequency-domain method. The raw data is to be transformed from the time domain into the frequency domain. The manner by which this was accomplished was the implementation of the Fourier Transform, which is mathematically defined using the transform equation:

$$F(\omega) = \int_{-\infty}^{\infty} f(t)e^{i\omega t} dt \quad (3.1)$$

where $f(t)$ = a function of time, $F(\omega)$ = amplitude as a function of frequency, and ω = circular frequency (radians per second). The inverse of the Fourier Transform is defined by the equation:

$$f(t) = \frac{1}{2\pi} \int_{-\infty}^{\infty} f(\omega)e^{-i\omega t} d\omega \quad (3.2)$$

Using the equations above, any function that is a function of time can be converted into a

function of frequency or vice versa. The only drawback associated with using these equations is that $f(t)$ must be a continuous function, which does not fit the description of the piecewise nature of digitally sampled data such as obtained in the bridge testing. For this reason, a different form of Fourier Transform must be used, known as the Discrete Fourier Transform, which is useful when data point values are known at regularly spaced intervals, which lends itself nicely to the problem at hand. The Discrete Fourier Transform is defined by the equation:

$$F_n = \sum_{k=0}^{N-1} f_k e^{2\pi i k n / N} \quad (\text{for } n = 0 \text{ to } N-1) \quad (3.3)$$

where N = number of sampled points and f_k = a set of N sampled points. The inverse form of the Discrete Fourier Transform is given by the equation:

$$f_k = \frac{1}{N} \sum_{n=0}^{N-1} F_n e^{-2\pi i k n / N} \quad (\text{for } k = 0 \text{ to } N-1) \quad (3.4)$$

This set of equations is extremely useful for engineering applications such as this, but there are still some problems. These equations require N^2 complex mathematical operations which, even with modern computing power, can take quite some time even for small data sets (Blevins, 1995). There is one other method that can reduce the computing time significantly. The Fast Fourier Transform, a numerical operation, can exploit the periodic and symmetric nature of trigonometric functions to greatly improve efficiency in comparison to the Discrete Fourier Transform. The number of computations for the Fast Fourier Transform is reduced to $N \log_2(N)$, which is approximately 100 times faster than the Discrete Fourier Transform for a set of 1000 data points (Bracewell, 2000).

In this way the natural frequencies are simply determined from the observation of the peaks on the graphs of the average normalised power spectral densities (ANPSDs). That's so called peak picking method. The ANPSDs are basically obtained by converting the measured accelerations to the frequency domain by a discrete Fourier transform (DFT). The peak picking method is initially based on the fact that the FRF goes through an extremum around the natural frequencies. The frequency at which this extremum occurs is a good estimate for the eigenfrequency. In the context of ambient vibration measurements only the FRF is replaced by the auto spectra of the ambient outputs (Bendat and Piersol 1993). The coherence function computed for two simultaneously recorded output signals has values close to one at the natural frequency. This fact also helps to decide which frequencies can be considered as natural.

For the peak picking method, 60,000 data points per channel are transformed to the frequency domain and averaged to estimate the power spectral densities. So all measured data (raw data) is used in the PP method. The average normalised power spectral densities (ANPSDs) are obtained through raw full data, raw longitudinal data, raw transverse data and raw vertical data respectively. The corresponding ANPSDs diagrams are shown in Figure 3.10. The peak points are clearly shown and then the eigen frequencies can be picked up. Note: the figures have been zoomed to focus on the frequency range of interest. The possible sequent frequencies picked up from ANPSDs diagrams are summarized in Table 3.3. It is demonstrated that the first vertical natural frequency of the Tennessee River Bridge is about 0.56Hz, while the first transverse natural frequency is around 0.76Hz. The

frequency 1.1Hz is coupled with vertical vibration and longitudinal vibration, while the frequency 1.9Hz is coupled with all three directions. The possible first longitudinal frequency would be 2.58Hz. All these frequencies need to be verified by more advanced stochastic subspace identification method.

The components of the mode shapes are normally determined by the values of the transfer functions at the natural frequencies. It is important to note that in the context of ambient testing, the transfer function does not mean the ratio of response over force, but rather the ratio of response measured by a roving sensor over response measured by a reference sensor. So every transfer function yields a mode shape component relative to the reference sensor. It is shown that the current rather sample peak picking method does not provide good mode shapes.

3.7 Stochastic Subspace Identification (SSI)

It is well known that a structural model can be describable by a set of linear, constant coefficient, second-order differential equations:

$$M\ddot{U}(t) + C\dot{U}(t) + KU(t) = F(t) \quad (3.5)$$

where, M , C and K are the time-invariant mass, damping and stiffness matrices, respectively, of the structure associated with the n generalized coordinates comprising the vector $U(t)$. $F(t)$ is a time-dependent vector of input forces. Equation (3.5) can be rewritten as a first-order system of differential equations in a number of ways. One commonly used reformulation is a state space representation

$$\dot{x}(t) = A_c x(t) + B_c u(t) \quad (3.6)$$

where, the state vector $x(t) = \begin{bmatrix} U(t), \dot{U}(t) \end{bmatrix}^T$, the state matrix A_c and the system control influence coefficient matrix B_c are defined by

$$A_c = \begin{bmatrix} 0 & I \\ -M^{-1}K & -M^{-1}C \end{bmatrix} \quad B_c = \begin{bmatrix} 0 \\ M^{-1}B_2 \end{bmatrix} \quad F(t) = B_2 u(t) \quad (3.7)$$

Furthermore, the output vector of interest, $y(t)$, can be a part of, or a linear combination of system states, such as

$$y(t) = C x(t) + D u(t) \quad (3.8)$$

Here C is a real output influence coefficient matrix and D is the out control influence coefficient matrix. Equations (3.6) and (3.8) constitute a continuous-time state-space model of a dynamic system. Continuous-time means that the expressions can be evaluated at each time instant.

Of course this is not realistic because experimental data are discrete in nature. The sample time and noise are always influencing the measurements. After sampling the continuous-time state-space model looks like

$$x_{k+1} = Ax_k + Bu_k \quad (3.9a)$$

$$y_k = Cx_k + Du_k \quad (3.9b)$$

where $x_k = x(k\Delta t)$ is the discrete time state vector; $A = \exp(A_c\Delta t)$ is the discrete state matrix; $B = [A - I]A_c^{-1}B_c$ is the discrete input matrix. Equation (3.9) forms a discrete-time state-space model of a dynamic system.

In practice there are always system uncertainties including process and measurement noises. The process noise is due to disturbances and modeling inaccuracies, whereas the measurement noise is due to sensor inaccuracy. If the stochastic components (noise) are included Equation (3.9) can be extended to consider process noise w_k and measurement noise v_k described as continuous-time stochastic state-space model

$$x_{k+1} = Ax_k + Bu_k + w_k \quad (3.10a)$$

$$y_k = Cx_k + Du_k + v_k \quad (3.10b)$$

It is difficult to determine accurately the individual process and measurement of noise characteristics. Therefore, some assumptions are required. Here the process noise w_k and measurement noise v_k are assumed to be zero-mean, white and with covariance matrices:

$$E\left[\begin{pmatrix} w_p \\ v_p \end{pmatrix} \begin{pmatrix} w_q^T & v_q^T \end{pmatrix}\right] = \begin{pmatrix} Q & S \\ S^T & R \end{pmatrix} \delta_{pq} \quad (3.11)$$

where E is the expected value operator and δ_{pq} is the Kronrcker delta. The sequences w_k and v_k are assumed statistically independent of each other.

Now we come to the practical problem: in the case of ambient vibration testing the input sequence u_k remains unmeasured and it disappears from (3.10)

$$x_{k+1} = Ax_k + w_k \quad (3.12a)$$

$$y_k = Cx_k + v_k \quad (3.12b)$$

The input is now implicitly modeled by the noise terms w_k and v_k . However the white noise assumptions of these noise terms can not be omitted. The consequence is that if this white noise assumption is violated, for instance if the input contains in addition to white noise some dominant frequency components, these frequency components cannot be separated from the eigenfrequencies of the system and they will appear as poles of the state matrix A .

Equation (3.12) constitutes the basis for the time-domain system identification through ambient vibration measurements. There have been several techniques to realize system identification algorithms based on Equation (3.12). The stochastic subspace identification algorithm is probably the most advanced method known up to date for ambient vibration measurement system identification. The subspace method identifies the state space matrices based on the measurements and by using robust numerical techniques such as QR-factorization, singular value decomposition (SVD) and least squares. Loosely said, the QR results in a significant data reduction, whereas the SVD is used to reject the noise (assumed to be represented by the higher singular values). Once the mathematical description of the structure (the state space model) is found, it is straightforward now to determine the modal parameters (by an eigenvalue decomposition): natural frequencies, damping ratios and mode shapes.

The key element of SSI is the projection of the row space of the future outputs into the row space of the past outputs. The main difference with the preceding algorithms is that the subspace algorithm is data driven instead of covariance driven so that the explicit formation of the covariance matrix is avoided. It is clear that the stochastic subspace identification is a time domain method that directly works with time data, without the need to convert them to correlations or spectra.

The stochastic subspace identification is applied to resampled data. The expected model order is chosen to be 90 and model order range is 2:1:100 that will be used to extract a model of order from 2 to 100. The stabilization diagrams are shown in Figure 3.11 a-c for longitudinal, vertical and transverse data respectively. The identified frequencies are listed in Table 3.4. It is demonstrated that they are identical to those obtained from peak picking method (table 3.4). So the frequencies listed in Table 3.4 will be used to calibrate the finite element model.

Excellent mode shapes have been extracted by SSI. The first three vertical mode shapes and transverse mode shapes are shown in Figure 3.12a-c and Figure 3.13a-b. Common to all system identification methods for ambient vibration measurements, it is not possible to obtain an absolute scaling of the identified mode shapes (e.g. mass normalization) because the input remains unknown.

3.8 Summary

Two complementary system identification methods are implemented to extract the dynamic characteristics of the Tennessee River bridge through ambient vibration testing. It has been shown how the modal parameters can be effectively extracted from ambient vibration data only by using the frequency domain based peak picking (PP) method and the time domain based stochastic subspace identification (SSI) technique.

In the PP method the natural frequencies are selected as the peaks of the ANPSDs. This can become a quite subjective task, especially if the peaks are not very clear. For the SSI method stabilization diagrams aid the engineer to select the true modes. One of the advantages of the SSI method is that the stabilization diagram can be constructed in an effective way. The computationally most heavy steps (QR and SVD) only have to be performed once. Afterwards models of increasing order are obtained by rejecting less singular values.

The advantages of the peak picking method are that it is easy to do and provides fast estimates. However, the damping has not been identified. In the PP method no modal model is fitted to the data, therefore operational deflection shapes are obtained in stead of mode shapes. If the modes are well separated, this is no major drawback, because an operational deflection shape is very similar to a mode shape.

The SSI technique is probably the most advanced method known for ambient vibration measurement and system identification. Based on stabilization diagram, the SSI technique can detect closely spaced frequencies that are possibly missed with the PP method. The computational load of the SSI technique is significantly higher than the PP method, the quality of the identification, however, is also higher. This fact is important since the modal parameters will serve as the key input to model updating, damage identification algorithms, structural monitoring and structural controls.

The weak point of the PP method is also its strong point: since no model has to fit to the data, the identification is very fast and it can be used on site to verify the quality of the measurements. For real applications, it is suggested that the peak picking method could be used to have a quick look at the overall dynamic behavior of the structure. Afterwards the stochastic subspace identification technique can be applied to detail or to ensure the results.

4. FINITE ELEMENT MODELING AND FREE VIBRATION ANALYSIS

4.1 General

Based on the general dynamic characteristics of steel-plate girder bridges and the proximity and activity of the seismic zones, the main bridge model was expected to remain elastic and displacements were anticipated to be small enough to neglect the material and geometric nonlinear

effects. Hence, the consideration of linear elastic small displacement analysis is considered to be appropriate.

Free vibration analysis is a key process in the dynamic analysis of a structure; the computed natural frequency and mode shapes succinctly describe the dynamic characteristics of a complex structure. The analytical model is calibrated and verified by comparing free vibration analysis results with ambient vibration measurements.

4.2 Finite Element Model

Three-dimensional linear elastic finite element models of the main span of the Tennessee River bridge have been constructed in SAP2000, a finite element analysis computer program. Developed for both the analytical modal analysis and earthquake response analysis, the model represents the structure in its current as-built configuration. The arch members, girders, stringers and floor beams are modeled by two-node frame elements that have three translational DOFs and three rotational DOFs at each node. All suspended wire ropes are modeled as the truss elements, a common frame element with released three rotational DOFs at each node. Wall type piers in the model are modeled as frame elements at both sides of the pier and at the top of the pier cap while shell elements serve as the webwalls.

In order to estimate the effect of the modeling of the bridge slab, two FE models (Model-1 and Model-2) are constructed. In FE Model-1, the concrete slab elements are not considered, where the effect of the concrete slab is simulated as equivalently concentrated joint forces for static analysis or concentrated joint masses for modal analysis. In Model-2, the 203.2 mm (8 in.) thickness concrete slab is modeled as shell elements. As a result, the Model-1 has a total of 500 frame elements and 120 shell elements with 507 nodes. The Model-2 results in a total of 507 nodes, 500 frame elements and 176 shell elements. The full 3-D view of above two FE models is shown in Figure 4.1.

Bridge bearings are modeled by a set of rigid elements connecting the superstructure and piers to simulate the actual behavior. The fixed bearing behavior at Pier 4 is modeled by simply releasing the rotational DOFs in the vertical bending plane of the bridge. The expansion bearing behavior at Pier 5 is modeled by assigning roller restraints in the longitudinal direction and hinge restraints in the transverse direction at the top joints of bearings. In other word, the DOFs allowed are the longitudinal translation and the vertical bending rotation. With those rigid elements of released rotational DOFs, relative displacement between the top and bottom shoes of the bearings can be obtained and thus indicate if the translation has exceeded the expansion capacity in seismic evaluation. Longitudinal springs are used to account for the restrained action from the adjacent spans at the both ends of the arch span in the longitudinal direction. Moreover, the foundations of the piers are simplified and modeled as fixed end supports.

Some assumptions and modeling approximations have to be made when creating a practical FE model of a bridge. Data inputs are based on design information and design blue prints. The FE model analyses do not account for construction tolerances or errors that can make as-built dimensions different from design dimensions. Therefore, the bridge FE model has to be checked by

field test results to satisfy the current conditions of a bridge. To achieve a suitable approximation of bridge dead load, the current FE model is first used to compare the dead load deformation of design with that of analytical prediction. The reasonable agreement has been achieved as shown in Table 4.1. It is demonstrated that the concrete slab (Model-2) only provides a slight stiffness in the vertical direction.

4.3 Free Vibration Analysis

An eigenvalue analysis is used to determine the undamped free vibration of the structural system. The eigensolution results in the “natural” mode shapes and frequencies of the structure. Free vibration analysis is required to calibrate the finite element model with the field ambient vibration test measurements. Free vibration analysis involves the solution of the following eigenvalue problem:

$$([K] - \omega^2[M])\{\phi\} = \{0\} \quad (4.1)$$

in which $[K]$ and $[M]$ are the structure (or global) stiffness matrix and the mass matrix, respectively; $\{\phi\}$ is the modal displacement vector. The eigenvalue of a mode (ω^2) is the square of the circular frequency of that mode (ω) and relates to the cyclical frequency (f) by the relation $f = \omega/2\pi$, and relates to the period of vibration (T) by the equation $T = 1/f$.

SAP2000 uses an “accelerated subspace iteration” algorithm to solve the eigenvalue problem. The subspace iteration method was developed by Bathe in 1971 and a detailed discussion of the method and its fundamentals can be found in Bathe (1982). Various techniques have been used to “accelerate” the basic subspace iteration method and the particular algorithm used in the SAP2000 program can be found in Wilson and Tetsuji (1983).

4.3.1 Model-1

The natural frequencies and mass participation for the lowest 15 modes are presented in Table 4.3. The natural frequency of the bridge ranges from 0.561 Hz to 1.988 Hz for the first 15 modes, and the period ranges from 1.781 sec to 0.503 sec. The natural frequencies listed in Table 4.3 and their mode shapes are used only to calibrate the finite element model. They are not used for the seismic response analysis.

Figures 4.2(a), (b) and (c) show the first mode shape in isometric, elevation and plan views, respectively. The natural frequency of this mode is 0.561 Hz. This mode has anti-symmetric shape in the main span. Based on mass participation ratio and from Figures 4.2(b) and (c), it is seen that this mode is the first vertical mode. Though the percentage of mass participation in the vertical direction is only 0.0030.

Figures 4.3(a), (b) and (c) show the second mode shape with a frequency of 0.717 Hz in isometric, elevation and plan views, respectively. Since the modal deformation is in the same direction, the mass participation for this mode is 21.2849%. Based on mass participation, the second

mode is noted as the first transverse mode. Therefore this is one of the very important modes that significantly contribute for the transverse seismic motion.

The third mode with a frequency of 0.973 Hz is shown in Figures 4.4(a), (b) and (c). The mass participation for this mode is only 0.0177% in transverse direction. It is observed that there exists the transverse modal deformation in an opposite direction between the deck and the rib of main span.

Figures 4.5(a), (b) and (c) show the fourth mode shape with a frequency of 1.149 Hz in isometric, elevation and plan views, respectively. The mode has a symmetric shape in vertical direction, the mass participation for this mode is 2.7265%. Based on mass participation, this mode is observed as the second vertical mode.

Figures 4.6(a), (b) and (c) show the fifth mode shape with a frequency of 1.320 Hz. The mass participation is only 0.0141%. Based on Figures 4.6(b) and (c), this mode is mainly a torsion mode with a little transverse of the rib.

The sixth mode shapes in isometric, elevation and plan views are shown in Figures 4.7(a), (b) and (c), respectively. The natural frequency of this mode is 1.399 Hz. Based on mass participation and from Figures 4.7(b) and (c), it is found that only the pier IV vibrates in longitudinal direction. The mass participation in the direction is 24.3415%.

Figures 4.8(a), (b) and (c) show the seventh mode shape with a frequency of 1.516 Hz. From mass participation and mode shape, it is seen that this mode is the first longitudinal mode. Mass participation for this mode is 25.4985% in the longitudinal direction.

The eighth mode shapes in isometric, elevation and plan views are shown in Figures 4.9(a), (b) and (c), respectively. The natural frequency of this mode is 1.557 Hz. Based on mass participation and from Figures 4.9(b) and (c), it is seen that this mode is the second transverse mode. Though the mass participation in the transverse direction is only 0.0001%.

Figures 4.10(a), (b) and (c) show the eighth mode shape with a frequency of 1.749 Hz, in the isometric, elevation and plan views respectively. The mass participation for this mode is 11.2142%. Based on mass participation, this mode is identified as the third vertical mode.

The tenth mode shape in isometric, elevation and plan views is shown in Figures 4.11(a), (b) and (c), respectively. The natural frequency of this mode is 1.838 Hz and the mass participation is 1.2857% in the transverse direction. Based on mass participation, this mode is treated as the third transverse mode.

4.3.2 Model-2

The natural frequencies and mass participation for the lowest 15 modes are presented in Table 4.4. The natural frequency of the bridge ranges from 0.562 Hz to 3.294 Hz for the first 15 modes, and the period ranges from 1.778 sec to 0.304 sec. The natural frequencies listed in Table 4.4

and their mode shapes are used only to calibrate the finite element model. They are not used for the seismic response analysis

Figures 4.12(a), (b) and (c) show the first mode shape in isometric, elevation and plan views, respectively. The natural frequency of this mode is 0.562 Hz. This mode has anti-symmetric shape in the main span. Based on mass participation ratio and from Figures 4.12(b) and (c), it is seen that this mode is the first vertical mode. Though the percentage of mass participation in the vertical direction is only 0.0032.

Figures 4.13(a), (b) and (c) show the second mode shape with a frequency of 0.861 Hz in isometric, elevation and plan views, respectively. Since the modal deformation is in the same direction, the mass participation for this mode is 14.8304%. Based on mass participation, the second mode is noted as the first transverse mode. Therefore this is one of the very important modes that significantly contribute for the transverse seismic motion.

Figures 4.14(a), (b) and (c) show the third mode shape with a frequency of 1.162 Hz in isometric, elevation and plan views, respectively. The mode has a symmetric shape in the vertical direction and the mass participation for this mode is 2.1737%. Based on mass participation, this mode is observed as the second vertical mode.

Figures 4.15(a), (b) and (c) show the seventh mode shape with a frequency of 1.573 Hz. From mass participation and mode shape, it is seen that this mode is the first longitudinal mode. Mass participation for this mode is 28.2276% in the longitudinal direction.

Figures 4.16(a), (b) and (c) show the eighth mode shape with a frequency of 1.762 Hz, in the isometric, elevation and plan views respectively. The mass participation for this mode is 12.2455% in the vertical direction. Based on mass participation, this mode is identified as the third vertical mode.

The thirteenth mode shapes in isometric, elevation and plan views are shown in Figures 4.16(a), (b) and (c), respectively. The natural frequency of this mode is 2.897 Hz. Based on mass participation and from Figures 4.17(b) and (c), it is seen that this mode is the second transverse mode. The mass participations in the vertical and longitudinal directions are the same as 0.0000%.

The natural frequency of fourteenth mode is 3.242 Hz. Based on mass participation, it is derived that this mode is the third transverse mode. The mass participations in the vertical, transverse and longitudinal directions are 0.0000%, 0.9373% and 0.0000%, respectively.

4.4 Finite Element Model Calibration and Verification

The FE modal analysis is checked afterwards by experimental modal analysis in the sense of natural frequencies and mode shapes. Usually, a perfectly calibrated model would match all experimentally determined mode shapes and frequencies exactly. To hope for such a perfect calibration is not realistic. Therefore, only the most structurally significant modes and frequencies are used in the model calibration process. In addition, the higher modes identified through ambient

vibration measurements are not reliable. The first three vertical modes, the first three transverse modes and the first longitudinal mode from field-testing are selected as calibration targets in current effort. Generally, it is hard for the mode shape to match perfectly for those chosen modes since the results of finite element method for the mode shapes are generated at the end nodes in the girders, while all measurements are taken by placing the instruments on the pavement just above the floor stringers due to the limited access to the actual floor beams.

Limited parameters such as mass, stiffness and the bearing spring stiffness in the longitudinal direction are used to correlate with the field test results. For the springs at the end of the arch span in longitudinal direction, a value of spring stiffness 1.751×10^5 kN/m (1000 kip/in) is found to match the first tested longitudinal frequency. Table 4.2 summarizes the identified and FE calculated frequencies. It is found that the analytical modal analysis results of Model-1 without the concrete slab shell elements agree well with the field test results. The errors are within 5%. The Model-2 gives comparable vertical and longitudinal frequencies with the Model-1. Considering the concrete slab of the deck system in the FE Model-2 will mainly influence the transverse behavior of the bridge. For example, the first transverse frequency of Model-2 is greater than that of Model-1 by 20%. It has been shown that the Model-2 over-estimates the bridge stiffness in the transverse direction.

Figures 4.18, 4.19 and 4.20 show the comparison of the first two vertical mode shapes and the first transverse mode shape. Usually, the traffic-induced excitation can produce clear acceleration records in the vertical direction, and the traffic combined with wind excitations can produce in the transverse direction. Since there is no excitation along the longitudinal direction, clear acceleration records in the longitudinal direction are not obtained. Therefore, the matching of the mode shape is difficult for this mode.

To make a start toward the seismic evaluation/retrofit, the dynamic properties of the Tennessee River bridge on Interstate Highway I-24 in Western Kentucky have been studied by analytical modal analysis with 3-D finite element method and experimental modal analysis with ambient vibration testing. Two complementary modal identification methods are implemented to extract the modal characteristics through ambient vibration testing. It has been shown how the modal parameters can be effectively extracted from output-data only induced by ambient vibrations by using the frequency domain based peak picking (PP) method and the time domain based stochastic subspace identification (SSI) technique. A good agreement of identified frequencies has been found between peak picking method in frequency domain and stochastic subspace identification method in time domain. However, stochastic subspace identification method provides a much better mode shape than the peak picking method. One of the advantages of the SSI method is that the stabilization diagram can be constructed in an effective way, which aids the engineer to select the true modes. The PP identification is very fast and efficient since no model has to be fitted to the data. The PP method can be used on site to verify the quality of the measurements for real applications.

The analytical modal analyses with 3-D finite element models of the bridge are comparable with the site experimental modal analysis. The FE Model-1 with the concrete slab simplified by concentrated joint forces or joint masses agrees well with the field test results. The concrete slab modeled by the shell elements only influences the transverse behavior of the bridge. It is suggested that the Model-1 could be the baseline FE model in the seismic evaluation/retrofit of the Tennessee

River main bridge.

5. SEISMIC EVALUATION OF THE MAIN BRIDGE

5.1 General

There are several seismic analysis methods in seismic evaluation of existing bridges including elastic analysis, inelastic pushover analysis, capacity spectrum analysis and nonlinear dynamic analysis (Priestly et al. 1996). Each approach incorporates different assumptions and varies in complexity of application. The most appropriate and cost-effective method for assessing the seismic vulnerability of a bridge structure should be reasonably selected.

In this work, the seismic response analyses of the main bridge and approach spans are performed by time-history method and response spectrum method, respectively. Time-history analysis is used because the bridge is assumed to behave linearly elastic with small displacements under the predicted earthquake loading. Time-history method is used instead of response spectrum method for the main bridge due to the importance of the bridge and also due to the lack of seismic considerations in its initial design. Using this analysis method can afford the engineer a complete description of the behavior of a structure at any time throughout an earthquake.

Time-history method for the seismic analysis involves the solution of the following equation of motion for forced vibration:

$$[M] \{ \ddot{u} \} + [C] \{ \dot{\beta} \} + [K] \{ u \} = -[M] \{ \ddot{u}_g \} \quad (5.1)$$

where $[M]$, $[C]$ and $[K]$ are global mass matrix, damping matrix and stiffness matrix, respectively. $\{ \ddot{u} \}$, $\{ \dot{\beta} \}$ and $\{ u \}$ are structural system nodal acceleration, velocity and displacement vectors, respectively. $\{ \ddot{u}_g \}$ is the earthquake motion for which response of the bridge has to be calculated. The SAP2000 computer program performs exact integration of the modal-response equations for a linear variation of the time-function between the input data time points. The damping coefficient exhibited by a structure during an earthquake event is difficult to predict. In this study, damping coefficients for all the modes are assumed to be 5%.

Traditionally, mode-superposition analysis was performed using a structure's eigenvectors as the basis for the analysis. Research (Wilson, Yuan, and Dickens, 1982) indicates that this is not the best starting point for a mode-superposition time-history analysis. Instead, a special set of load-dependent, orthogonal Ritz vectors yields more accurate results than the same number of natural mode shapes. Ritz vector analysis significantly reduces computing time. The reason that Ritz vector analysis yields better results than an equal number of eigenvectors is because the Ritz vectors take into account the spatial distribution of dynamic loading. In fact, the spatial distribution of loading serves as a starting load vector to begin the process of finding appropriate Ritz vectors. Subsequent Ritz vectors are formed based on the preceding Ritz vector and the neglected inertial effects. In contrast, the eigenvectors are computed from the stiffness and mass matrices only, and therefore, cannot account for the spatial distribution of loading. Eigenvectors that are orthogonal to loading do not participate in the structural response even if they are at or near the forcing frequency.

Usually, time-histories representing the 250-year event and the 500-year event were

generated for the vertical and two orthogonal horizontal directions (Street et al. 1996). The definition of the 250-year event is: the peak horizontal particle acceleration, at the top of bedrock, which has a 90% probability of not being exceeded in 250 years (i.e. 10% probability of exceedance). Likewise, the 500-year event has a 90% probability of not being exceeded in 500 years. A recurrence rate (return period) can be calculated for the earthquakes, which would produce the 250- and 500-year events.

For the seismic zones affecting Kentucky, the 250-year and 500-year events defined in Street et al. (1996) correspond to the earthquake and near the maximum credible earthquake, respectively. For the bridge location in this study, borders of Marshall and Livingston Counties, Kentucky, a time-history with peak horizontal acceleration of 15% gravity (see Figure 5.1) represents the AASHTO design earthquake. The time-history for the “near maximum credible earthquake” (500-year event) has a peak horizontal acceleration of 30% gravity (see Figure 5.2) in Marshall and Livingston Counties.

5.2 Seismic Response Analysis

The seismic response of the Tennessee River Bridge is calculated for the 250-year and 500-year earthquakes. The earthquake duration is 20.5 seconds consisting of 4100 data points at 0.005-second intervals. The input motions along longitudinal, transverse and vertical directions can be found in Figures 5.1 and 5.2. For 250-year event, the peak ground accelerations along longitudinal, transverse and vertical directions are 165, 147 and 164 cm/sec^2 , respectively. For 500-year event, the peak ground accelerations along longitudinal, transverse and vertical directions are 289.19, 178.36 and 290.59 cm/sec^2 , respectively.

The bridge structure is subjected to all the three orthogonal components of each event (longitudinal, transverse and vertical) simultaneously. To provide conservative stress and displacement results, the bridge is subjected to two combinations of the longitudinal and transverse components with respect to the longitudinal and transverse directions of the bridge for each event. For the first combination, the longitudinal component of the event is placed along the longitudinal direction of the bridge (x -direction) and the transverse component of the event is placed along the transverse direction of the bridge (y -direction). For the second combination, the longitudinal component of the event is placed along the transverse direction of the bridge while the transverse component of the event is placed along the longitudinal direction of the bridge. In above two combinations, vertical component is applied along the vertical direction of the bridge.

5.3 Seismic Evaluation

5.3.1 The Superstructure

Tables 5.1 presents the maximum seismic stresses of the main bridge selected elements resulting from the combined loading of DL+EQ. In all cases, the combined stresses are well below the yield stress. Consequently, the bridge elements keep in elastic state under maximum credible seismic event, and therefore the linear elastic assumption is verified.

The maximum axial stress resulting from the dead load (DL) is found to be 16.05 ksi (111 MPa) in frame element 43. The maximum stress resulting from dead and earthquake load (EQ) is 28.73 ksi (198 MPa) in element 43, which is less than the steel yield stress of 50 ksi (345 MPa)

5.3.2 The Substructure

Tables 5.2 and 5.3 show the maximum seismic forces and stress at bottom of Pier 4 and Pier 5 resulting only from earthquake loads. It can be found that the results are very small in both piers. At the bottom of Pier 5, the maximum bending stress is 1.62 ksi (11.2 MPa). In all cases, the maximum shear stress is not greater than 0.2 ksi (1.4 MPa).

5.3.3 The Bearings

Since the superstructure of the bridge is connected to the substructure through bearings, it is necessary to check these bearings against loss-of-span and anchor bolt shear failure. The maximum seismic shear forces at two fixed bearings over Pier 4 and the seismic shear force Capacity/Demand (C/D) Ratios, $r_{C/D} = V_c/V_d$, for each anchor bolt are presented in Table 5.4. The anchor bolt capacity V_c is calculated by assuming the nominal shear strength of each bolt as 48 ksi (331 MPa). The resultant of base shear is calculated as the square root of the sum of squares of the longitudinal and transverse base shears. Then the seismic demand (V_d) is calculated by multiplying by 1.25 as per FHWA Retrofitting Manual. As shown in Table 5.4, the seismic shear force C/D ratios ($r_{C/D}$) are greater than 1.0 in the case of 250-year earthquake. But these C/D ratios are less than 1.0 under 500-year earthquake event. Therefore, the supports with fixed bearings on the Pier 4 need to be retrofitted under 500-year earthquake event. The shear capacity of each fixed bearing can be increased by providing additional two A325 anchor bolts, or by replacing the bearing with seismic isolation system.

In Table 5.4, the ratio of the maximum seismic pullout force to dead load force, $\rho_{S/G}$, over the fixed bearings is less than 0.28, which can be expressed as a factor of safety of 3.5 against overturning. Consequently, the pullout of anchor bolts is not expected.

The bearings over Pier 5 are of expansion type having a slotted bottom chord member attached to the bottom shoe of the bearing. Therefore expansion is allowed to a limited extent. In this study, the displacement Capacity/Demand (C/D) ratios $C/D = \frac{\Delta_s(c) - \Delta_i(d)}{\Delta_{eq}(d)}$, Section A.4.2, FHWA

Retrofitting Manual, are calculated for these bearings and presented in Table 5.5. $\Delta_s(c)$ is the allowable displacement. $\Delta_i(d)$ is the maximum possible movement resulting from a 90°F (32°C) maximum differential temperature. $\Delta_{eq}(d)$ is the maximum calculated relative movement due to earthquake loading. The C/D ratios are greater than 1.0 and hence loss-of-span cannot occur due to displacement consideration.

6. SEISMIC EVALUATION OF THE APPROACH SPANS

6.1 General

The plan and elevation of the approaches of Tennessee River Bridge on I-24, located symmetrically in the both sides of the main span, are shown in Figure 2.2. The approach at each side consists of 4 spans with a total length of 238.38m (782.08 ft.) which provides a 11.96m (39.25 ft.) wide roadway. The spans in both the approaches are supported on piers through fixed bearings and expansion bearings as indicated in Figures 6.1 and 6.2. All the piers and End Bents are founded on piles which extend up to 25.60m (84 ft.) to 8.53m (28 ft.) depending on the sites.

The approaches have two girders and the floor system. The floor system consists of a 203.2mm (8 in.) thickness concrete slab supported by three longitudinal stringers (typical W24×68 spaced at 2.838m or 111.75 in.) and the bracing system. The stringers are placed on the transverse floor beams. The typical sections of the floor beams are 1.302m (51.25 in.) in depth, 7.94mm (0.3125 in.) in web thickness, 304.8mm (12 in.) in flange width and 41.28mm (1.625 in.) in flange thickness. The typical section of the diagonal bracings is W7×21.5. The piers consist of two tapered shafts (approximately 2.74m or 9 ft. in diameter) connected by a 3-foot thick wall supported by the pile foundation.

6.2 Structural Modeling

The approach spans are idealized as a simple structural system depending on the type of the bearings on the top of the piers. This simple structural system is regarded as the single degree of freedom system (SDOF) for the mathematical model of the bridge. The mass of the SDOF system is assumed to be contributed by the mass of the superstructure and one-third mass of the piers. The calculated results are shown in Table 6.1. Seismic Evaluation and Retrofit of Bridges (Harik I.E., et al., 1997) demonstrates the calculation of the transverse stiffness and longitudinal stiffness of the mathematical model.

As noted in the research report (Harik I.E., et al., 1999), representative models with maximum and minimum stiffness are adopted in the force and displacement calculations, respectively, due to the unavailability of detailed site soil investigation. The total transverse stiffness and total longitudinal stiffness, assuming that the piers are fixed at the bottom of pile caps (used for force calculation), are 4,248 kN/mm and 72.78 kN/mm, respectively. The total longitudinal stiffness is 45.7 kN/mm when the piers are assumed to extend up to an imaginary depth equal to half of length of piles and fixed at that level (used for displacement calculation). The extended part of the pier (Figure 6.3) has the same structural properties with the original one. This simplified method is adopted for the conservative estimation of seismic forces and displacements in this study.

6.3 Seismic Response Analysis

Since the bridge is located on the boundary of Marshall and Livingston counties in Kentucky

and near the New Madrid Seismic Zone, it is analyzed under seismic motion corresponding to 0.15g earthquake of the 250-year event and 0.3g earthquake of the 500-year event. In this work, seismic analysis of the simplified SDOF models for the approach spans is carried out using the response spectrum method. Figures 6.4 to 6.7 illustrate the recommended response spectra developed by Street et al (1996). Damping ratio of the response spectra is 5%. The results of the seismic analysis are utilized to determine the possibility of any loss-of-span due to the excessive longitudinal displacements at expansion bearings or bearing failure when the shear strength of the anchor bolts is insufficient in fixed bearings.

The influence of the vertical seismic component on longitudinal displacements is expected to be very small and hence it is not considered in this study. In the analysis of the force Capacity/Demand, the combined seismic force of the bolts under longitudinal earthquake loading and transverse earthquake loading is considered. In the analysis of the displacement Capacity/Demand, only longitudinal earthquake loading is considered. The research results indicated that longitudinal seismic waves had caused more damages than transverse for multi-span simple bridges (Zimmerman and Brittain, 1979).

In response spectrum analysis, site soil coefficient S is assumed to be 1.5. The C_s is limited to 2.0A for soil profile type III as per AASHTO (Division IA, section 3). The calculated results are shown in Tables 6.2 and 6.3, respectively.

6.4 Capacity/Demand Ratios

For the approach spans, the bearing force Capacity V_c /Demand V_d ratios $r_{C/D}$ are calculated as per A.4.3 of FHWA Seismic Retrofitting Manual for Highway Bridges (Buckle et al., 1995). The anchor bolt capacity V_c is calculated by assuming the nominal shear strength of one bolt as 188.6 kN (42.4 kips). The resultant of the shear force is calculated as the square of the sum of squares of the longitudinal and transverse shear forces. It should be noted that a coefficient of 0.3 is considered during the combination of orthogonal seismic forces. Then the seismic demand (V_d) is calculated by multiplying by 1.25 as per FHWA Retrofitting Manual. The calculated results are shown in Table 6.4. The seismic shear force Capacity/Demand ratios ($r_{C/D}$) of the anchor bolts for some of the bearings are less than 1.0 under the 250-year earthquake. But those C/D ratios of the anchor bolts for all supports are less than 1.0 under 500-year earthquake event. Therefore, retrofit of the bearings is recommended. For the bearings with $C/D < 0.5$, seismic retrofit is strongly recommended.

For the 250-year earthquake, all A307 anchor bolts at both bearings on Pier 1 could be replaced by the corresponding A490 anchor bolts with the same diameters. And four A307 anchor bolts at each bearing on Pier 2 could be replaced by 4 corresponding A325 anchor bolts with the same diameter.

For the maximum credible 500-year earthquake, eight A307 anchor bolts at each bearing on Pier 1 could be replaced by 12 A490 anchor bolts with the diameters of 1-3/4". Half of the A307 anchor bolts at each bearing on Pier 2 could be replaced by 6 corresponding A490 anchor bolts with the same diameters. And four A307 anchor bolts at each bearing on Pier 3 could be replaced by 4 corresponding A325 anchor bolts with the same diameters.

For the approach spans, the expansion bearing displacement Capacity/Demand ratios $C/D = \frac{\Delta_s(c) - \Delta_i(d)}{\Delta_{eq}(d)}$ are calculated as per A.4.2 of FHWA Seismic Retrofitting Manual for Highway

Bridges (Buckle et al., 1995). The calculated results are shown in Table 6.5. $\Delta_s(c)$ is the available displacement. $\Delta_i(d)$ is the maximum possible displacement due to a 32°C (90°F) maximum differential temperature effect and $\Delta_{eq}(d)$ is the maximum displacement due to earthquake. The C/D ratios are greater than 1.0 and hence loss-of-span cannot occur due to the displacement consideration.

7. CONCLUSIONS AND RECOMMENDATIONS

7.1 General

The parallel Tennessee River Bridges, located on the boundary of Marshall and Livingston Counties in Kentucky, are near the New Madrid Seismic Zone. Thus, the bridges may be subjected to future severe earthquakes. It is important to evaluate the bridges for projected seismic events [i.e. 0.15g (250-year event) and 0.3g (500-year event) in this study].

7.2 Main Bridge

The seismic evaluation of the main bridge consisted of field ambient vibration testing, three-dimensional finite element modeling and seismic response analysis using the time-history method. Field testing was mainly carried out to identify the natural frequencies and their mode shapes. These frequencies and mode shapes have been compared with the results from the calibrated finite element models. Comparisons have been performed for three vertical modes, three transverse modes and one longitudinal mode.

The three-dimensional finite element models were developed with frame elements, shell elements, truss elements and spring elements. These models have been calibrated with the field test results for natural frequencies and mode shapes. Frequencies from the field test for the first modes in the vertical, transverse and longitudinal directions are 0.565 Hz, 0.744 Hz and 1.563 Hz, respectively. Frequencies from the finite element Model-1 for the first modes in the vertical, transverse and longitudinal directions are 0.561 Hz, 0.717 Hz and 1.516 Hz, respectively. Reasonable agreement between the field testing and finite element model analysis has been obtained.

Seismic response analyses have been carried out using the time-history method. Stresses for selected structural members have been calculated for different seismic excitation combinations. For the superstructure, the maximum stress resulting from dead load and earthquake load is 28.73 ksi (198 MPa), which is less than the steel yield stress of 50 ksi (345 MPa). In all cases, the maximum shear stress of the substructure at the bottom of Pier 4 and Pier 5 resulting only from earthquake loads is not greater than 0.2 ksi (1.4 MPa). Consequently, retrofit of the structural elements is not required.

The maximum seismic shear forces at two fixed bearings on Pier 4 and the seismic shear force Capacity/Demand ratios (rC/D) for each anchor bolt were determined. The seismic shear force C/D ratios are greater than 1.0 in the case of the 250-year earthquake. For the 500-year event, the C/D ratios are less than 1.0. Therefore, the supports with fixed bearings on the pier of the main bridge need to be retrofitted under the maximum credible 500-year earthquake.

The bearings on Pier 5 are of expansion bearings and the displacement Capacity/Demand ratios (C/D) are greater than 1.0 and hence loss-of-span is not probable.

7.3 Approach Spans

Seismic analysis of the simplified single-degree-of-freedom models for the approach spans has been carried out using the response spectrum method using a 5% damping ratio. The analysis is carried out to determine the possibility of any loss-of-span to longitudinal displacements at expansion bearings or bearing failure when the shear strength of the anchor bolts is insufficient in fixed bearings. The seismic shear force Capacity/Demand ratios ($r_{C/D}$) of the anchor bolts for some of the bearings are less than 1.0 under the 250-year earthquake. The C/D ratios of the anchor bolts for all fixed bearings are less than 1.0 under the 500-year earthquake event. Therefore, seismic retrofit is recommended. For the bearings with $C/D < 0.5$, retrofit is strongly recommended. The displacement C/D ratios are greater than 1.0 and hence loss-of-span is not probable.

REFERENCES

AASHTO (1996), Standard Specifications for Highway Bridges, 16th Edition, American Association of State Highway and Transportation Officials, Washington D.C.

AASHTO (1998), LRFD Bridge design Specifications, Second Edition, American Association of State Highway and Transportation Officials, Washington D.C.

Abdel-ghaffer, A.M. and R. H. Scanlan (1985a), Ambient Vibration Studies of Golden Gate Bridge: I. Suspended Structure, ASCE J. of Engrg. Mech., 111(4), 463-482.

Abdel-ghaffer, A.M. and R. H. Scanlan (1985b), Ambient Vibration Studies of Golden Gate Bridge: II. ASCE J. of Engrg. Mech., 111(4).

Alampalli, S., and Fu, G., (1994), "Instrumentation for Remote and Continuous Monitoring of Structural Condition," Paper No.940261 Presented at the Transportation Research Board's 73rd Annual Meeting, Washington D.C..

Andersen, P., Brincker, R. and Kirkegaard, P.H. (1996). "Theory of covariance equivalent ARMAV models of civil engineering structures." Proceedings of IMAC14, the 14th International Modal Analysis Conference, Dearborn, MI, 518-524.

Bathe, K.J., (1982), Finite Element Procedures in Engineering Analysis, Prentice-Hall, Inc., Englewood Cliffs, New Jersey, Chapter 12.

Bendat, J.S. and Piersol, A.G. (1993). Engineering applications of correlation and spectral analysis. 2nd edition, John Wiley & Sons, New York.

Blevins, Robert D., (1995), Formulas for Natural Frequency and Mode Shape, Krieger Publishing Company, Malabar, Florida.

Bracewell, Ronald N., (2000), The Fourier Transform and Its Applications, Third Edition McGraw Hill.

Buckland, P.G., et al., (1979), "Suspension Bridge Vibrations: Computed and Measured," Journal of the Structural Division, Vol. 105, No. ST5, 859-874.

Buckle, I.G. and I. M. Friedland (editors, 1995), Seismic Retrofitting Manual for Highway Bridges, Report No. FHWA-RD-94-052, Federal Highway Administration.

Chapra, S.C., and Canale, R.P., (1988), Numerical Methods for Engineers, 2nd Edition, McGraw-Hill, Inc., New York, New York, Chapter 13.

De Roeck, G. and Peeter, B. (1999). MACEC2.0 – Modal Analysis on Civil Engineering Constructions, Department of Civil Engineering, Catholic University of Leuven, Belgium. <http://www.bwk.kuleuven.ac.be/bwk/mechanics/macec>

De Roeck, G., Peeters, B. and Ren, W.X. (2000). "Benchmark Study on System Identification

through Ambient Vibration Measurements.” Proceedings of IMAC-XVIII, the 18th International Modal Analysis Conference, San Antonio, Texas, 1106-1112.

Doll, H., (1994), “Eigenfrequencies and Normal Modes of the Norderelb Bridge Near Hamburg: Numerical and Measuring Investigations,” Proceedings of the 12th International Modal Analysis Conference, Honolulu, Hawaii, 449-455.

EERI (1990), Loma Prieta Earthquake Resistance Report, Earthquake Spectra, Special supplement to Vol.6, 448.

EERI (1995), Northridge Earthquake Resistance Report, Earthquake Spectra, Special supplement to Vol.11, 116.

Ewins, D.J. (1986). Modal testing: theory and practice. Research Studies Press Ltd., England.

Farrar, C., White, K., and Mayes, R., (1995), “Vibration Testing of the I-40 Bridge Before and After the Introduction of Damage,” Presented at the North-American Workshop on Instrumentation and Vibration Analysis of Highway Bridges, Cincinnati, Ohio.

Harik, I.E., D. Dietz, C. Hill and M.W. Guo (1997), Seismic Evaluation and Retrofit of Bridges, Research Report KTC-96-5, Kentucky Transportation Center, University of Kentucky.

Harik, I.E., D. L. Allen, R. L. Street, M.W. Guo, R.C. Graves, J. Harrison and M. J. Gawry (1997a), Free and Ambient Vibration of Brent-Spence Bridge, ASCE J. of Struct. Engrg., 123(9), 1262-1268.

Harik, I.E., D. L. Allen, R. L. Street, M. W. Guo, R.C. Graves, J. Harrison, and M. J. Gawry(1997b), Seismic Evaluation of Brent-Spence Bridge, ASCE J. of Struct. Engrg., 123(9), 1269-1275.

Harik, I.E., Madasamy, C., Chen, D.L., Zhou, L.N., Sutterer, K. Street, R.L., and Allen, D.L. (1998), Seismic Evaluation of the Ohio River Bridge on US51 at Wickliffe, Kentucky, Research Report, KTC-98-20, Kentucky Transportation Center, University of Kentucky.

Harik, I.E., Madasamy, C., Chen, D.L., Zhou, L.N., Sutterer, K. Street, R.L., and Allen, D.L. (1999a), Seismic Evaluation of the US41 Northbound Bridge over the Ohio River at Henderson, KY, Research Report, KTC-99-16, Kentucky Transportation Center, University of Kentucky.

Harik, I.E., Vasudevan, K., Madasamy, C., Chen, D.L., Zhou, L.N., Sutterer, K. Street, R.L., and Allen, D.L. (1999b), Seismic Evaluation of the US41 Southbound Bridge over the Ohio River at Henderson, KY, Research Report, KTC-99-17, Kentucky Transportation Center, University of Kentucky.

Hudson, D.E., (1977), “Dynamic Tests of Full-Scale Structures”, Journal of the Engineering Mechanics Division, Vol. 103, No.EM6, 1141-1157.

Jacob, K., (1995), “Geotechnical and Seismological Aspects of New York Seismic Code

Provisions,” National Center for Earthquake Engineering Research Bulletin, Vol. 9, No. 3.

James III, G.H., Carne, T.G. and Lauffer, J.P. (1995). "The natural excitation technique (NExT) for modal parameter extraction from operating structures." *International Journal of Analytical and Experimental Modal Analysis*, 10(4), 260-277.

Johnston, A.C., (1982), “A Major Earthquake Zone on the Mississippi,” *Scientific American*, Vol. 246, No. 4, 60-68.

Johnston, A.C., (1985), “A Brief Overview of the Geology, Seismicity and Seismic Hazard of the Central Mississippi Valley Area,” Presented at A Regional Seminar on Earthquake Fundamentals for the Mississippi Valley, Memphis, Tennessee.

Johnston, A.C. and Nava, S.J. (1985), “Recurrence Rates and Probability Estimates for the New Madrid Seismic Zone”, *Journal of Geophysical Research*, Vol. 90, No. B8, 6737-6753.

Maia, N.M.M. and Silva, J.M.M. Edited. (1997). *Theoretical and experimental modal analysis*. Research Studies Press Ltd., England.

Mayes, R.L., et al., (1992), “AASHTO Seismic Isolation Design Requirements for Highway Bridges,” *Journal of Structural Engineering*, Vol. 118, No. 1, 284-304.

Morteza A. M., M. Torkamani and H. E. Lee, (2002). “Dynamic Behavior of Steel Deck Tension-Tied Arch Bridges to Seismic Excitation”, *Journal of Bridge Engineering*, Vol. 7, No.1, 57-67.

National Highway Institute (NHI) Course No. 13063, (1996), “Seismic Bridge Design Applications,” Notes from Sessions 1 & 2.

Paultre, P., Proulx, J., and Talbot, M., (1995), “Dynamic Testing Procedures for Highway Bridges Using Traffic Loads,” *Journal of Structural Engineering*, Vol. 121, No. 2, 362-376.

Priestly, M.J.N., F. Seible and G. M. Calvi, *Seismic Design and Retrofit of Bridges*, John-Wiley & Sons, Inc., 1996.

Roeder C. W., G. Macrae, P. Crocker, K. Arima and S. Wong, (2000). “Dynamic Response and Fatigue of Steel Tied-Arch Bridge”, *Journal of Bridge Engineering*, Vol. 5, No.1, 14-21.

Saiidi, M., Douglas, B., and Feng, S. (1994), “Prestress Force Effect on Vibration Frequency of Concrete Bridges,” *Journal of Structural Engineering*, Vol. 120, No. 7, 2233-2241.

Shahawy, M.A., (1995), “Non-destructive Strength Evaluation of Florida Bridges,” *Proceedings of SPIE Nondestructive Evaluation of Aging Infrastructure Conference*, Oakland, California.

Shama, A. A., J. B. Mander, S. S. Chen and A. J. Aref, (2001). “Ambient Vibration and Seismic Evaluation of a Cantilever Truss Bridge”, *Engineering Structures*, 23(2001), 1281-1292

Shelley, S.J., et al., (1995), “Dynamic Testing (Vibration Analysis) of Highway Bridges,” Notes

Presented at the North-American Workshop on Instrumentation and Vibration Analysis of Highway Bridges, Cincinnati, Ohio.

Street, R., Z. Wang, I. E. Harik, D. L. Allen and J. J. Griffin (1996), Source Zones, Recurrence Rates, and Time Histories for Earthquakes Affecting Kentucky, Report No.KTC-96-4, Kentucky Transportation Center, University of Kentucky.

Van der Auweraer, H. and Hermans, L. (1999). "Structural modal identification from real operating conditions." *Sound and Vibration*, 33(1), 34-41.

Van Overschee, P. and De Moor, B. (1996). *Subspace identification for linear systems: theory, implementation and applications*, Kluwer Academic Publishers, Dordrecht, Netherlands

Ventura, C.E., Felber, A.J., and Prion, G.L., (1994). "Seismic Evaluation of a Long Span Bridge by Modal Testing", *Proceedings of the 12th International Modal Analysis Conference*, Honolulu, Hawaii, 1309-1315.

Wendichansky, D.A., Chen, S.S., and Mander, J.B., (1995). "In-Situ Performance of Rubber Bearing Retrofits," Presented at National Seismic Conference on Bridges and Highways, San Diego, California.

Wilson, E.L. and A. Habibullah (1998), *SAP2000 - Structural Analysis Users Manual*, Computers and Structures, Inc.

Wilson, E.L., M.W. Yuwan, and J.M. Dickens (1982), *Dynamic Analysis by Direct Superposition of Ritz Vectors*, *Earthquake Engineering and Structural Dynamics*, 10, 813-823.

Wilson, E.L., and Tetsuji, I.J., (1983), "An Eigensolution Strategy for Large Systems," *Computers and Structures*, Vol. 16, 259-265.

Zimmerman, R. M. and Brittain, R. D. (1979), *Seismic Response of Multi-simple Span Highway Bridges*, *Proceedings of the 3rd Canadian Conference on Earthquake Engineering*, Montreal, 1091-1120.

Table 3.1 Different Stations per Setup

Setup	Moveable Stations	Base Stations
-------	-------------------	---------------

(1)	(2)	(3)
SL1	L1, L2, L3, L4	L8, L11, R11
SL2	L5, L6, L7, L8	L8, L11, R11
SL3	L9, L10, L11, L12	L8, L11, R11
SL4	L12, L13, L14, L15	L8, L11, R11
SR1	R1, R2, R3, R4	R8, R11, L11
SR2	R5, R6, R7, R8	R8, R11, L11
SR3	R9, R10, R11, R12	R8, R11, L11
SR4	R12, R13, R14, R15	R8, R11, L11

Table 4.1 Comparisons of Dead Load Deformation

Panel Point	Model-1		Model-2		Design	
	mm	in.	mm	in.	mm	in.
1	18.796	0.740	16.358	0.644	20.422	0.804
2	34.722	1.367	30.404	1.197	37.490	1.476
3	48.717	1.918	43.002	1.693	53.340	2.100
4	60.858	2.396	54.102	2.130	67.056	2.640
5	71.476	2.814	64.033	2.521	77.470	3.050
6	80.442	3.167	72.619	2.859	83.820	3.300
7	87.071	3.428	79.096	3.114	86.360	3.400

Table 4.2 Identified and Calculated Frequencies

Mode	Model-1 (Hz)	Model-2 (Hz)	Peak-Picking (Hz)	Stochastic Subspace Identification	
				Frequency (Hz)	Damping Ratio (%)
1 st vertical	0.561	0.562	0.567	0.565	1.3
2 nd vertical	1.149	1.162	1.100	1.109	2.5
3 rd vertical	1.749	1.762	1.483	1.488	1.3
1 st transverse	0.717	0.861	0.767	0.744	4.4
2 nd transverse	1.557	2.897	1.267	1.242	1.4
3 rd transverse	1.838	3.242	2.300	2.301	1.5
1 st longitudinal	1.516	1.573	1.583	1.563	1.1

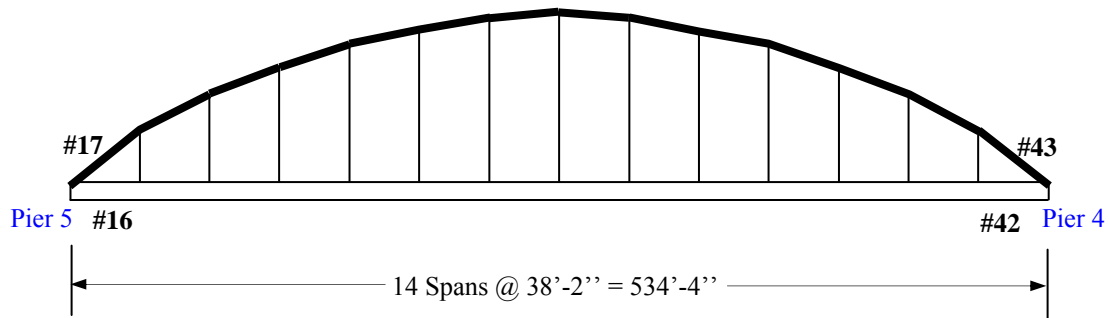
Table 4.3 Natural Frequencies and Mass Participation of the Main Span of the Bridge for Model-1
(Exact Eigen System)

Mode Number	Angular Frequency (rad/sec)	Circular Frequency (Hz)	Period (Sec)	Mass Participation			Cumulative Mass Participation		
				X-DIR	Y-DIR	Z-DIR	X-SUM	Y-SUM	Z-SUM
1	3.528	0.561	1.781	0.4202	0.0000	0.0030	0.4202	0.0000	0.0030
2	4.507	0.717	1.394	0.0000	21.2849	0.0000	0.4202	21.2849	0.0030
3	6.117	0.973	1.027	0.0000	0.0177	0.0000	0.4202	21.3025	0.0030
4	7.217	1.149	0.871	0.7608	0.0000	2.7265	1.1810	21.3025	2.7296
5	8.291	1.320	0.758	0.0000	0.0141	0.0001	1.1810	21.3167	2.7296
6	8.792	1.399	0.715	24.3415	0.0000	0.0000	25.5226	21.3167	2.7296
7	9.527	1.516	0.659	25.4985	0.0000	8.7602	51.0211	21.3167	11.4898
8	9.783	1.557	0.642	0.0000	0.0001	0.0000	51.0211	21.3168	11.4898
9	10.992	1.749	0.571	22.6905	0.0000	11.2142	73.7116	21.3168	22.7040
10	11.546	1.838	0.544	0.0000	1.2857	0.0000	73.7116	22.6025	22.7040
11	12.140	1.932	0.518	0.0000	0.0008	0.0000	73.7116	22.6032	22.7040
12	12.358	1.967	0.508	0.0000	0.2927	0.0000	73.7116	22.8959	22.7040
13	12.459	1.983	0.504	0.0000	0.0327	0.0000	73.7116	22.9286	22.7040
14	12.489	1.988	0.503	0.0001	0.0023	0.0000	73.7117	22.9308	22.7040
15	12.494	1.988	0.503	0.0000	0.0034	0.0000	73.7117	22.9342	22.7040

Table 4.4 Natural Frequencies and Mass Participation of the Main Span of the Bridge for Model-2

(Exact Eigen System)

Mode Number	Angular Frequency (rad/sec)	Circular Frequency (Hz)	Period (Sec)	Mass Participation			Cumulative Mass Participation		
				X-DIR	Y-DIR	Z-DIR	X-SUM	Y-SUM	Z-SUM
1	3.533	0.562	1.778	0.4186	0.0000	0.0032	0.4186	0.0000	0.0032
2	5.411	0.861	1.161	0.0000	14.8304	0.0000	0.4186	14.8304	0.0032
3	7.299	1.162	0.861	0.3794	0.0000	2.1737	0.7980	14.8304	2.1770
4	7.499	1.193	0.838	0.0000	6.5723	0.0000	0.7980	21.4027	2.1770
5	8.427	1.341	0.746	0.0000	0.0001	0.0000	0.7980	21.4029	2.1770
6	8.792	1.399	0.715	24.3408	0.0000	0.0000	25.1389	21.4029	2.1770
7	9.886	1.573	0.636	28.2276	0.0000	8.2668	53.3664	21.4029	10.4438
8	11.069	1.762	0.568	20.3796	0.0000	12.2455	73.7460	21.4029	22.6893
9	12.727	2.025	0.494	0.0000	0.9448	0.0000	73.7460	22.3477	22.6893
10	13.991	2.227	0.449	0.1573	0.0000	0.0083	73.9033	22.3477	22.6976
11	16.182	2.576	0.388	0.0000	0.1206	0.0000	73.9033	22.4683	22.6976
12	16.689	2.656	0.376	0.0000	0.0003	0.0000	73.9033	22.4686	22.6976
13	18.202	2.897	0.345	0.0000	0.0000	0.0000	73.9033	22.4686	22.6976
14	20.368	3.242	0.308	0.0000	0.9384	0.0000	73.9033	23.4070	22.6976
15	20.695	3.294	0.304	0.0000	0.0000	0.0000	73.9033	23.4070	22.6976



Elevation

Table 5.1 Maximum seismic stresses of the bridge elements resulting from the combined loading of DL+EQ

Number of structural member		16	17	42	43	
DL (ksi)		7.56	-15.88	7.25	-16.05	
250-year event	EQ (ksi)	Case-1	3.78	-4.65	3.12	-5.21
		Case-2	2.32	-5.63	2.63	-6.41
	σ (ksi)	Case-1	11.34	-20.53	10.37	-21.26
		Case-2	9.88	-21.51	9.88	-22.46
500-year event	EQ (ksi)	Case-1	6.50	-11.13	5.24	-12.68
		Case-2	5.09	-7.30	4.31	-9.35
	σ (ksi)	Case-1	14.06	-27.01	12.49	-28.73
		Case-2	12.65	-23.18	11.56	-25.40

Note: All structural steel members calculated in Table 5.1 to be 50 ksi Y.P. steel

Table 5.2 Maximum seismic forces and stresses at bottom of Pier 5 and Pier 4 resulting from 250-Year event

Quantity	Units	Pier 5		Pier 4	
		Case-1	Case-2	Case-1	Case-2
F_x	kip	544.9	388.7	394.0	396.1
F_y	kip	295.0	310.2	290.2	280.3
F_z	kip	2406	1914	2386	1866
M_x	kip.in	28960	24120	28490	24300
M_y	kip.in	276500	223100	162600	145600
M_z	kip.in	8408	7520	27760	35030
σ	ksi	0.67	0.54	0.46	0.40
τ	ksi	0.04	0.03	0.06	0.07

Note:
$$\sigma = \frac{F_z}{A} + \frac{M_x}{S_x} + \frac{M_y}{S_y} ; \quad \tau = \frac{\sqrt{F_x^2 + F_y^2}}{A} + \frac{M_z C}{J_z}$$

Table 5.3 Maximum seismic forces and stresses at bottom of Pier 5 and

Pier 4 resulting from 500-Year event

Quantity	Units	Pier 5		Pier 4	
		Case-1	Case-2	Case-1	Case-2
F_x	kip	988.7	1170.0	862.3	735.2
F_y	kip	832.7	738.8	828.2	733.9
F_z	kip	5925	4835	5967	4774
M_x	kip.in	93690	86040	93740	85090
M_y	kip.in	641900	654300	418500	367800
M_z	kip.in	19210	19530	70350	52180
σ	ksi	1.62	1.58	1.20	1.04
τ	ksi	0.09	0.09	0.16	0.12

Note: $\sigma = \frac{F_z}{A} + \frac{M_x}{S_x} + \frac{M_y}{S_y}$; $\tau = \frac{\sqrt{F_x^2 + F_y^2}}{A} + \frac{M_z C}{J_z}$

Table 5.4 Maximum seismic shear forces at two fixed bearings over Pier 4 and the seismic shear

force Capacity/Demand
ratios ($r_{C/D}$) for each anchor bolt

	Quantity	Units	CASE-1		CASE-2	
			(1)	(2)	(1)	(2)
250-year event	F_x	kip	209.3	234.3	221.0	208.7
	F_y	kip	99.3	90.5	121.1	115.9
	$r_{C/D}$	–	1.59	1.47	1.46	1.55
	$\rho_{S/G}$	–	0.15	0.14	0.14	0.14
500-year event	F_x	kip	506.2	510.3	382.4	405.9
	F_y	kip	227.6	274.1	186.9	214.7
	$r_{C/D}$	–	0.66	0.64	0.87	0.80
	$\rho_{S/G}$	–	0.267	0.274	0.246	0.222

Note:

(1) Seismic Shear Force Capacity/Demand ratio:

$$r_{C/D} = V_c / V_d$$

where V_c – the anchor bolt capacity

V_d – the seismic demand, coefficient 1.25 is considered.

(2) For anchor bolts– steel A325, 4Ø1.75” at each bearing

Nominal shear strength for each bolt is 115.4 kips (513.3 kN).

(3) $\rho_{S/G}$ – the ratio of the maximum seismic pullout force to dead load force

Table 5.5 Displacement Capacity/Demand ratios of the

bearings over Pier 5

	$\Delta_s(c)$	$\Delta_i(d)$	$\Delta_{eq}(d)$		C/D	
			Case-1	Case-2	Case-1	Case-2
250-year event	65 in. (165 cm)	3.75 in. (9.53 cm)	0.62 in. (1.58 cm)	0.75 in. (1.91 cm)	98.8	81.7
500-year event	65 in. (165 cm)	3.75 in. (9.53 cm)	2.25 in. (5.72 cm)	1.75 in. (4.45 cm)	27.2	35

Note: Capacity/Demand ratio $C/D = \frac{\Delta_s(c) - \Delta_i(d)}{\Delta_{eq}(d)}$

$\Delta_s(c)$ – the allowable displacement.

$\Delta_i(d)$ – the maximum possible movement resulting from a 90°F (32°C) maximum differential temperature.

$\Delta_{eq}(d)$ – the maximum calculated relative movement due to earthquake loading

Table 6.1 Calculation of weight for SDOF system

	Superstructure				Piers		
	Span 1	Span 2	Span 3	Span 4	Pier 1	Pier 2	Pier 3
	(Span 9)	(Span 8)	(Span 7)	(Span 6)	(Pier 8)	(Pier 7)	(Pier 6)
Weight (kips)	1381	1342	1342	1362	524	1045	1180

Note: One-third weight of the piers is considered in the above table.

Table 6.2 Seismic force of the approach bridge

	Period (sec)	C_s		Seismic Force (kN)	
		250-year event	500-year event	250-year event	500-year event
Transverse	0.17	0.3	0.6	9080	18161
Longitudinal	1.372	0.20	0.31	6808	10620

Table 6.3 Longitudinal displacement of the approach bridge

Period (sec)	C_s		Displacement (in.)			
	250-year event	500-year event	250-year event		500-year event	
			End Bent 1 (End Bent 2)	Pier 4 (Pier 5)	End Bent 1 (End Bent 2)	Pier 4 (Pier 5)
1.73	0.20	0.26	5.87	11.74	7.54	15.08

**Table 6.4 Seismic shear force Capacity/Demand ratios ($r_{C/D}$)
for each anchor bolt**

		V_c (kN)	V_d (kN)	$r_{C/D}$	
Pier 1 (Pier 8)	250-year event	188.6	457.6	0.41	
	500-year event	188.6	915.2	0.21	
Pier 2 (Pier 7)	250-year event	Case-1	188.6	211.3	0.89
		Case-2	188.6	117.3	1.61
	500-year event	Case-1	188.6	331.8	0.57
		Case-2	188.6	221.1	0.85
Pier 3 (Pier 6)	250-year event	Case-1	188.6	146.8	1.28
		Case-2	188.6	81.4	2.32
	500-year event	Case-1	188.6	230.4	0.82
		Case-2	188.6	153.5	1.23

Note: (1) Seismic Shear Force Capacity/Demand ratio:

$$r_{C/D} = V_c / V_d$$

where V_c – one anchor bolt capacity

V_d – the combined seismic force demand, coefficient 1.25 is considered.

(2) For anchor bolts– steel A307, 8Ø1.5” at each bearing

Nominal shear strength for each bolt is 188.6 kN (42.4 kips).

**Table 6.5 Displacement C/D ratios for expansion
bearings of the approach bridge**

		$\Delta_s(c)$	$\Delta_i(d)$	$\Delta_{eq}(d)$	C/D
250-year event	End Bent 1 (End Bent 2)	24 in. (60.96 cm)	2.74 in. (6.96 cm)	5.87 in. (14.91 cm)	3.62
	Pier 4 (Pier 5)	47 in. (119.38cm)	1.39 in. (3.53 cm)	11.74 in. (29.82 cm)	3.88
500-year event	End bent 1 (End Bent 2)	24 in. (60.96 cm)	2.74 in. (6.96 cm)	7.54 in. (19.15 cm)	2.82
	Pier 4 (Pier 5)	47 in. (119.38 cm)	1.39 in. (3.53 cm)	15.08 in. (38.30 cm)	3.02

Note: Capacity/Demand ratio $C/D = \frac{\Delta_s(c) - \Delta_i(d)}{\Delta_{eq}(d)}$

$\Delta_s(c)$ – the allowable displacement.

$\Delta_i(d)$ – the maximum possible movement resulting from a 90°F (32°C)

maximum differential temperature.

$\Delta_{eq}(d)$ – the maximum calculated relative movement due to earthquake loading



Figure 2.1a Roadway View of Tennessee River Bridges on I-24



Figure 2.1b Side View of Tennessee River Bridges on I-24



Figure 2.1c Side View Showing the Main Span of Tennessee River Bridges on I-24



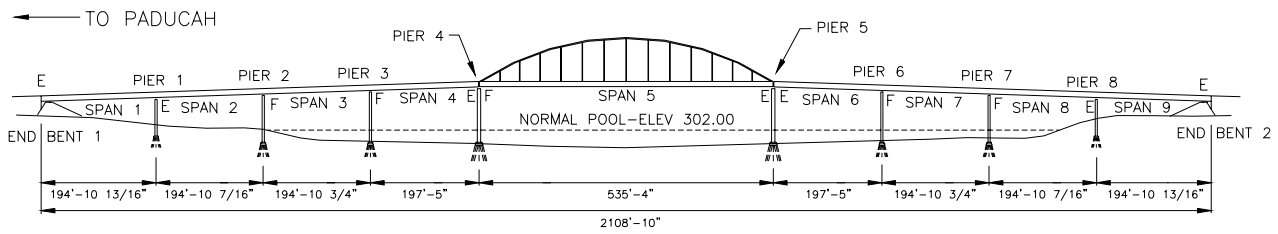
Figure 2.1d View Showing the Roadway of Tennessee River Bridges on I-24



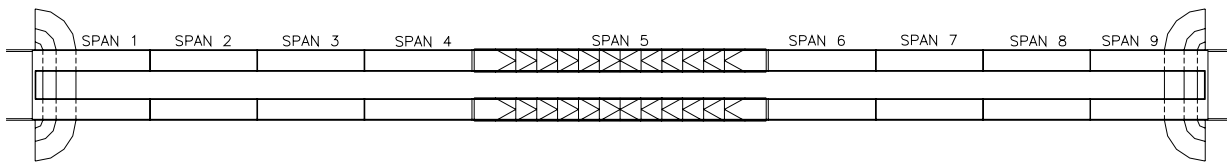
Figure 2.1e Side View Showing the Approach Span of Tennessee River Bridges on I-24



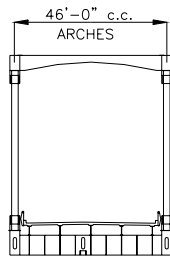
Figure 2.1f Bottom View Showing the Bearings of Tennessee River Bridges on I-24



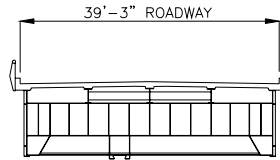
ELEVATION



PLAN



SECTION THRU TIED ARCH SPAN



SECTION THRU GIRDER SPAN

Figure 2.2 Layout of Tennessee River Bridges on I-24

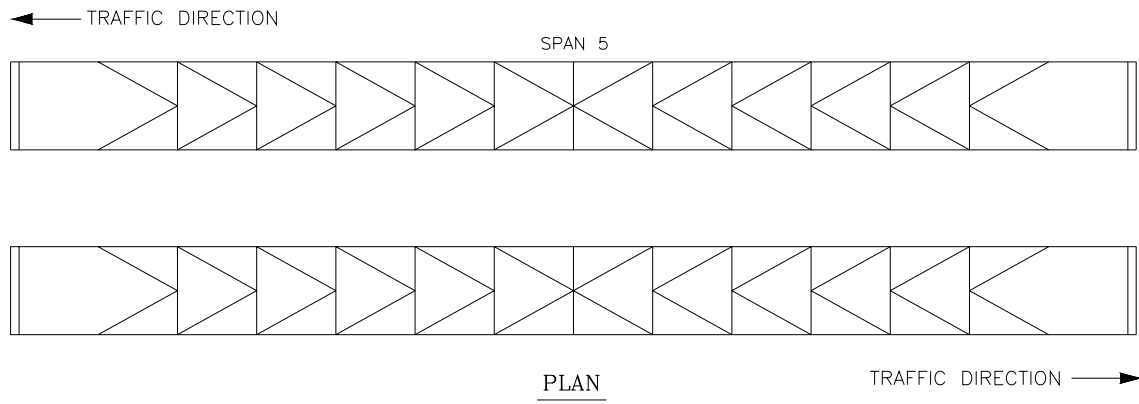
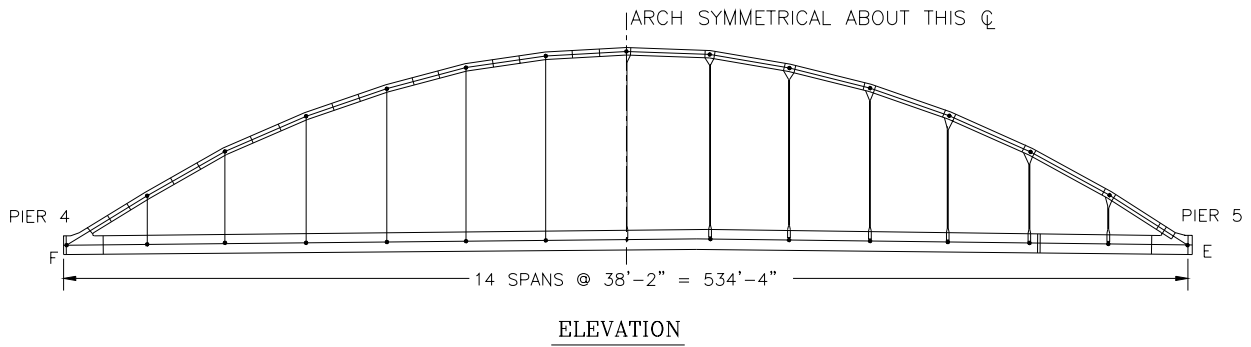


Figure 2.3 Main Span Plan and Elevation Views of Tennessee River Bridges



Figure 2.4 View Showing the Superstructure under Roadway of Tennessee River Bridges



Figure 2.5
Bearing of
River



Expansion
Tennessee
Bridges



Figure 3.1 Triaxial Accelerometers Mounted on the Aluminum Block



Figure 3.2 Data Acquisition System on Site

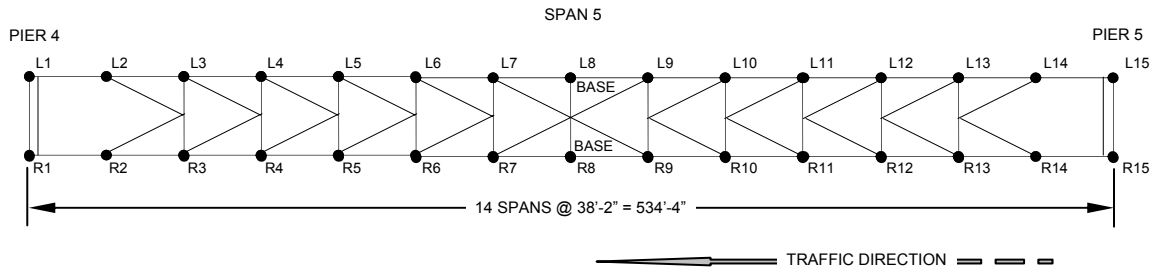


Figure 3.3 The Test Setup and a view on the Measurement Locations

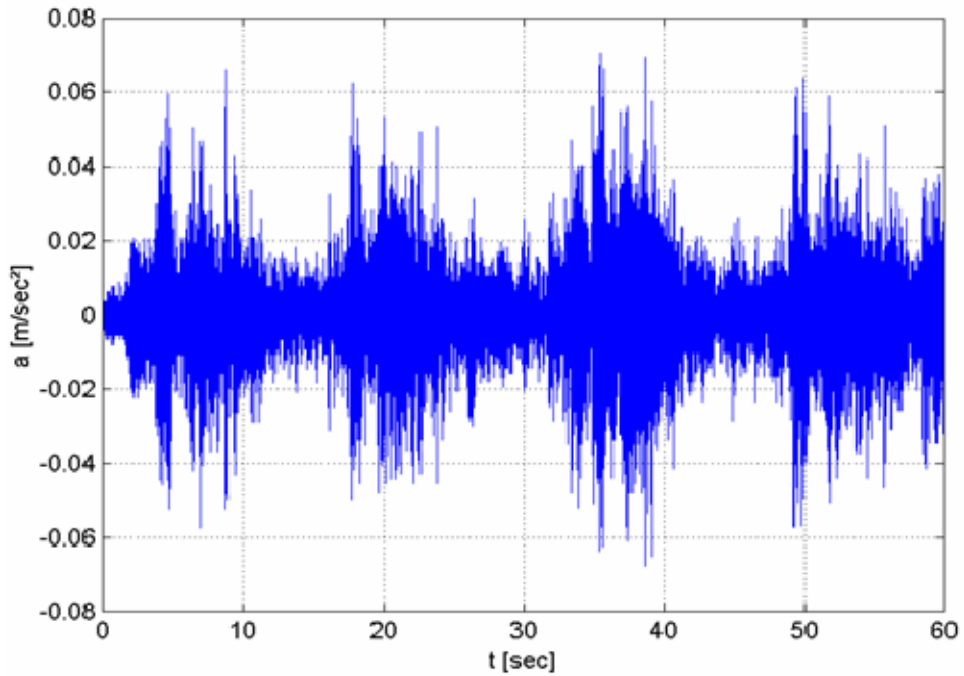


Figure 3.4a Raw Longitudinal Time History Data at Station L8

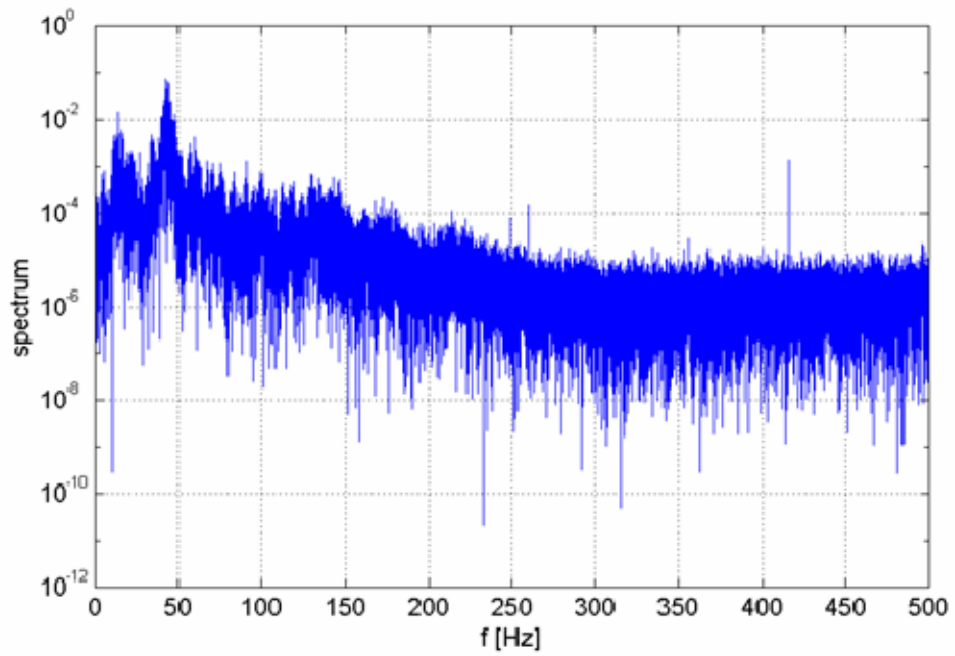


Figure 3.4b Raw Longitudinal Power Spectral Density at Station L8

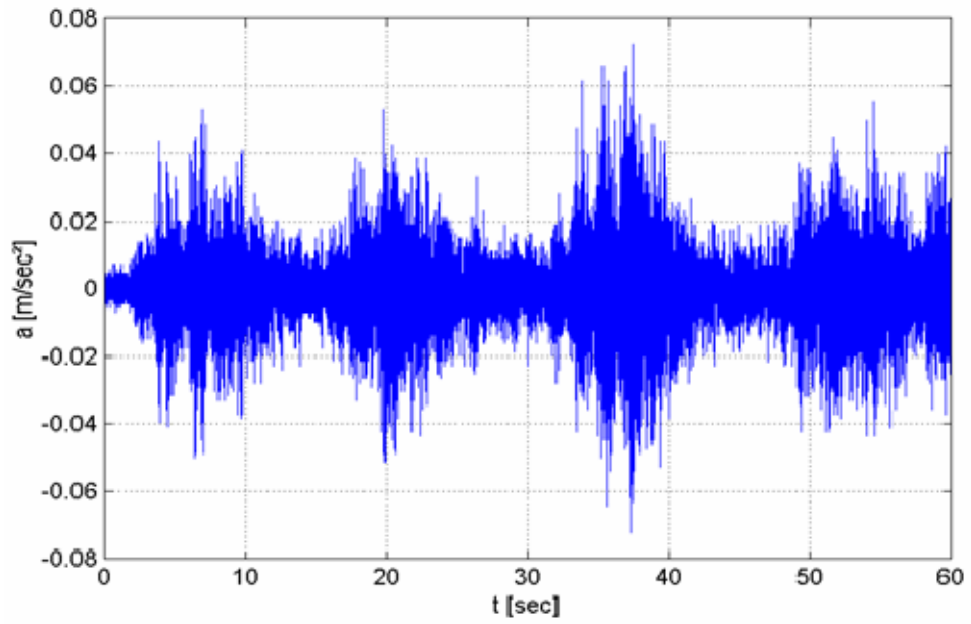
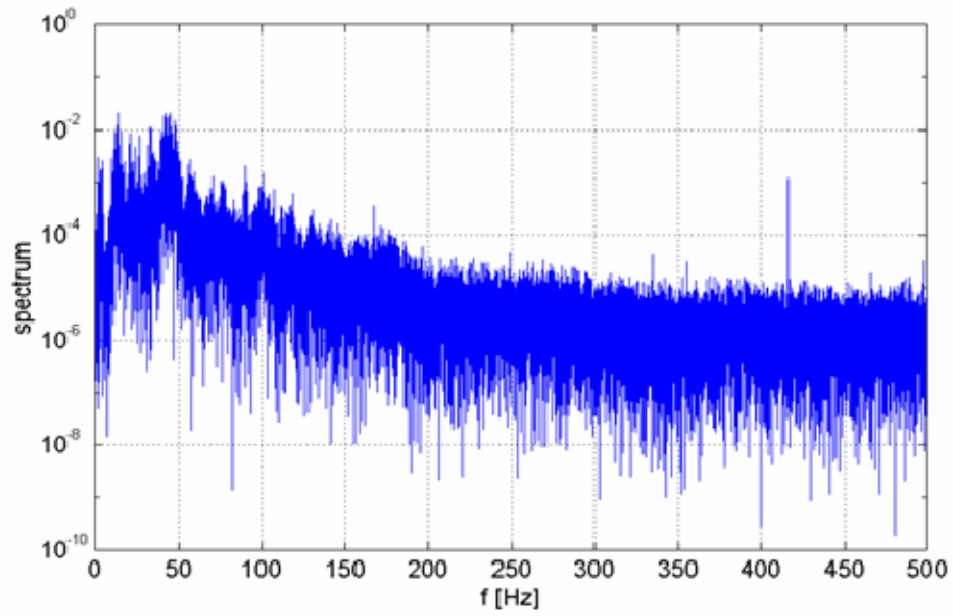


Figure
Raw

3.5a



Transverse Time History Data at Station L8

Figure 3.5b Raw Transverse Power Spectral Density at Station L8

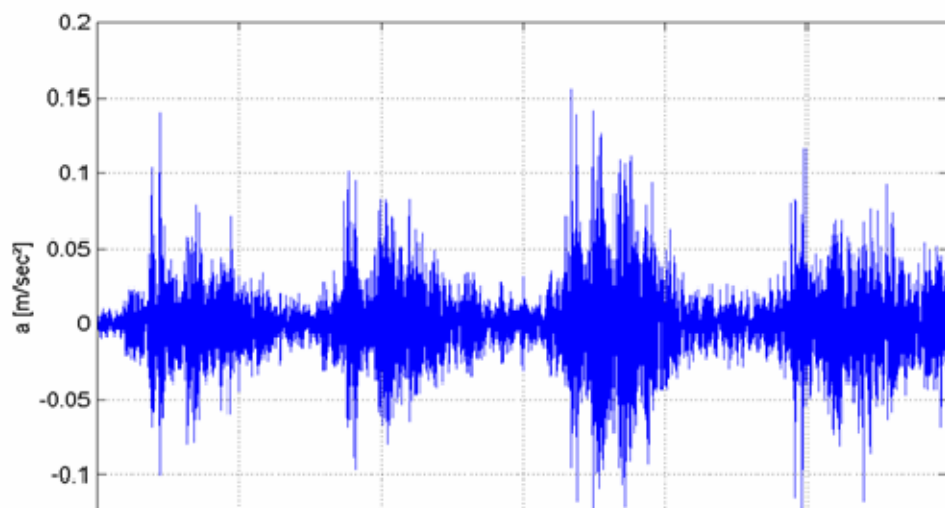
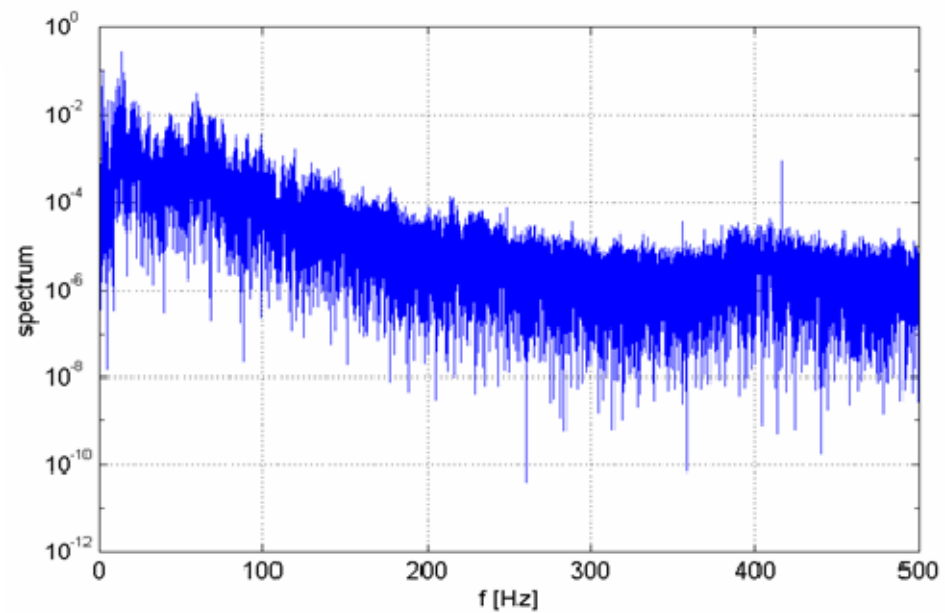
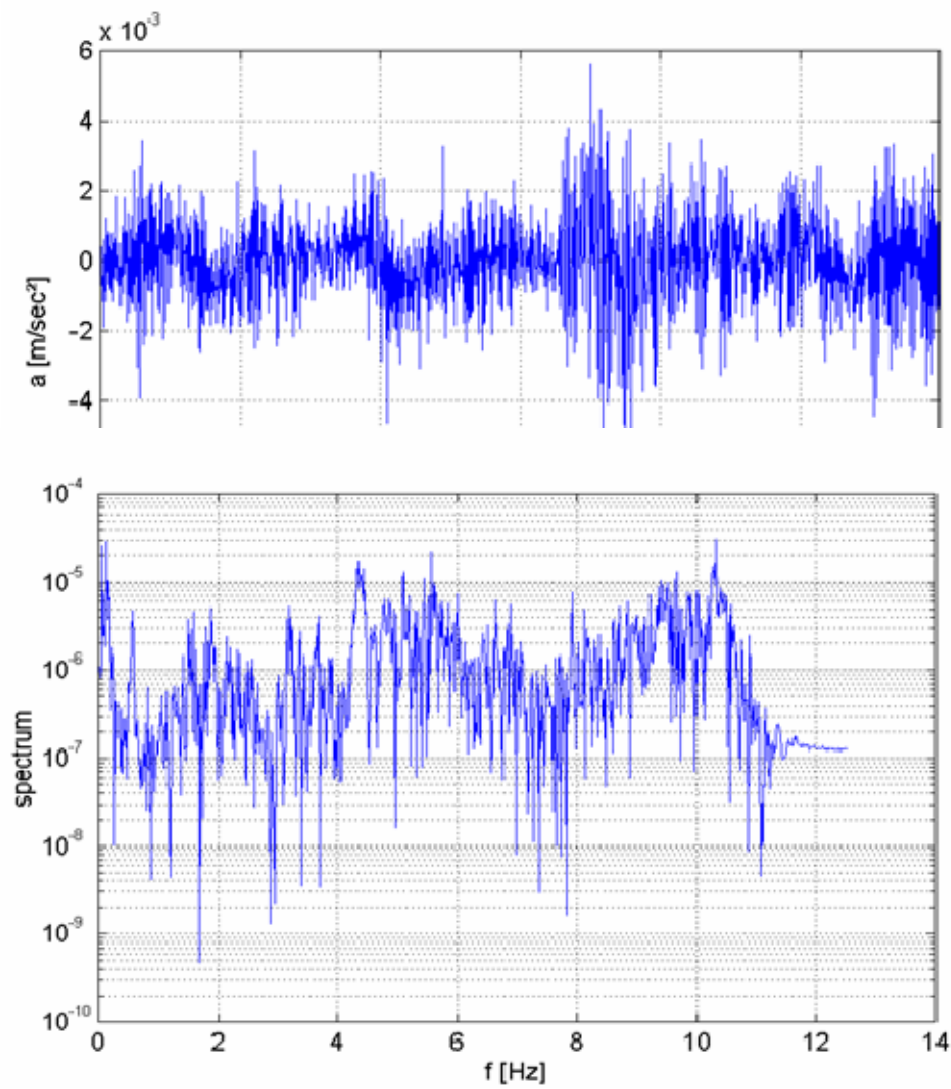


Figure
Time
Data
L8



3.6a Raw
Vertical
History
at Station

Figure 3.6b Raw Vertical Power Spectral Density at Station L8



Figure

3.7a

Resampled Longitudinal Time History Data at Station L8

Figure 3.7b Resampled Longitudinal Power Spectral Density at Station L8

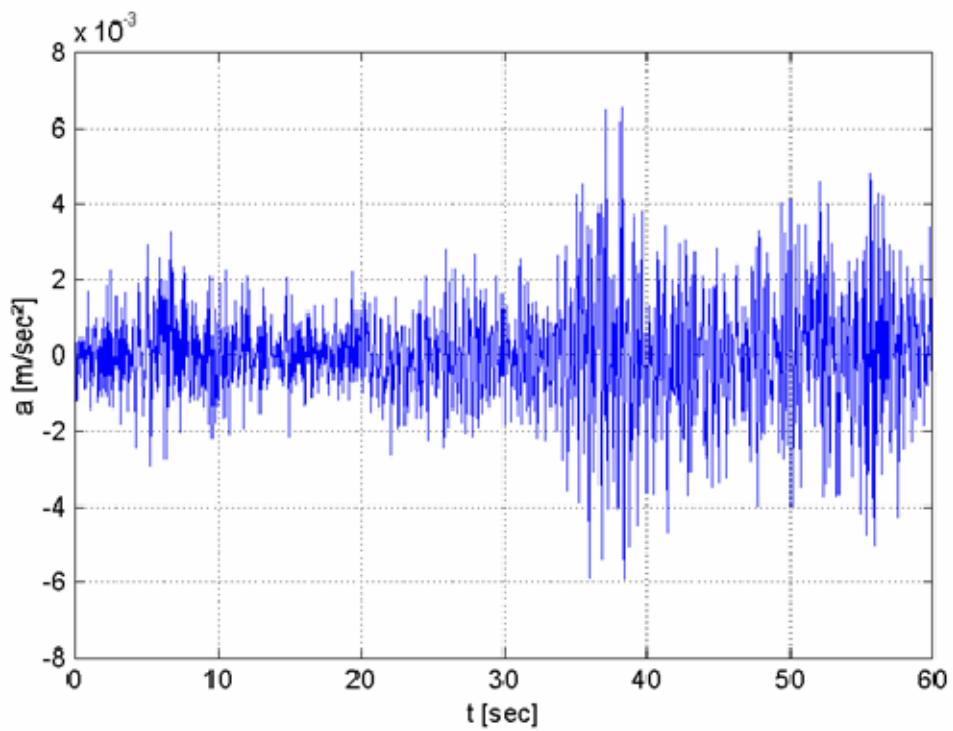


Figure 3.8a Resampled Transverse Time History Data at Station L8

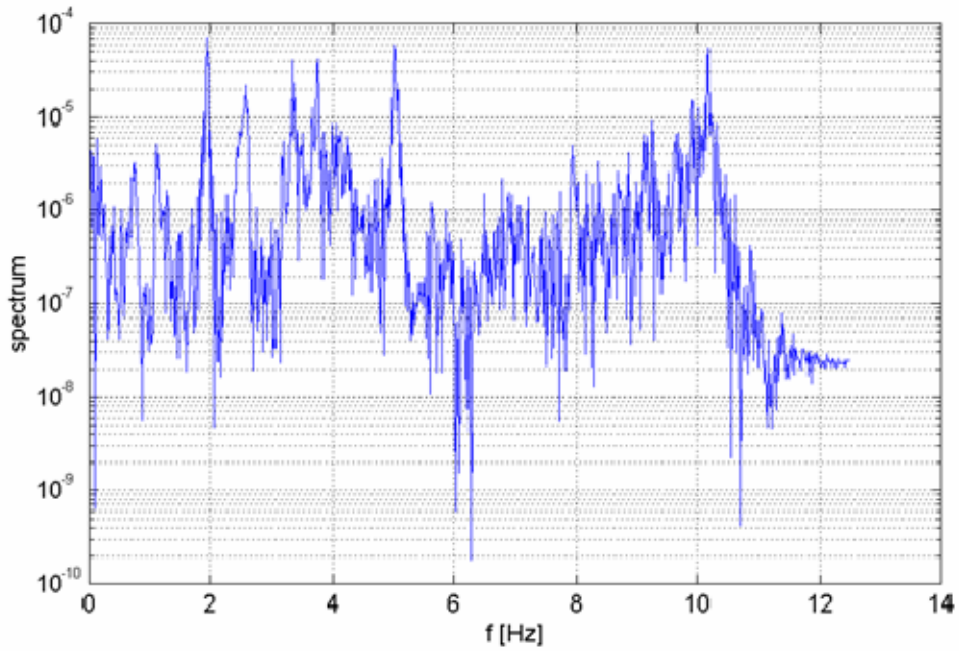
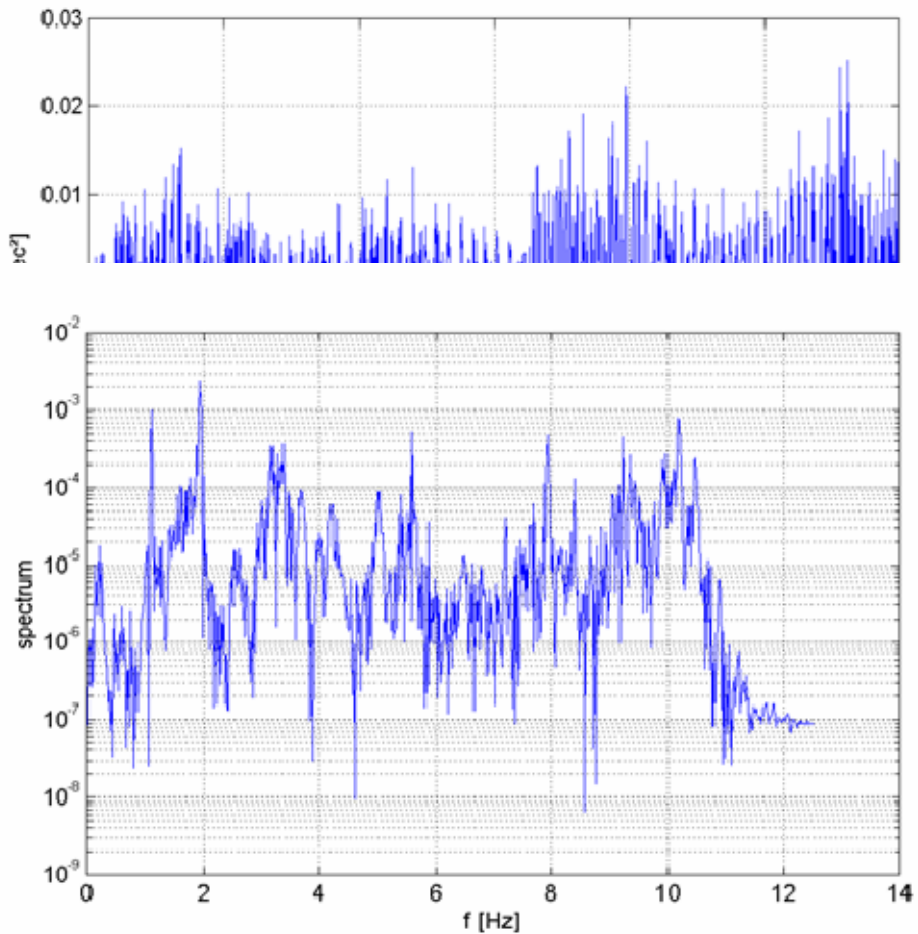


Figure 3.8b Resampled Transverse Power Spectral Density at Station L8



Figure

3.9a

Resampled Vertical Time History Data at Station L8

Figure 3.9b Resampled Vertical Power Spectral Density at Station L8

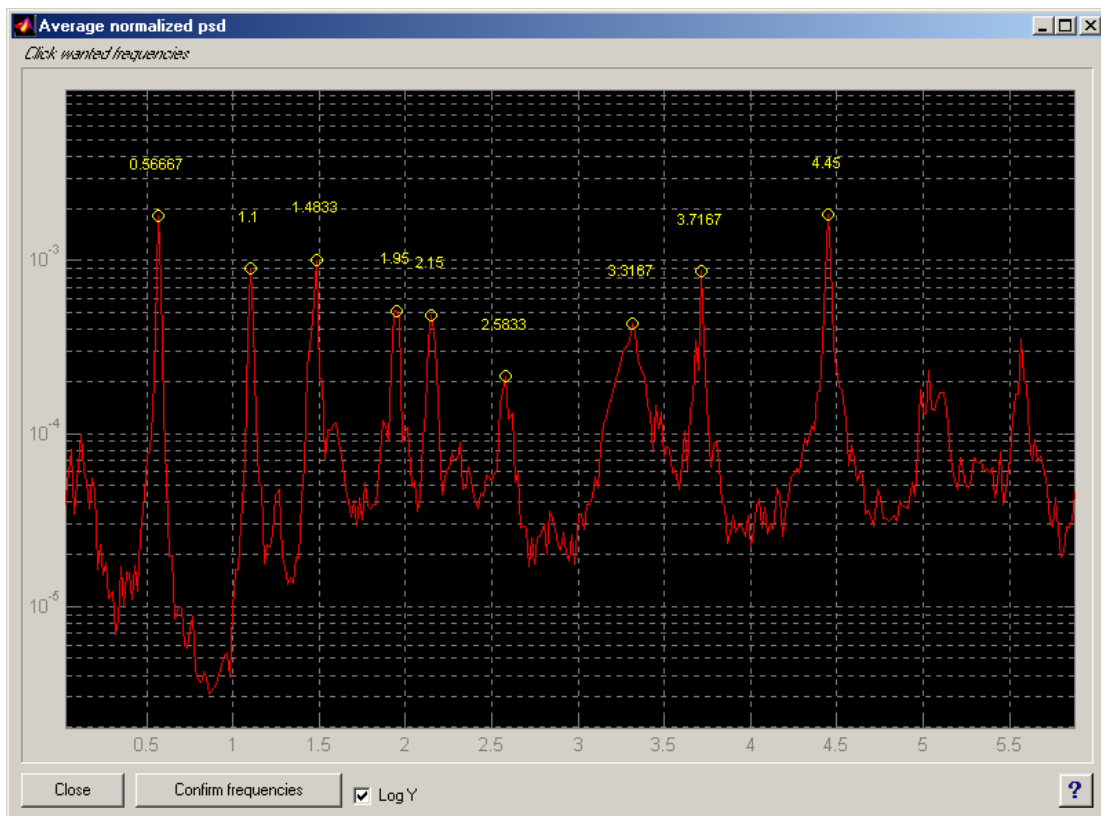


Figure 3.10a Full Average Normalized Power Spectral Density

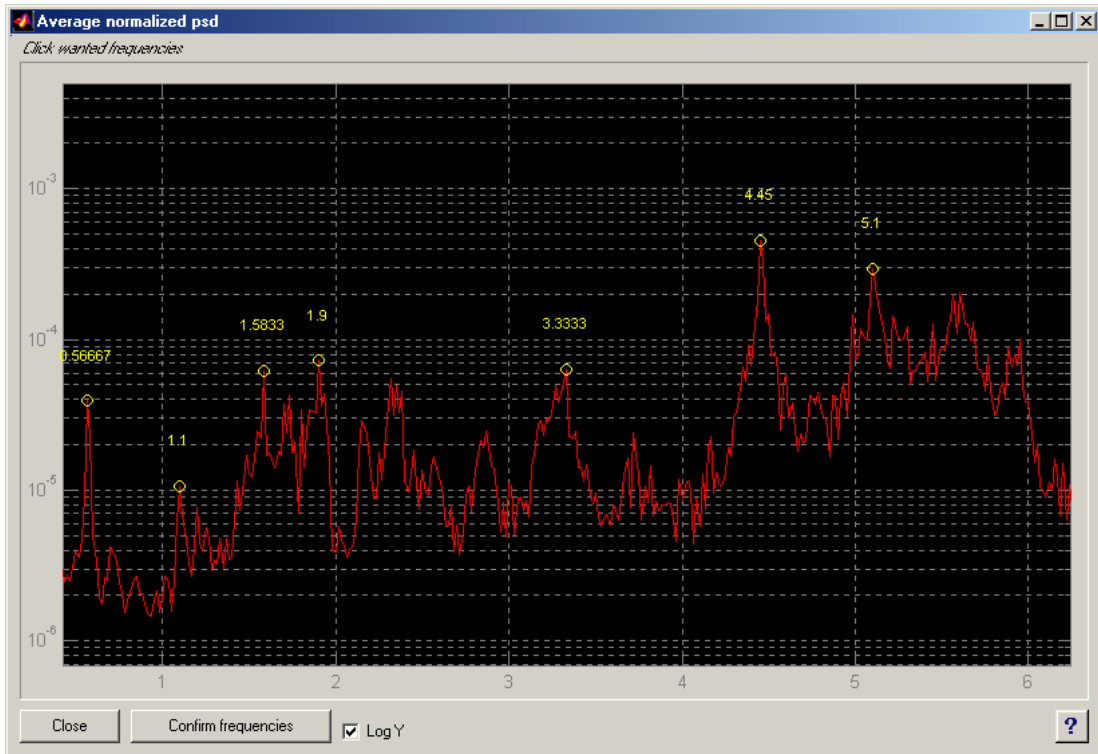


Figure 3.10b Longitudinal Average Normalized Power Spectral Density

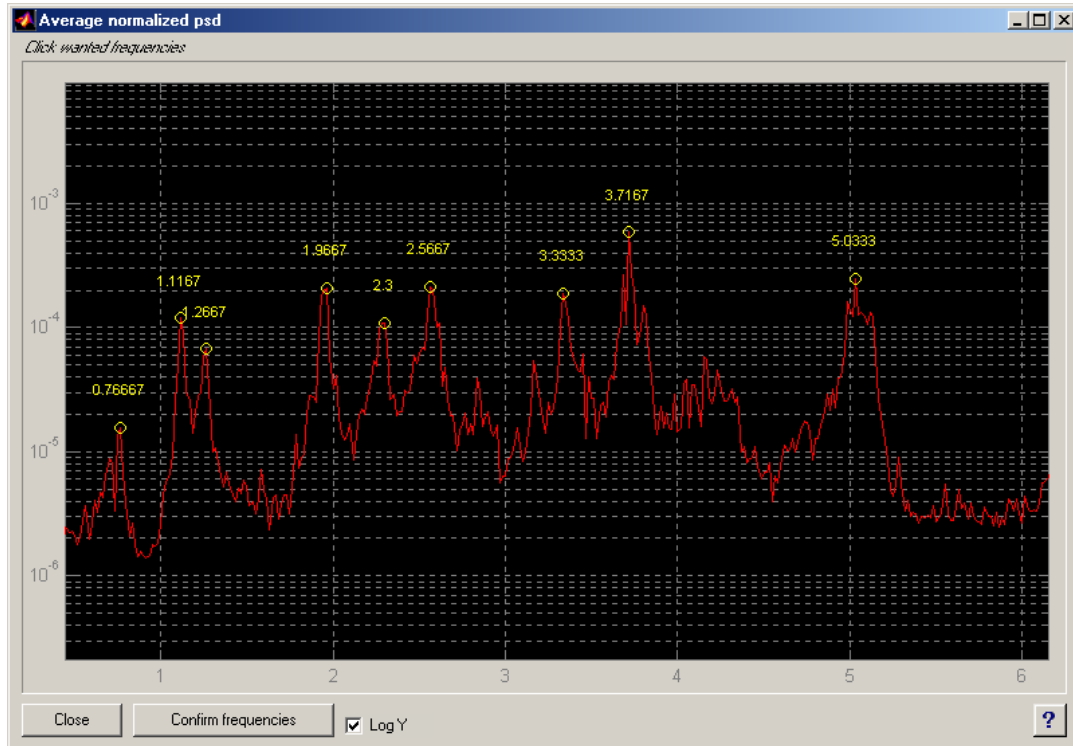


Figure 3.10c Transverse Average Normalized Power Spectral Density

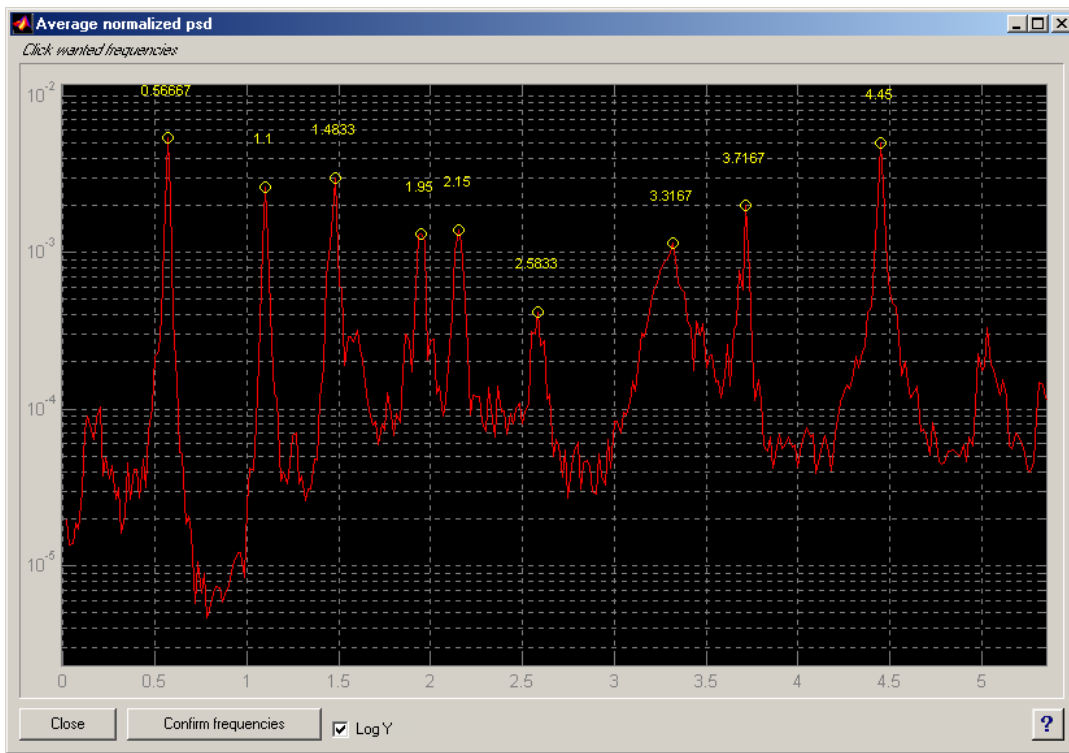
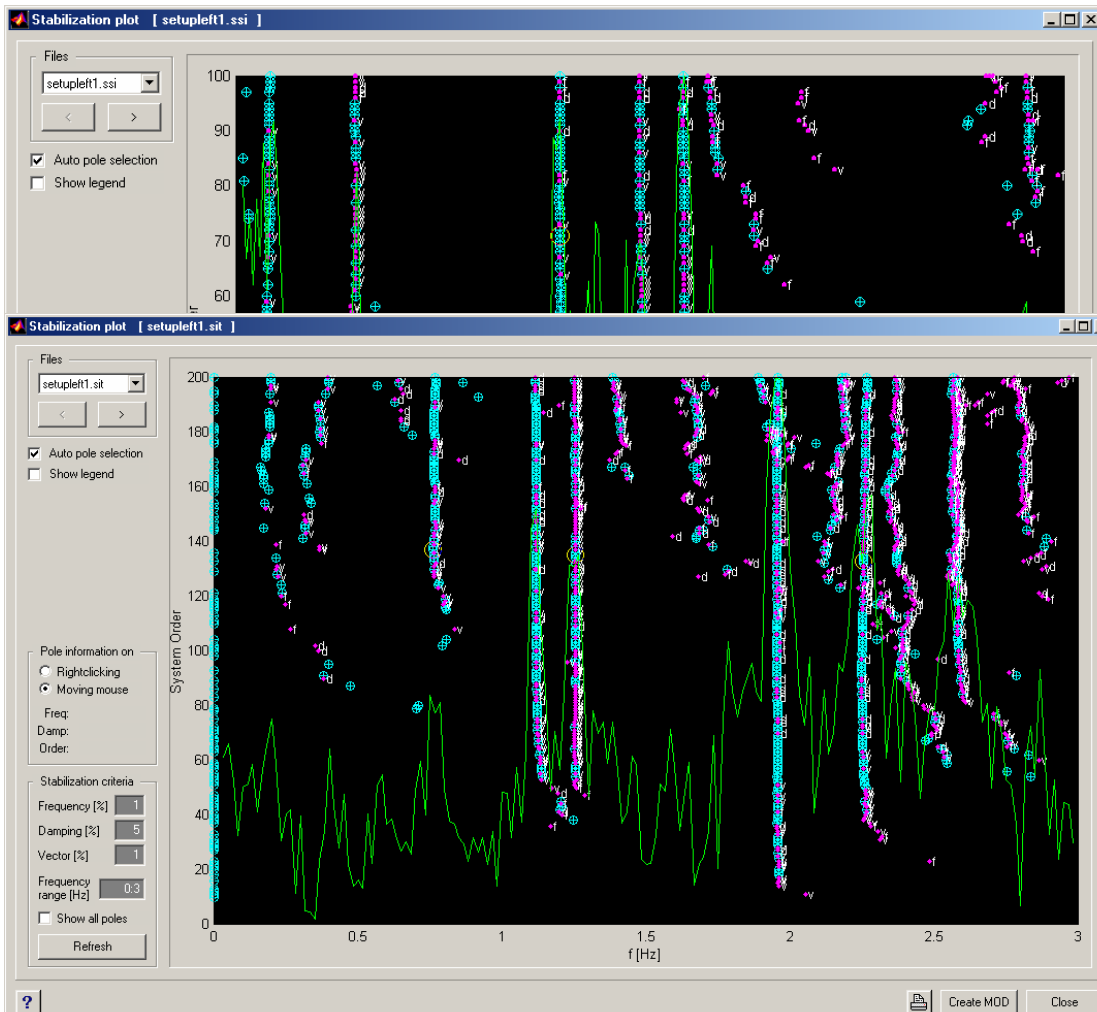


Figure 3.10d Vertical Average Normalized Power Spectral Density



Figure

3.11a Stabilization Diagram of Longitudinal Data

Figure 3.11b Stabilization Diagram of Transverse Data

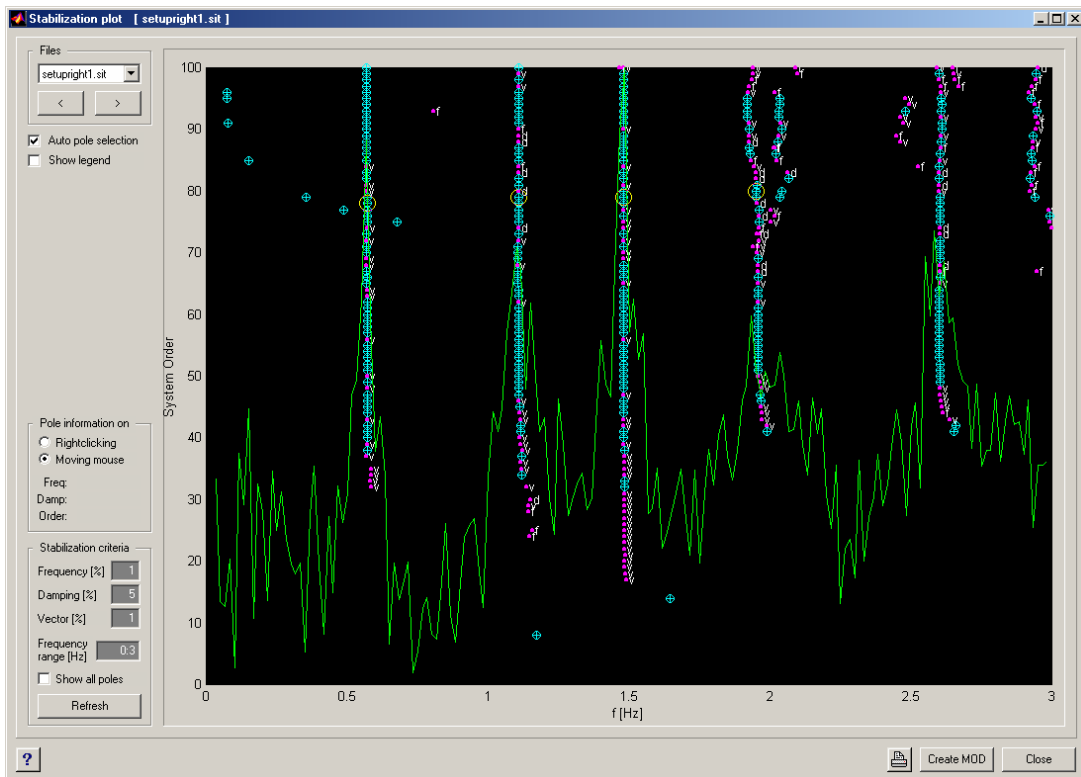


Figure 3.11c Stabilization Diagram of Vertical Data

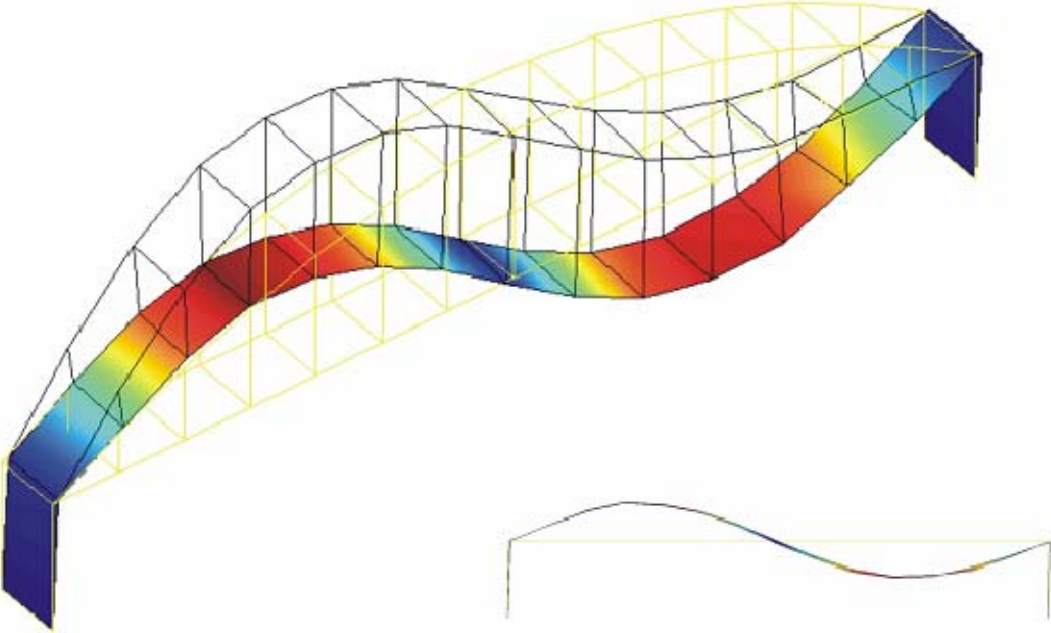


Figure 3.12a The first Vertical Mode Shape ($f=0.565\text{Hz}$, damping ratio=1.3%)

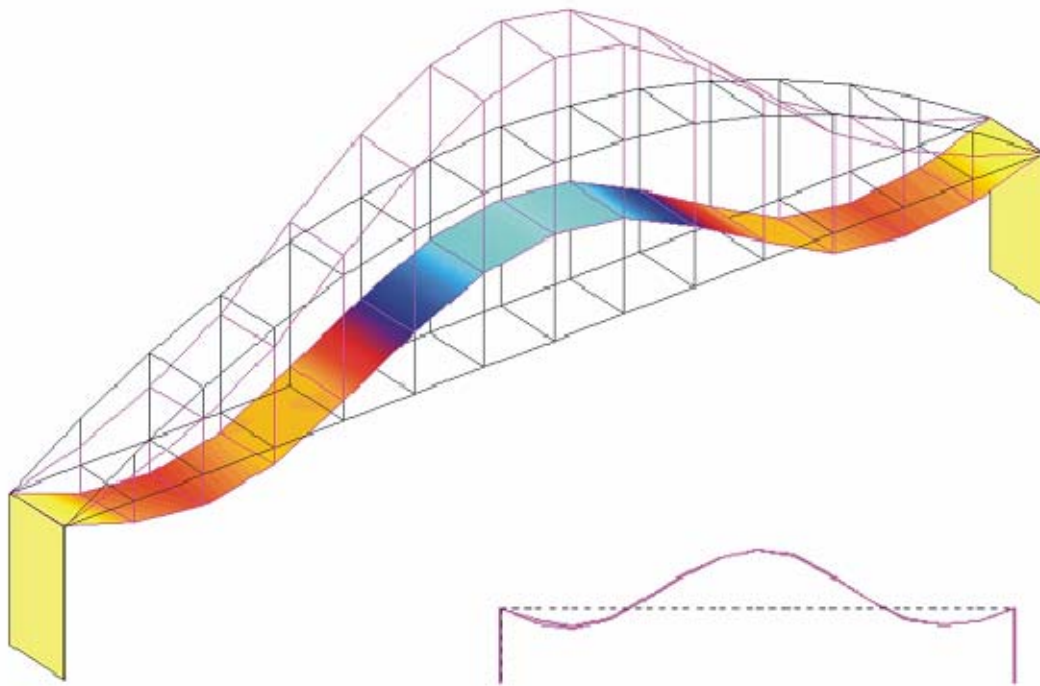


Figure 3.12b The Second Vertical Mode Shape ($f=1.109\text{Hz}$, damping ratio=2.5%)

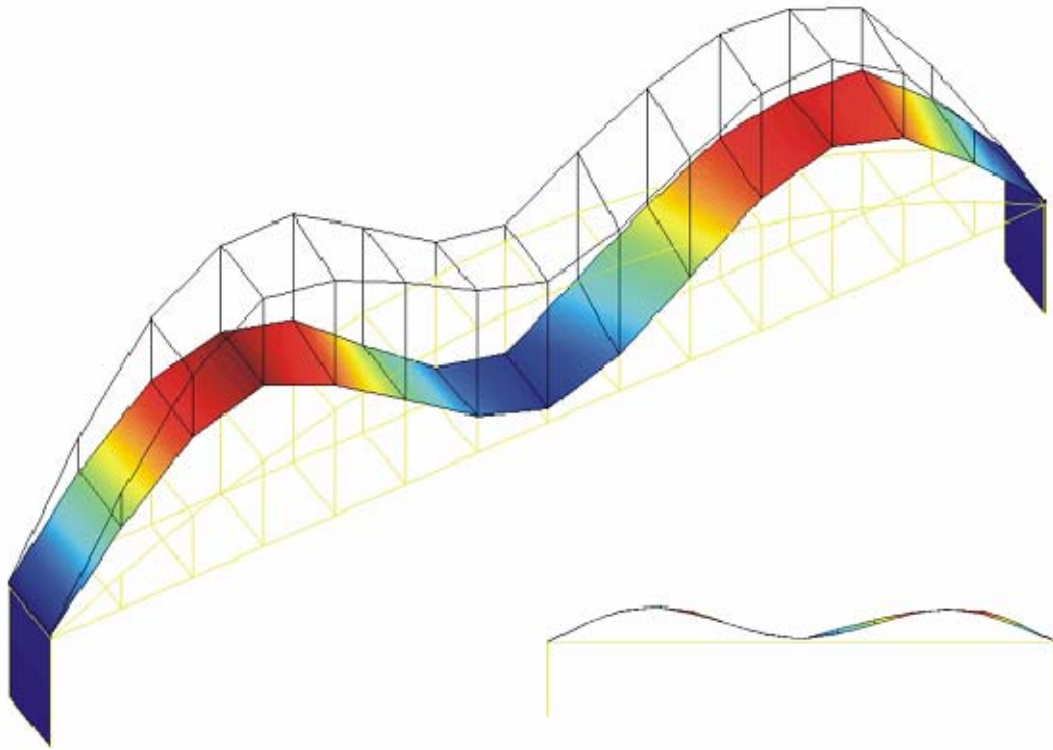


Figure 3.12c The Third Vertical Mode Shape ($f=1.488\text{Hz}$, damping ratio=1.3%)

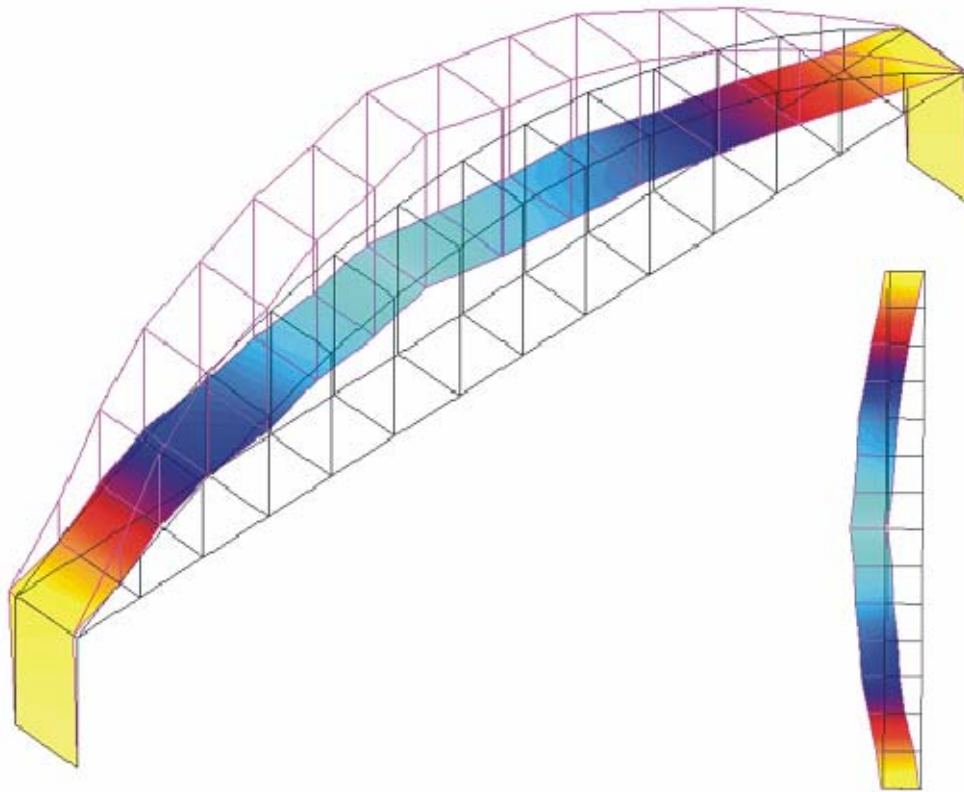


Figure 3.13a The First Transverse Mode Shape ($f=0.744\text{Hz}$, damping ratio=4.4%)

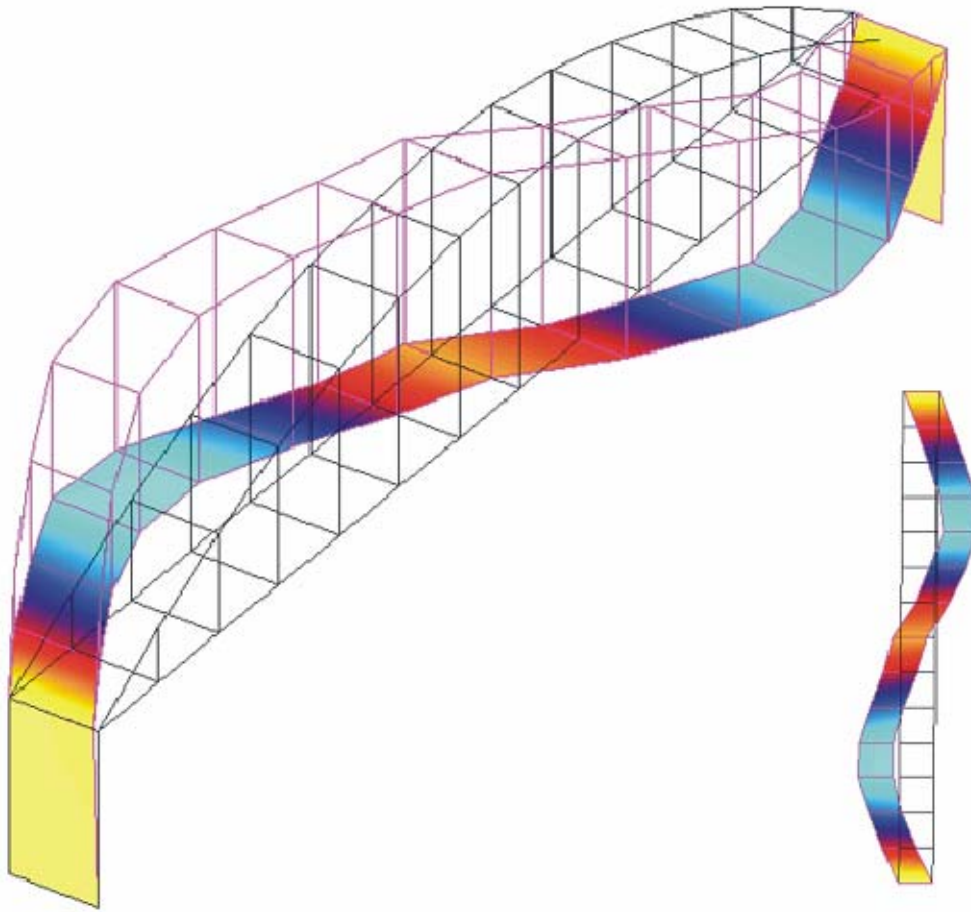
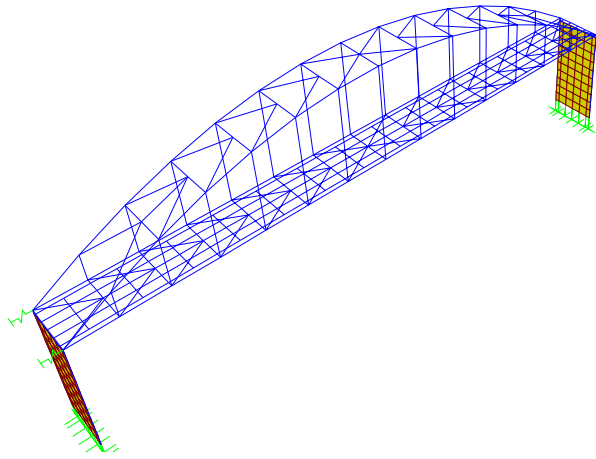
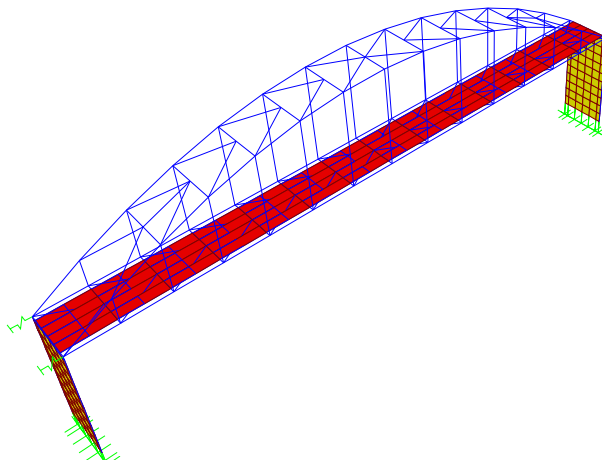


Figure 3.13b The Second Transverse Mode Shape ($f=1.242\text{Hz}$, damping ratio=1.4%)

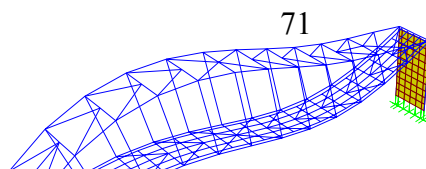


(a) Model-1

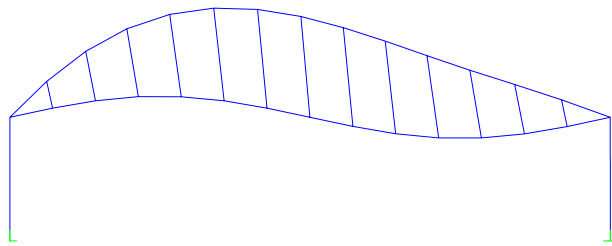


(b) Model-2

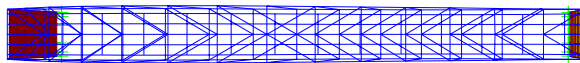
Figure 4.1 3-D View of the FE Models



(a) Isometric View

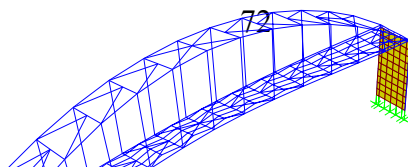


(b) Elevation View

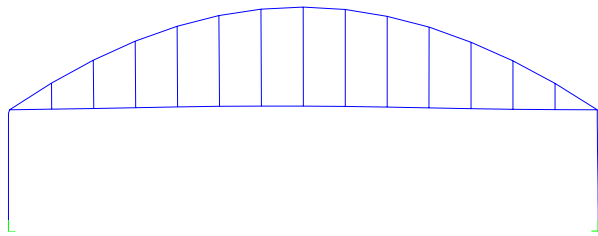


(c) Plan View

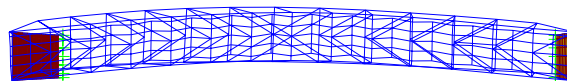
Figure 4.2 Mode Shape of the First Natural Frequency for Model-1
(1st Vertical Mode Shape, 0.561 Hz)



(a) Isometric View

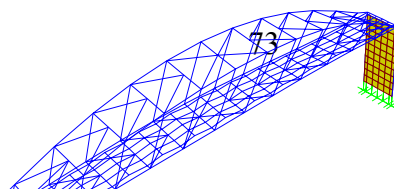


(b) Elevation View

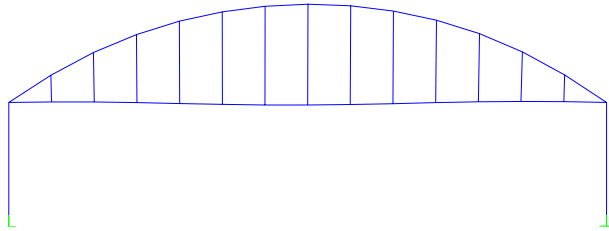


(c) Plan View

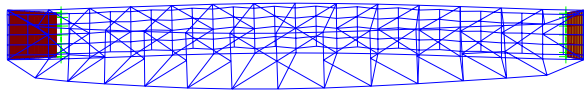
Figure 4.3 Mode Shape of the Second Natural Frequency for Model-1
(1st Transverse Mode Shape, 0.717 Hz)



(a) Isometric View

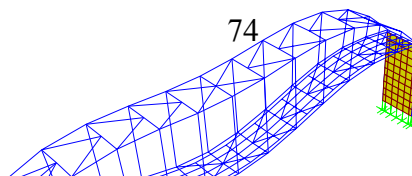


(b) Elevation View

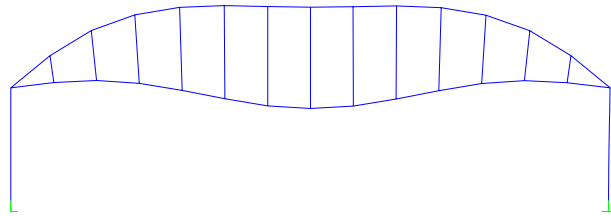


(c) Plan View

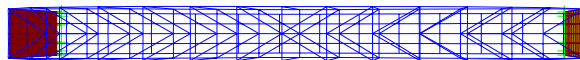
Figure 4.4 Mode Shape of the Third Natural Frequency for Model-1
(0.973 Hz)



(a) Isometric View

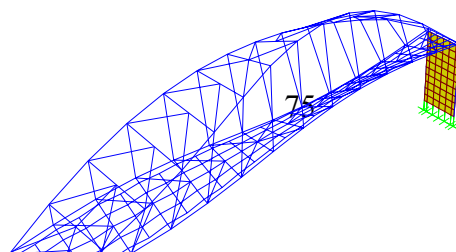


(b) Elevation View

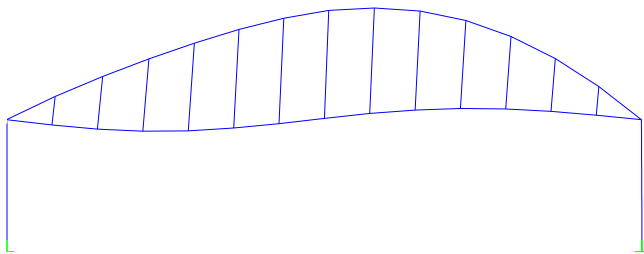


(c) Plan View

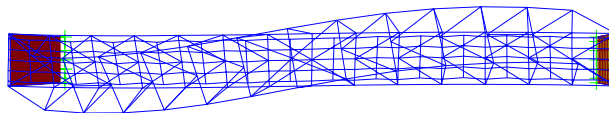
Figure 4.5 Mode Shape of the Fourth Natural Frequency for Model-1
(2nd Vertical Mode Shape, 1.149 Hz)



(a) Isometric View

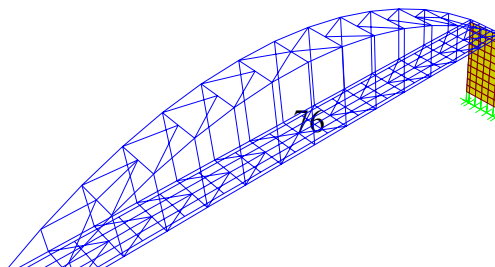


(b) Elevation View

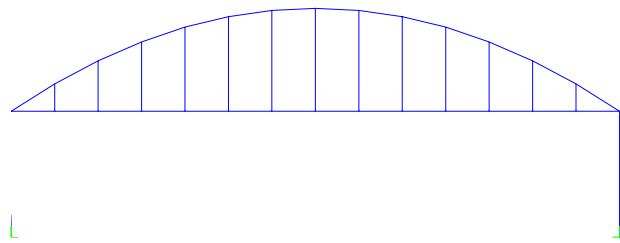


(c) Plan View

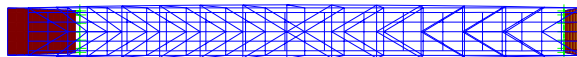
Figure 4.6 Mode Shape of the Fifth Natural Frequency for Model-1 (1.320 Hz)



(a) Isometric View

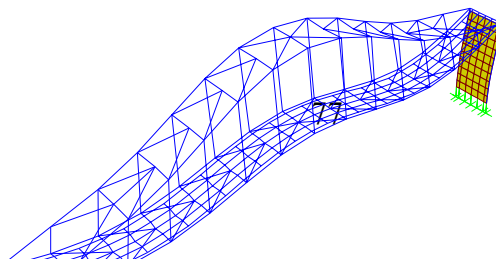


(b) Elevation View

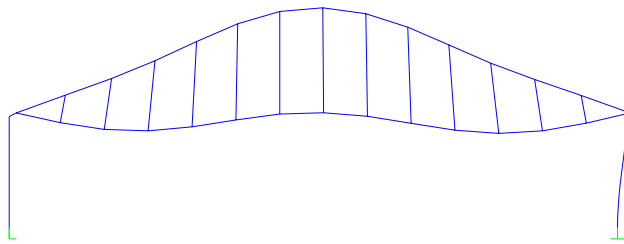


(c) Plan View

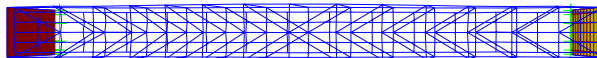
Figure 4.7 Mode Shape of the Sixth Natural Frequency for Model-1
(1.399 Hz)



(a) Isometric View

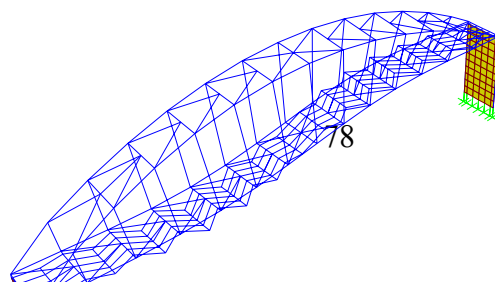


(b) Elevation View

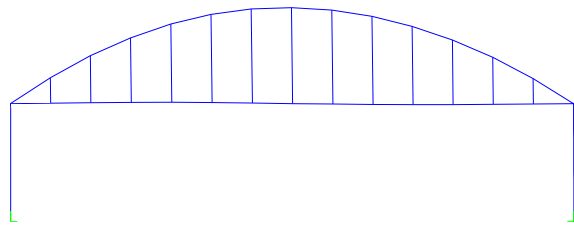


(c) Plan View

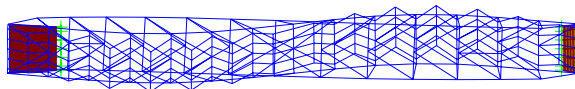
Figure 4.8 Mode Shape of the Seventh Natural Frequency for Model-1
(1st Longitudinal Mode Shape, 1.516 Hz)



(a) Isometric View

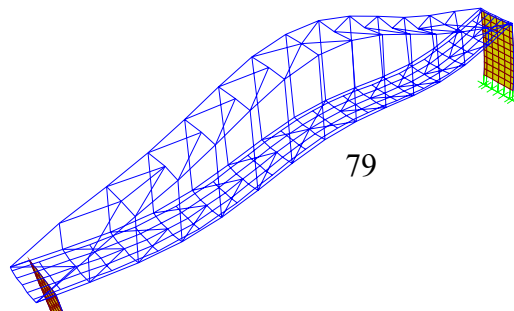


(b) Elevation View

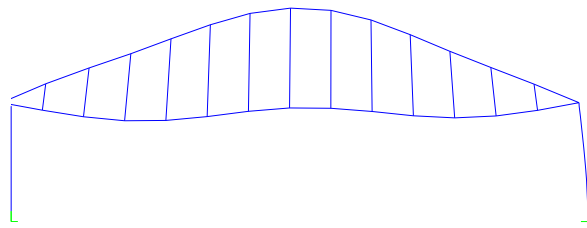


(c) Plan View

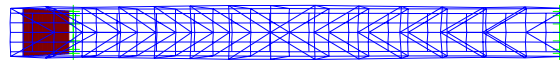
Figure 4.9 Mode Shape of the Eighth Natural Frequency for Model-1
(2nd Transverse Mode Shape, 1.557 Hz)



(a) Isometric View

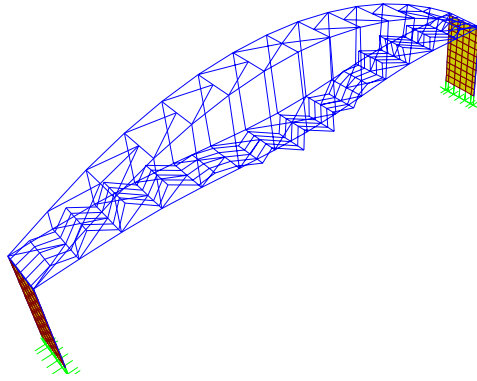


(b) Elevation View

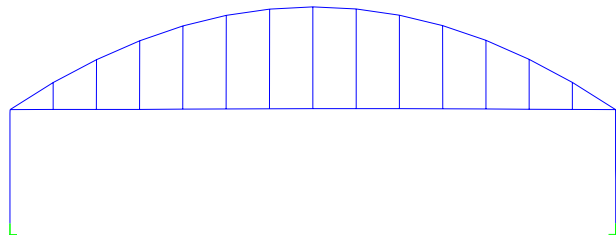


(c) Plan View

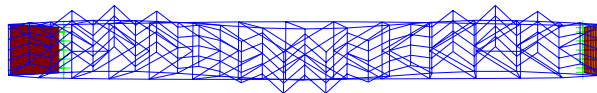
Figure 4.10 Mode Shape of the Ninth Natural Frequency for Model-1
(3rd Vertical Mode Shape, 1.749 Hz)



(a) Isometric View

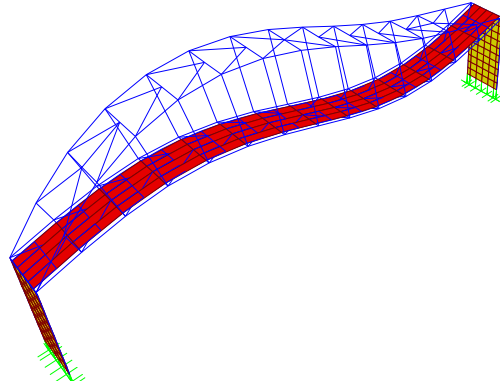


(b) Elevation View

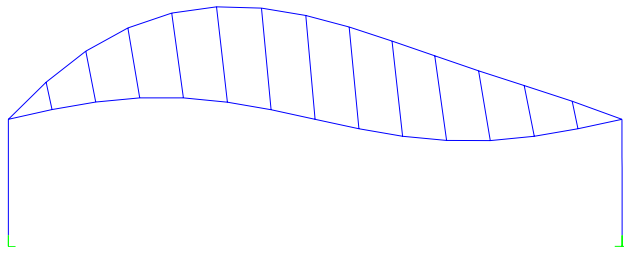


(c) Plan View

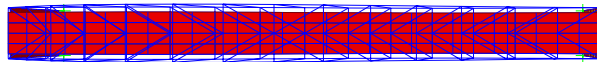
Figure 4.11 Mode Shape of the Tenth Natural Frequency for Model-1
(3rd Transverse Mode Shape, 1.838 Hz)



(a) Isometric View

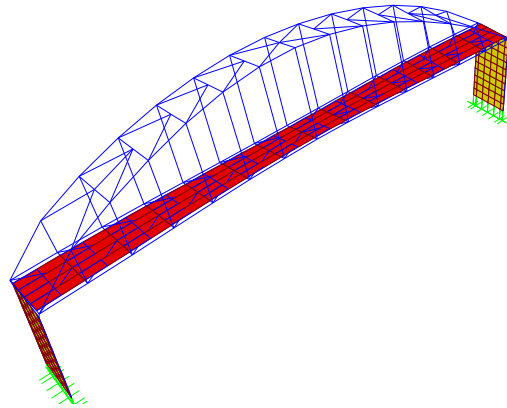


(b) Elevation View

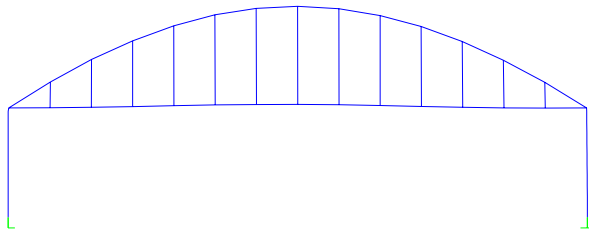


(c) Plan View

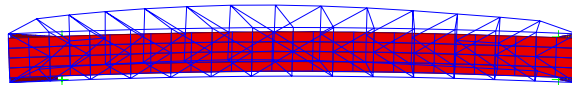
Figure 4.12 Mode Shape of the First Natural Frequency for Model-2
(1st Vertical Mode Shape, 0.562 Hz)



(a) Isometric View

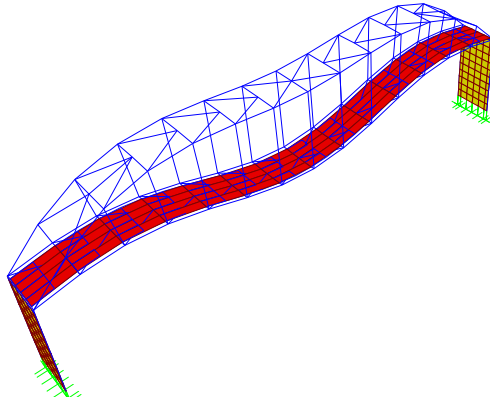


(b) Elevation View

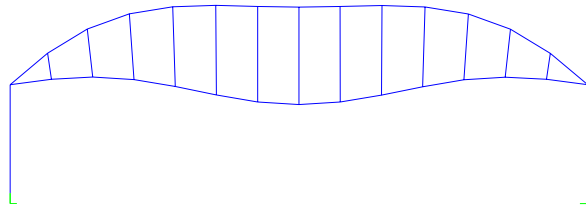


(c) Plan View

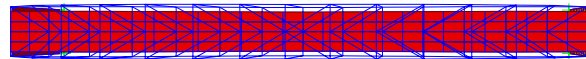
Figure 4.13 Mode Shape of the Second Natural Frequency for Model-2
(1st Transverse Mode Shape, 0.861 Hz)



(a) Isometric View

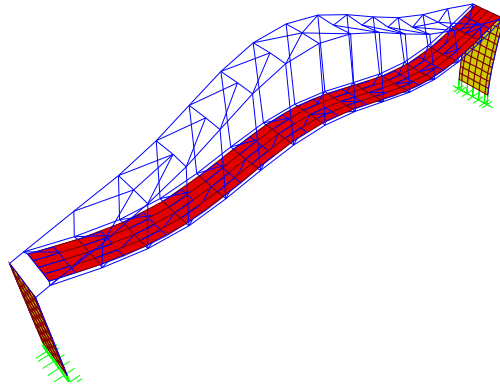


(b) Elevation View

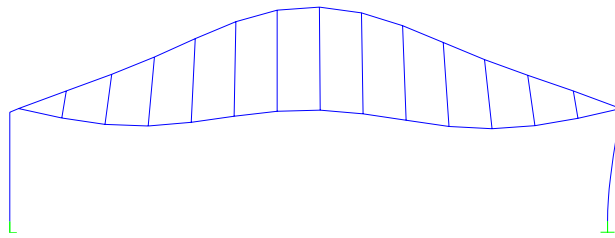


(c) Plan View

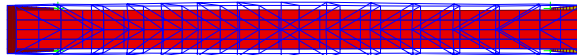
Figure 4.14 Mode Shape of the Third Natural Frequency for Model-2
(2st Vertical Mode Shape, 1.162 Hz)



(a) Isometric View

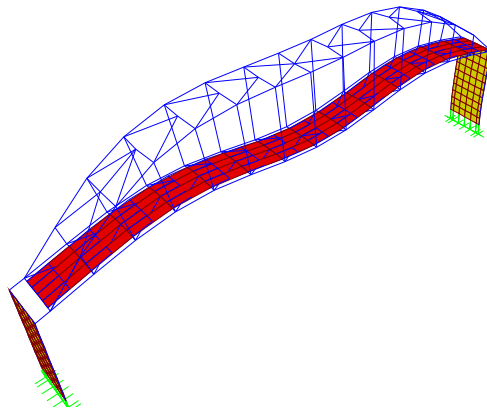


(b) Elevation View

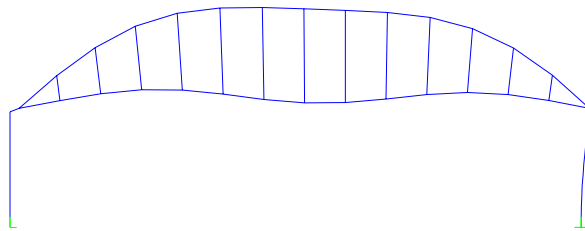


(c) Plan View

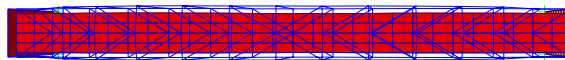
Figure 4.15 Mode Shape of the Seventh Natural Frequency for Model-2
(1st Longitudinal Mode Shape, 1.573 Hz)



(a) Isometric View

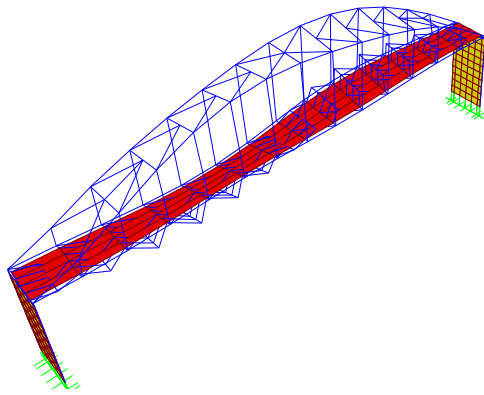


(b) Elevation View

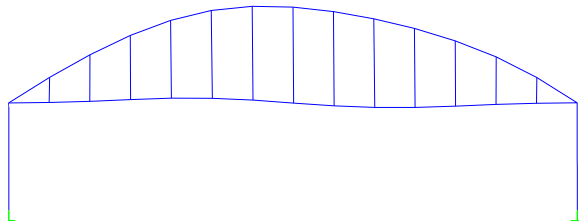


(c) Plan View

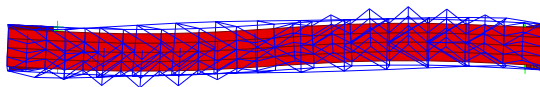
Figure 4.16 Mode Shape of the Eighth Natural Frequency for Model-2
(3st Vertical Mode Shape, 1.762 Hz)



(a) Isometric View



(b) Elevation View



(c) Plan View

Figure 4.17 Mode Shape of the Thirteenth Natural Frequency for Model-2
(2st Transverse Mode Shape, 2.897 Hz)

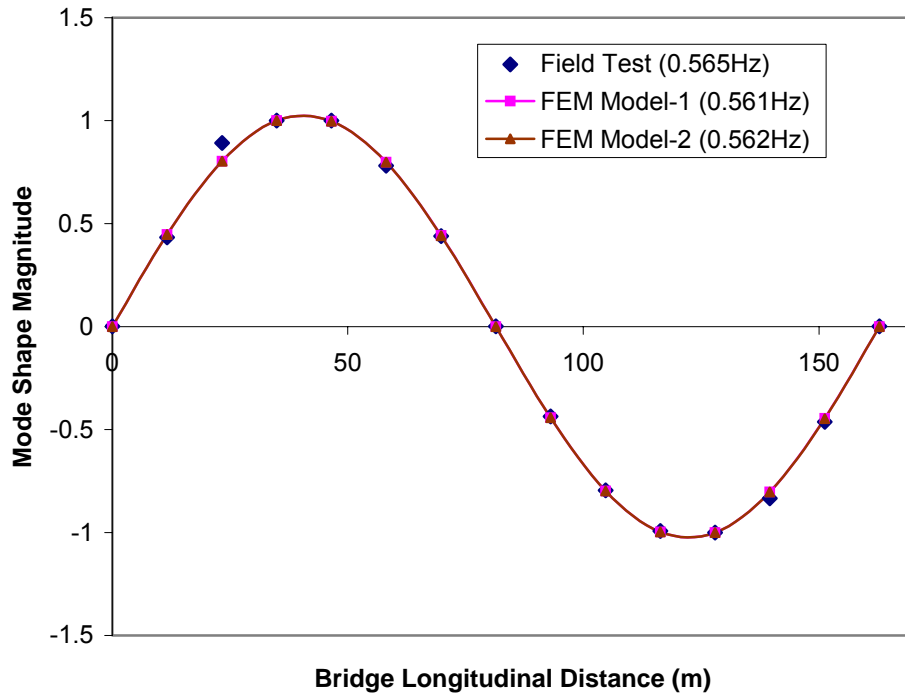


Figure 4.18 Comparison of 1st Vertical Mode Shapes

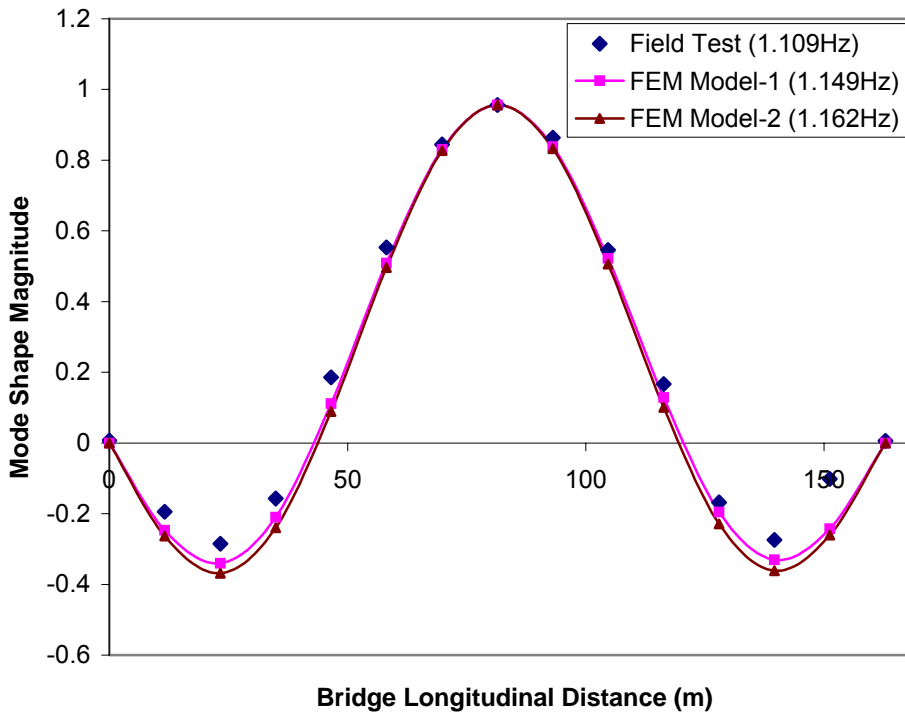


Figure 4.19 Comparison of 2nd Vertical Mode Shapes

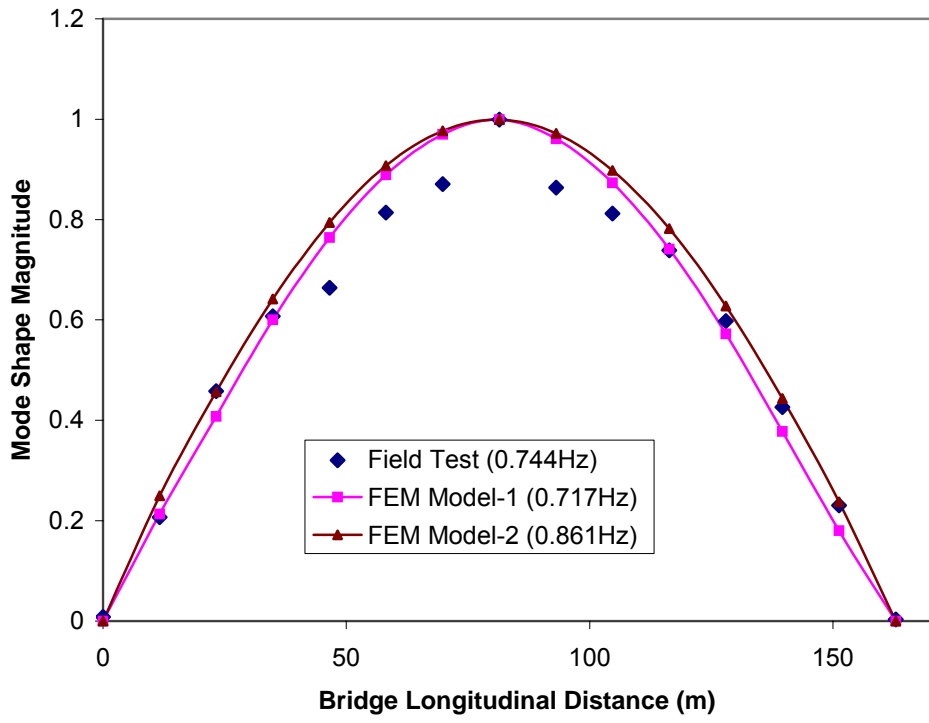
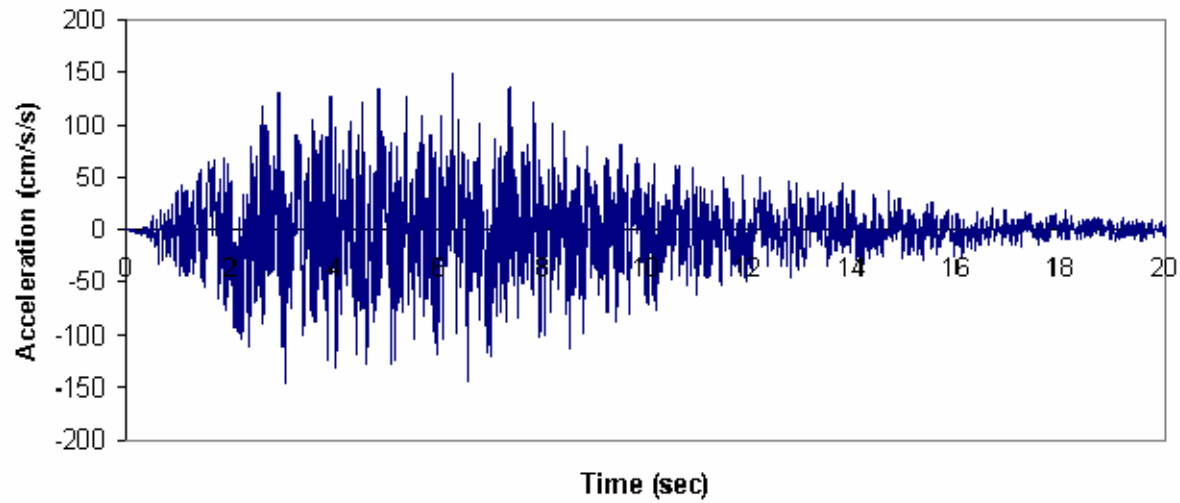


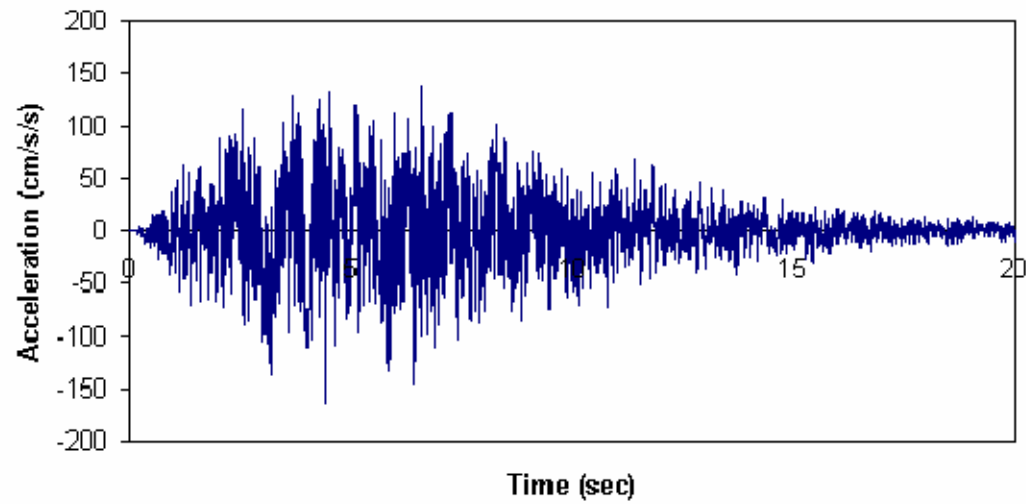
Figure 4.20 Comparison of 1st Transverse Mode Shapes



Acceleration time history for component-1 of the 250-Year event for counties identified by 0.15g-1

(b) Acceleration time history for component-1

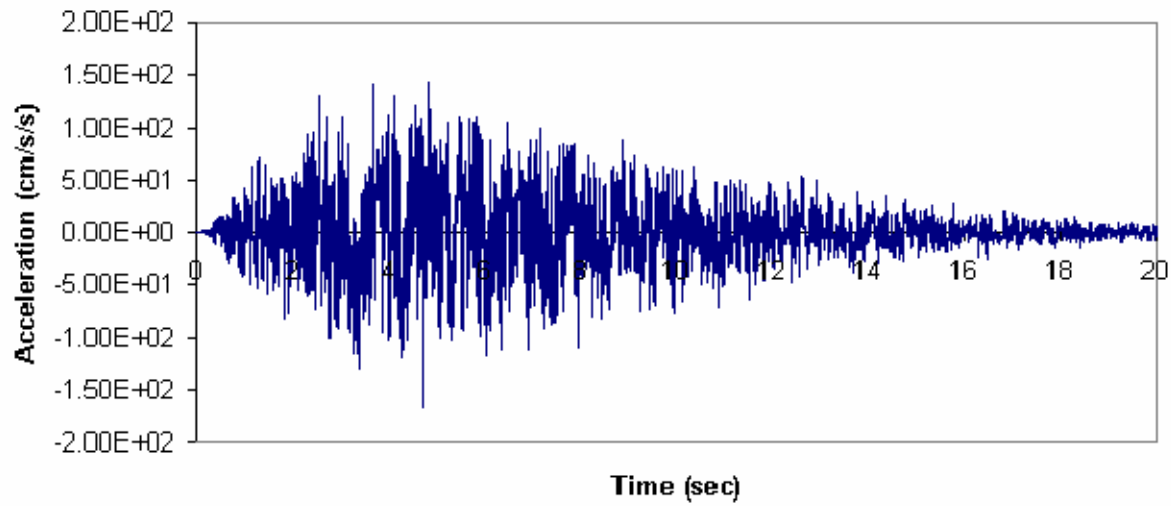
Figure 5.1 (cont') Time-history and Response Spectra Identification Map of the Commonwealth of Kentucky for 250-year Event Earthquake



Acceleration time history for component-2 of the 250-Year event for counties identified by 0.15g-1

(c) Acceleration time history for component-2

Figure 5.1 (cont') Time-history and Response Spectra Identification Map of the Commonwealth of Kentucky for 250-year Event Earthquake



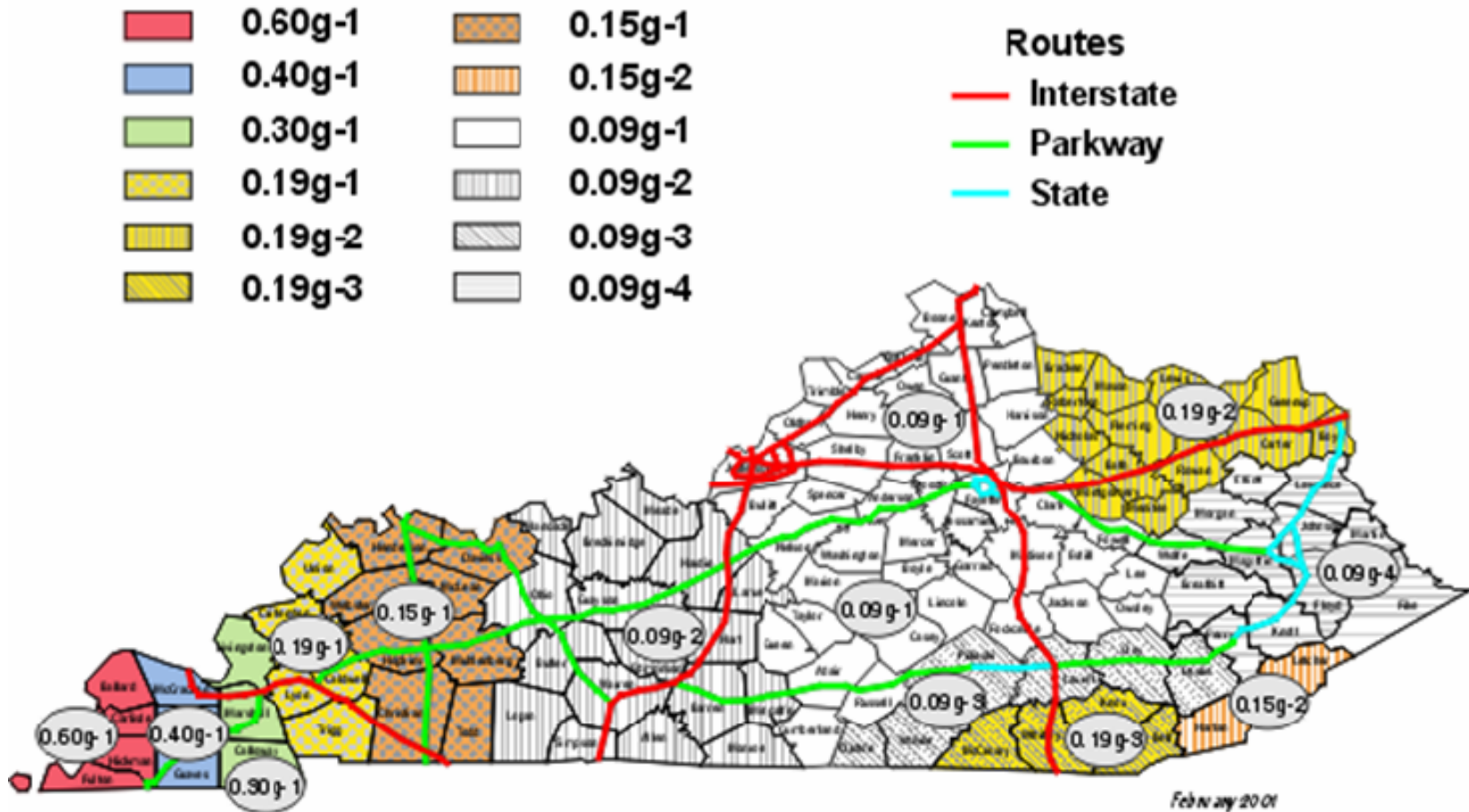
Acceleration time history for component-3 of the 250-Year event for counties identified by 0.15g-1

(d) Acceleration time history for component-3

Figure 5.1 (cont') Time-history and Response Spectra Identification Map of the Commonwealth of Kentucky for 250-year Event Earthquake

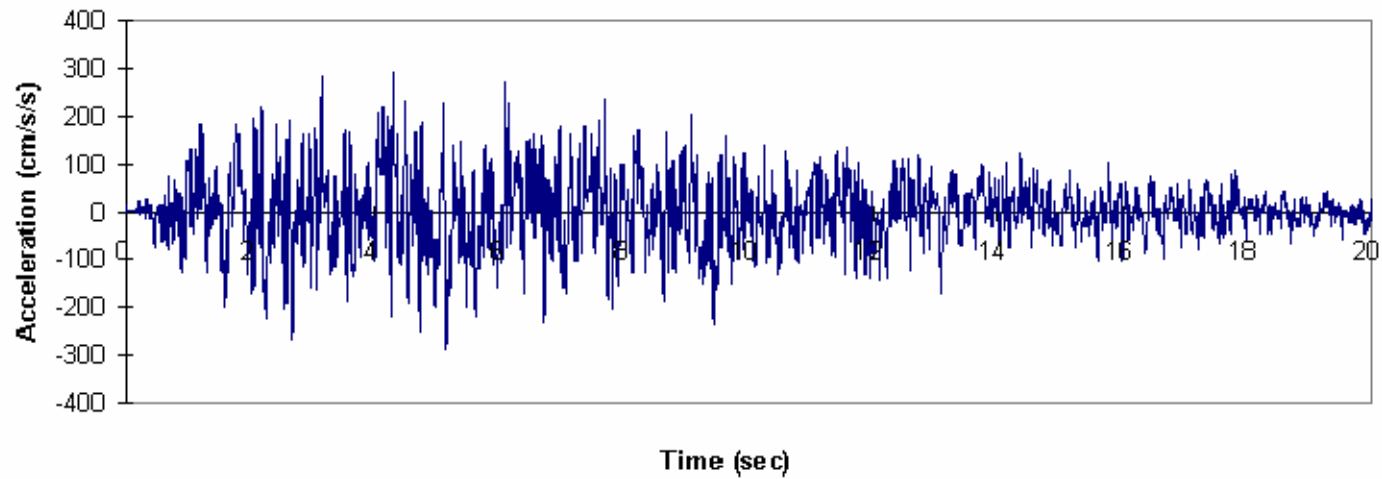
Time History-Response Spectra (TR-500Y-0.xxg-x)

Identification Map for 90 Percent Probability of Not Being Exceeded in **500 Years**



(a) Response spectra identification map

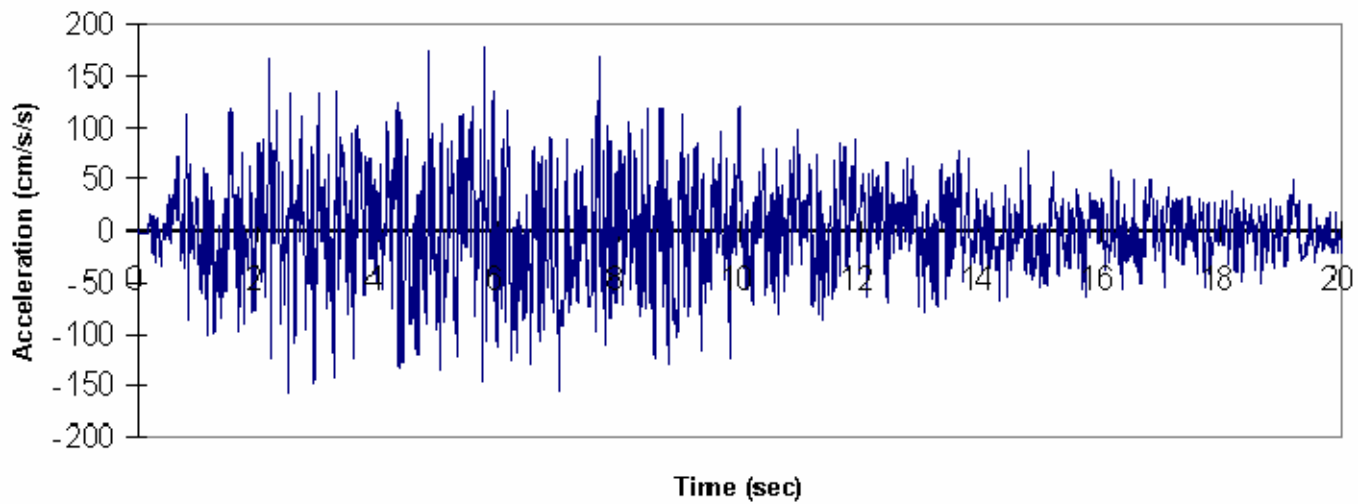
Figure 5.2 Time-history and Response Spectra Identification Map of the Commonwealth of Kentucky for 500-year Event Earthquake



Acceleration time history for component-1 of the 500-Year event for counties identified by 0.3g-1

(b) Acceleration time history for components-1

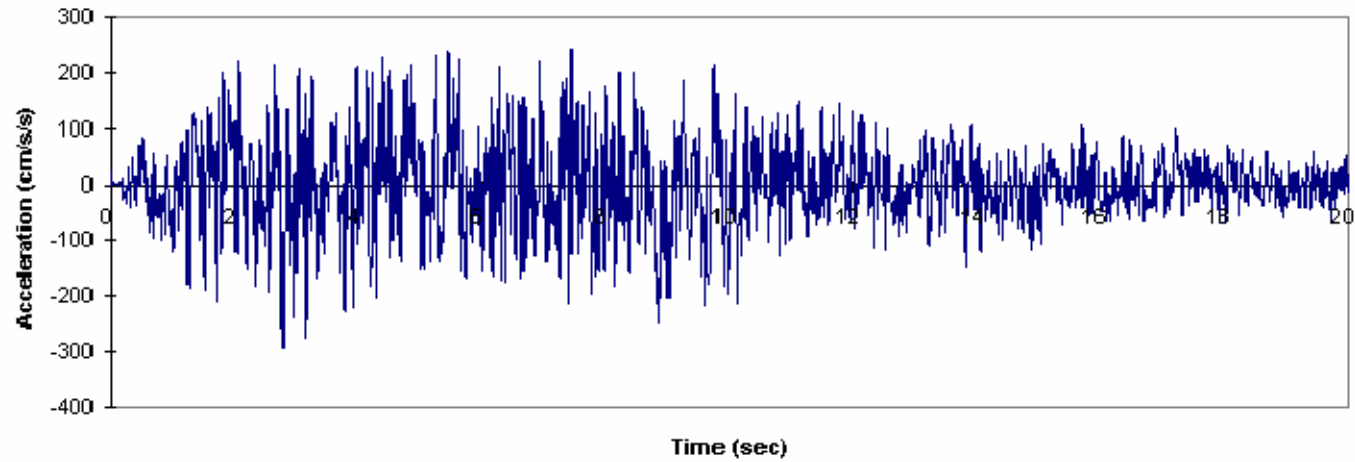
Figure 5.2 (cont') Time-history and Response Spectra Identification Map of the Commonwealth of Kentucky for 500-year Event Earthquake



Acceleration time history for component-2 of the 500-Year event for counties identified by 0.3g-1

(c) Acceleration time history for component-2

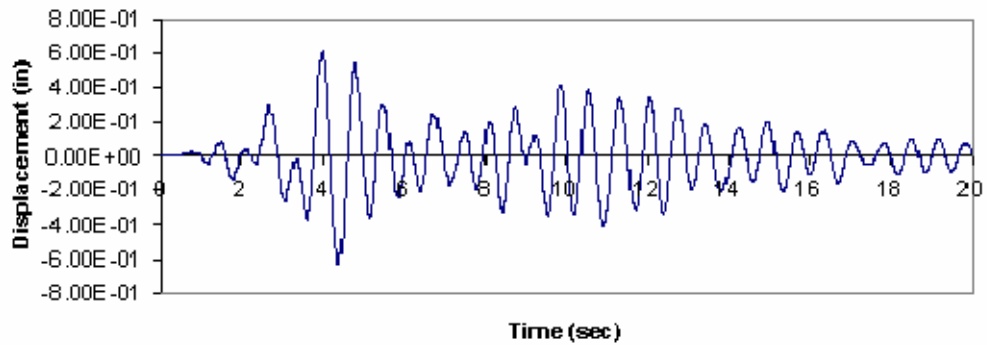
Figure 5.2 (cont') Time-history and Response Spectra Identification Map of the Commonwealth of Kentucky for 500-year Event Earthquake



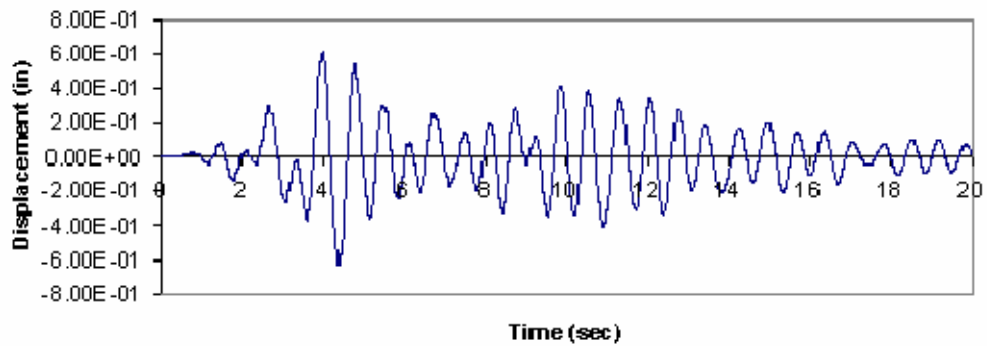
Acceleration time history for component-3 of the 500-Year event for counties identified by 0.3g-1

(d) Acceleration time history for component-3

Figure 5.2 (cont') Time-history and Response Spectra Identification Map of the Commonwealth of Kentucky for 500-year Event Earthquake



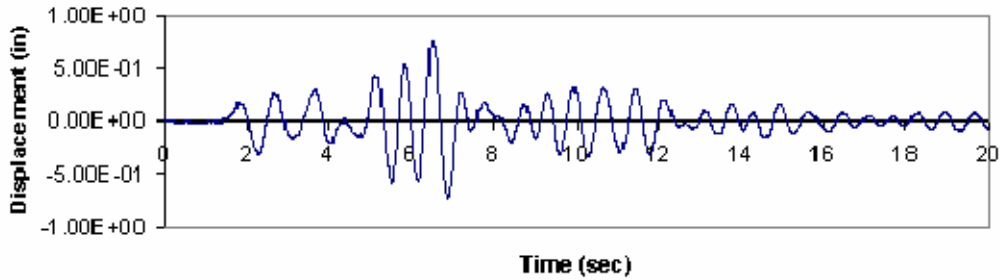
Time history of relative longitudinal displacement between top (Joint 1) and bottom (Joint 303) of the bearing



Time history of relative longitudinal displacement between top (Joint 1) and bottom (Joint 303) of the bearing

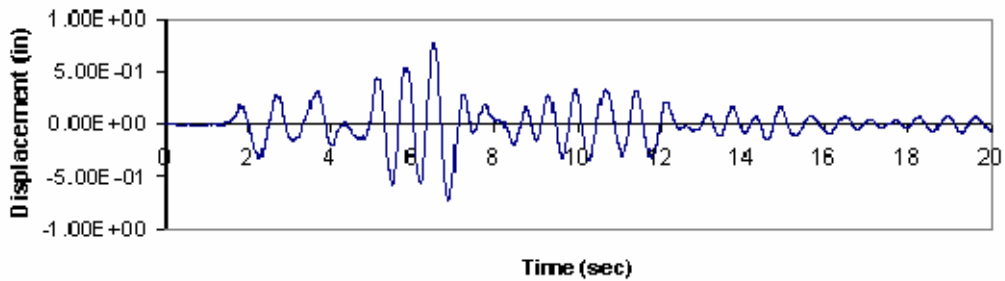
CASE-1: 250-Year (0.15g-1)

Figure 5.3 Time-history of Relative Longitudinal Displacement between Top and Bottom of the Bearings on Pier 5 for 250-year Event (Case-1, $\xi=0.05$)



Time history of relative longitudinal displacement between top (Joint 1) and bottom (Joint 303) of the bearing

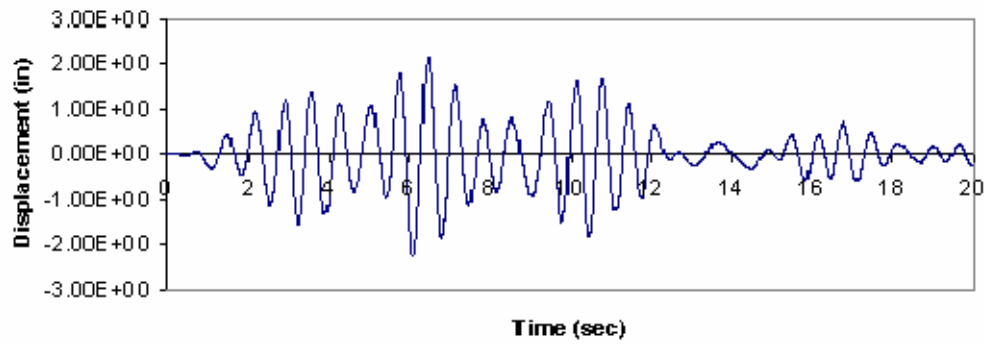
CASE-2: 250-Year (0.15g-1)



Time history of relative longitudinal displacement between top (Joint 1) and bottom (Joint 303) of the bearing

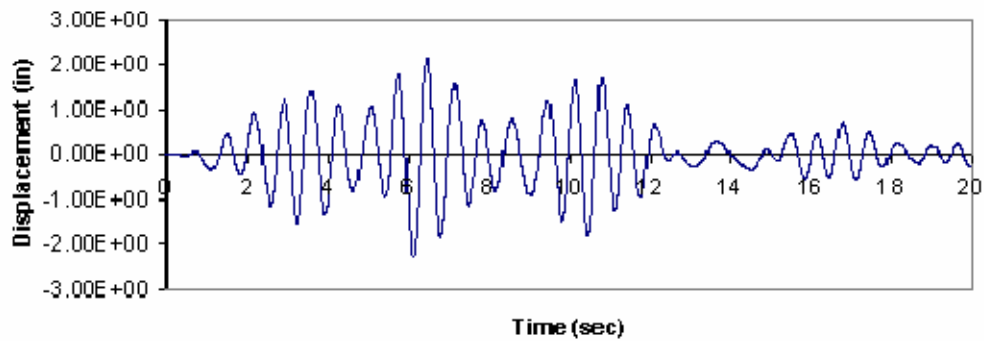
CASE-2: 250-Year (0.15g-1)

Figure 5.4 Time-history of Relative Longitudinal Displacement between Top and Bottom of the Bearings on Pier 5 for 250-year Event (Case-2, $\xi=0.05$)



Time history of relative longitudinal displacement between top (Joint 1) and bottom (Joint 303) of the bearing

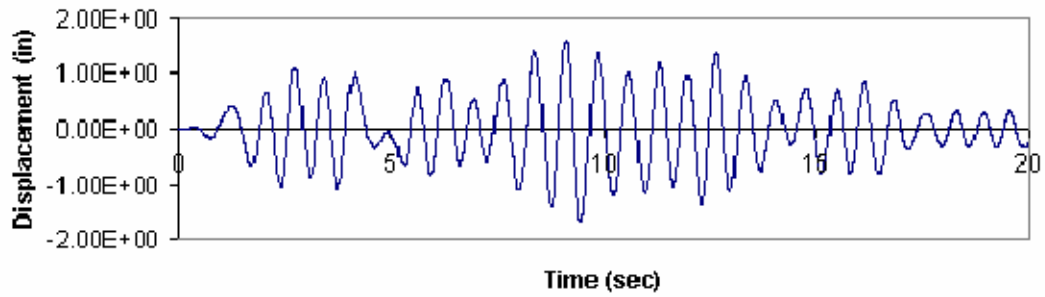
CASE-1: 500-Year (0.3g-1)



Time history of relative longitudinal displacement between top (Joint 1) and bottom (Joint 303) of the bearing

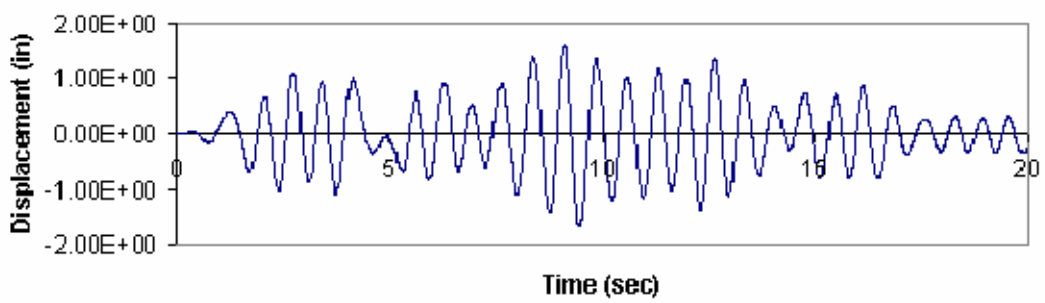
CASE-1: 500-Year (0.3g-1)

Figure 5.5 Time-history of Relative Longitudinal Displacement between Top and Bottom of the Bearings on Pier 5 for 500-year Event (Case-1, $\xi=0.05$)



Time history of relative longitudinal displacement between top (Joint 1) and bottom (Joint 303) of the bearing

CASE-2: 500-Year (0.3g-1)



Time history of relative longitudinal displacement between top (Joint 1) and bottom (Joint 303) of the bearing

CASE-2: 500-Year (0.3g-1)

Figure 5.6 Time-history of Relative Longitudinal Displacement between Top and Bottom of the Bearings on Pier 5 for 500-year Event (Case-2, $\xi=0.05$)

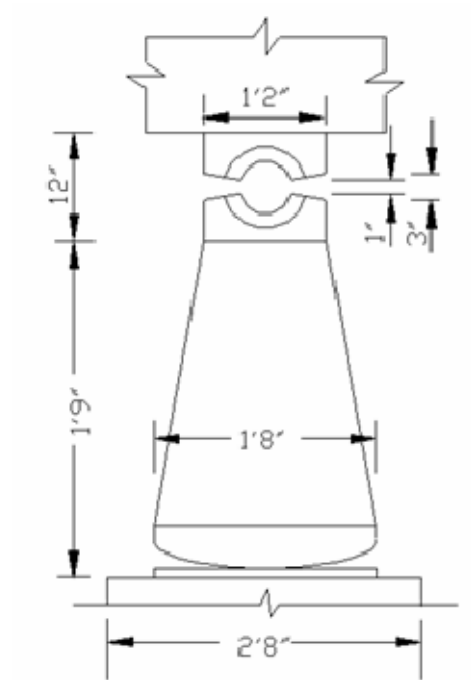


Figure 6.1 Expansion

bearing for Pier 1 and Pier 8

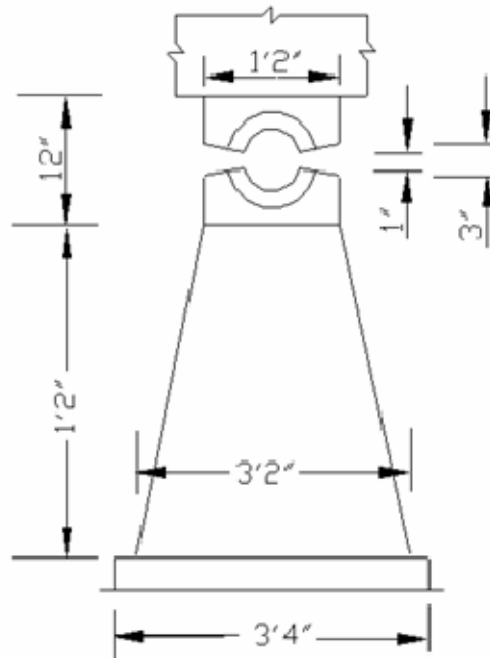
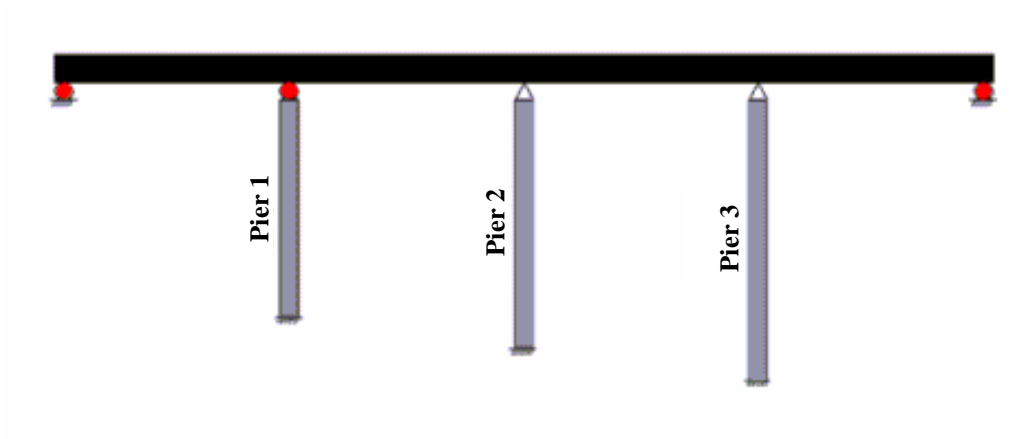
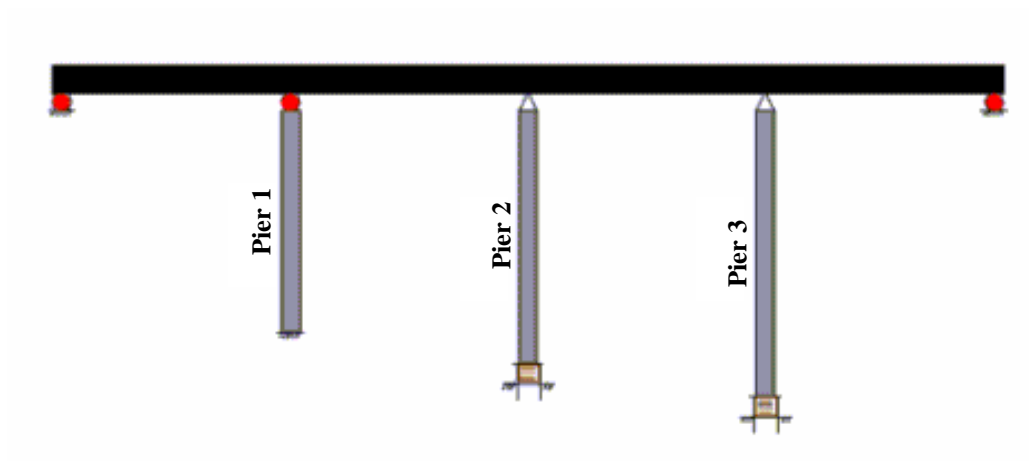


Figure 6.2 Fixed bearing for Pier 2, Pier 3, Pier 6 and Pier 7



(a) Assuming that the piers are fixed at the bottom of pile caps
(used for force calculation)



(b) Assuming that the piers are extended to a depth of half length of the piles and fixed at that
level (used for displacement calculation)

Figure 6.3 Calculation model for the longitudinal analysis

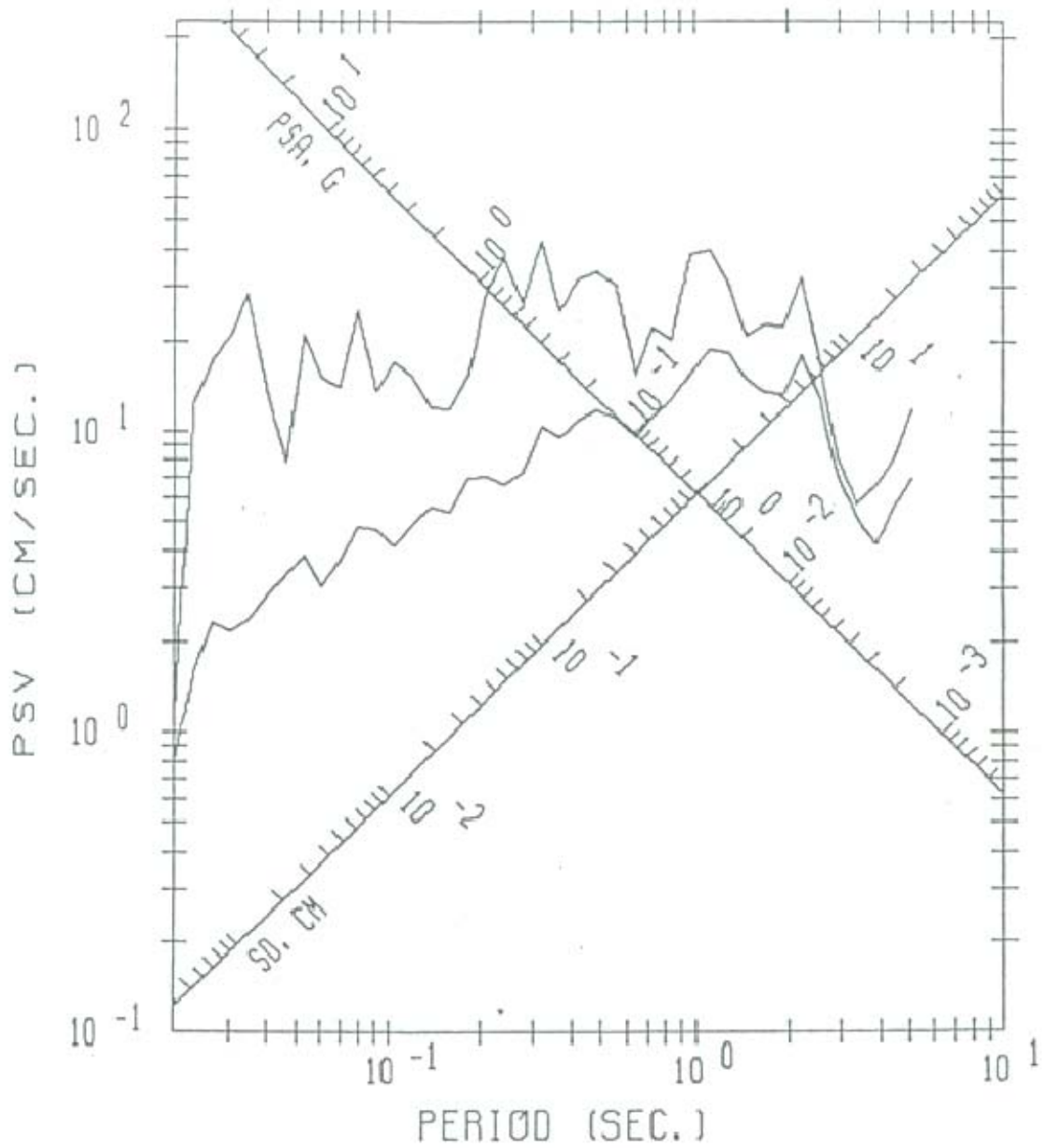


Figure 6.5 Response spectra for the transverse component of the 250-year event for counties identified by 0.15g-1 (Damping ratio=0.00 and 0.05)

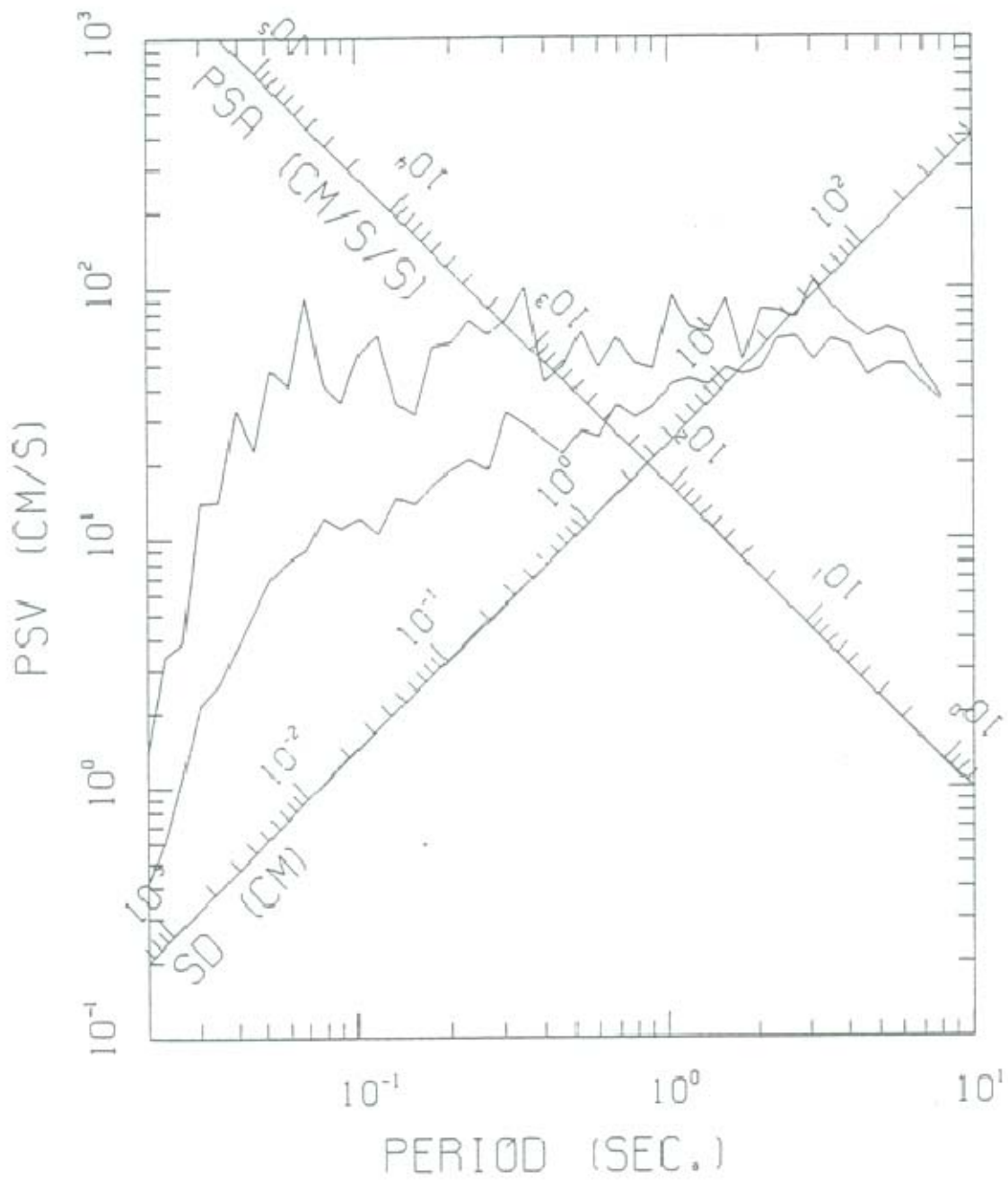


Figure 6.6 Response spectra for the horizontal component of the 500-year event for counties identified by 0.30g-1 (Damping ratio=0.00 and 0.05)

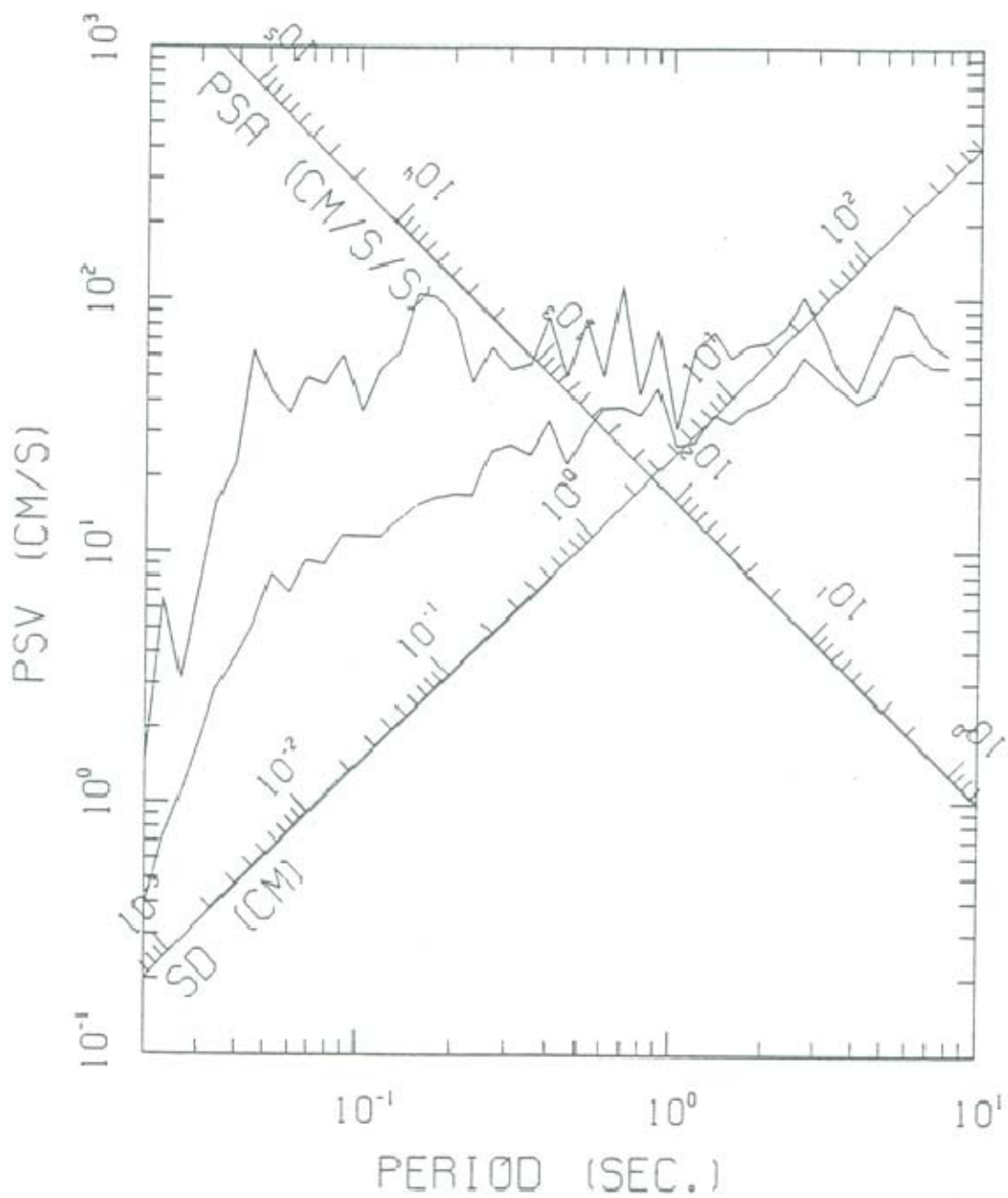


Figure 6.7 Response spectra for the transverse component of the 500-year event for counties identified by 0.30g-1 (Damping ratio=0.00 and 0.05)

For more information or a complete publication list, contact us at:

KENTUCKY TRANSPORTATION CENTER

176 Raymond Building
University of Kentucky
Lexington, Kentucky 40506-0281

(859) 257-4513
(859) 257-1815 (FAX)
1-800-432-0719
www.ktc.uky.edu
ktc@engr.uky.edu

The University of Kentucky is an Equal Opportunity Organization